공학석사 학위논문

100°C 이하 저온 열원에 적용된 유기 랭킨 사이클의 성능에 관한 연구

Studies on the Performance of Organic Rankine Cycle Applied to Low Temperature Heat Source below 100°C

2016년 2월

서울대학교 대학원

기계항공공학부

이 지 성

100°C 이하 저온 열원에 적용된
유기 랭킨 사이클의 성능에 관한 연구

Studies on the Performance of
Organic Rankine Cycle Applied to Low Temperature
Heat Source below 100°C

지도교수 김 민 수

이 논문을 공학석사 학위논문으로 제출함

2015년 11월

서울대학교 대학원
기계항공공학부
이 지 성

이지성의 공학석사 학위논문을 인준함
2015년 12월

위 원 장 _____ (인)

부위원장 _____ (인)

위 원 _____ (인)

Abstract

Studies on the Performance of Organic Rankine Cycle Applied to Low Temperature Heat Source below 100ºC

Ji Sung Lee
Department of Mechanical and Aerospace Engineering
The Graduate School
Seoul National University

In this study, the performance of Organic Rankine Cycle (ORC) applied to low temperature heat source was investigated to provide meaningful information and better understanding on ORC. In previous studies of ORC, the types of heat source were mainly geothermal heat, solar heat, biomass combustion waste heat whose temperatures range from 150ºC to 350ºC. However, although waste heat below 100ºC generated from industrial process (e.g. food, beverage, fiber industry) and PEM fuel cell has a large portion of overall waste heat, it isn't sufficiently utilized for waste heat recovery.

Therefore, it is necessary to investigate operating characteristics of ORC using waste heat from heat source under 100°C. In order to verify the performance of ORC applied to heat source below 100°C, experiment was conducted to investigate the effects of some key parameters (e.g. evaporation pressure, condensation pressure, mass flow rate, etc.) and the optimal operating condition which has maximum generation work. Results show that the maximum generation work was about 234 W and the thermal efficiency of ORC was about 4%, when the range of heat input was from 3 kW to 6 kW. By experiment of ORC applied to low temperature heat source, it was confirmed that ORC can obtain the additional generating power from waste heat under 100°C.

Keywords: Organic Rankine Cycle, Scroll Expander, Waste Heat Recovery, Low Temperature Heat Source, Industrial Waste Heat, PEM fuel cell Waste Heat, R-245fa

***Identification Number*: 2013-23833**

Contents

List of Figures

List of Tables

Nomenclature

P_c	Critical pressure (MPa)
T_c	Critical temperature (^oC)
T_{bp}	Boiling point temperature (^oC)
PEMFC	Proton Exchange Membrane Fuel Cell
ORC	Organic Rankine Cycle
ODP	Ozone Depletion Potential relative to R11
GWP	Global Warming Potential relative to CO_2
h	Heat transfer coefficient (W m^{-2} K^{-1})
D_h	Hydrauric diameter (m)
k	Thermal conductivity (W m^{-1} K^{-1})
Re	Reynolds number
Pr	Prandtl number
μ	Dynamic viscosity (Pa s^{-1})
ρ	Density (kg m^{-3})
x	Quality
Bo	Boiling number
q"	Heat flux (W m^{-2})
G	Mass flux (kg m^{-2} s^{-1})
DSH	Degree of Super Heating (^oC)
DSC	Degree of Sub Cooling (^oC)
GPH	Gallon per hour (Gal h^{-1})

RPM	Revolution per minute (rev min^{-1})
cps	Centi poise (g cm^{-1} s^{-1})
RT	Refrigeration tons (=3.52 kW)
E	Exergy (W)
Q	Heat (J)
W	Work (J)
T_f	Frictional torque (N m)
η	Efficiency
D	Exergy destruction (W)
R_p	Pressure ratio

Subscript

r	Refrigerant
v	Saturated vapor
l	Saturated liquid
tp	Two phase
sp	Single phase
cell	Fuel cell
w	Water
eva	Evaporator
cond	Condenser
exp	Expander
th	Thermal

sat	Saturation
0	Dead state
h	Hot
r	Refrigerant
exg	Exergy
0	Dead state

Chapter 1. Introduction

1.1 Background of the Study

In recent decades, global energy crisis and global warming problem have been great issues. By 2035, the world's population is expected to reach 8.7 billion and the primary energy consumption is projected to increase by 37% between 2013 and 2035 [1, 2]. The growing fossil fuel use for transportation and industry, the decreasing crude oil production, and the political and social unrest of major oil supplying countries has accelerated the global energy crisis. Furthermore, due to increasing carbon dioxide emissions which have the largest portion of the overall anthropogenic greenhouse gas emissions, the global land-ocean temperature has been increasing steadily and the abnormal climate has been occurring more frequently. Especially, the 42% of the global carbon dioxide emissions comes from the primary energy consumption for generating electricity [3]. Therefore, in order to overcome these problems, it is most important to improve the efficiency of the conventional or novel power generation systems and find new type of energy sources such as renewable energy, alternative energy and so on.

Considering the feasibility of application and the impact to the energy and

climate problem, it is most essential to increase the conversion efficiencies of the utilization of available energy sources [4]. Because improving energy efficiency plays a key role towards planning to make energy security and fulfilling climate and environmental regulations. There are several ways to increase conversion efficiencies of generating electricity such as co-generation using waste heat, developing new type of power generation cycle and so on. Among these ways, recovering waste heat from conventional power cycle or engine exhaust and industrial waste heat sources has been evaluated as most effective method. Because roughly two-thirds of the fuel used to generate power is lost as waste heat during fossil-fuelled power generation [5]. Waste heat sources are classified according to the temperature rage as: high temperature (>650^{o}C), medium temperature (230~650^{o}C), low temperature or low-grade (<230^{o}C) [6]. According to statistical information, the low temperature waste heat sources accounts for 50% of overall heat generated from industry [7]. In this respect, organic Rankine cycle (ORC) has been spotlighted as the viable technology to produce electrical power from low-grade heat sources due to lower ebullition temperature and pressure, simpler structure, and lower cost of maintenance compared to conventional steam cycle. Furthermore, the ORC applied to waste heat recovery is expected to be helpful to the reduction of greenhouse gas emissions which would have been produced if

fossil fuel was to be used for the conventional power generation system [8].

Likewise, the ORC has several benefits and potentials for applying to waste heat recovery. In this study, in order to provide meaningful information and better understanding on the ORC, the performance of the ORC applied to low temperature heat source was investigated. Especially, unlike the previous studies on the ORC, the experiments was conducted to investigate the characteristics of the ORC utilizing waste heat below 100^{o}C.

1.2 Overview on the Organic Rankine Cycle

The steam Rankine cycle has been used for transforming on large scale thermal energy into electrical power as the most important method. By using water as working fluid, it is possible to lessen the concerns about toxicity, flammability, consumption work of the pump, thermal/chemical stability, cost, and so on. However, when steam cycle is used as small and medium scale power plant, there are many disadvantages such as need of superheating to prevent condensation during expansion process, risk of erosion of turbine blades, excess pressure in evaporator, and complex and expensive turbines [9].

With this background, in order to overcome these problems, it was necessary to partially mitigate the limitations of water by selecting an alternative working fluid. As shown in Table 1.1 and Fig. 1.1, Organic fluids having higher molecular mass and lower boiling point/critical temperature than water have been proposed in so called “organic Rankine cycle”.

Due to the same fundamentals of operating of both of the ORC and the conventional steam cycle, these cycles have few similarities about cycle configurations, components and applications. However, because these cycles use different working fluids, the characteristics of these cycles appear differently depending on situations. The ORC has several advantages over traditional steam Rankine cycle. For example, less heat is needed during the

Table 1.1 Properties of water and organic fluids

Substance	**Molecular mass (kg/kmol)**	**P_c (MPa)**	**T_c (°C)**	**T_{bp} (°C)**
Water	18.02	22.06	373.95	99.974
R245fa	134.05	3.64	154.05	14.90
R245ca	134.05	3.93	174.42	25.13
R11	137.37	4.408	197.96	23.71
R113	187.38	3.392	214.06	47.59
R114	170.92	3.257	145.68	3.49
R123	152.93	3.662	183.68	27.82
R134a	102.03	4.06	101.03	-26.07
R141b	116.95	4.25	204.50	32.05

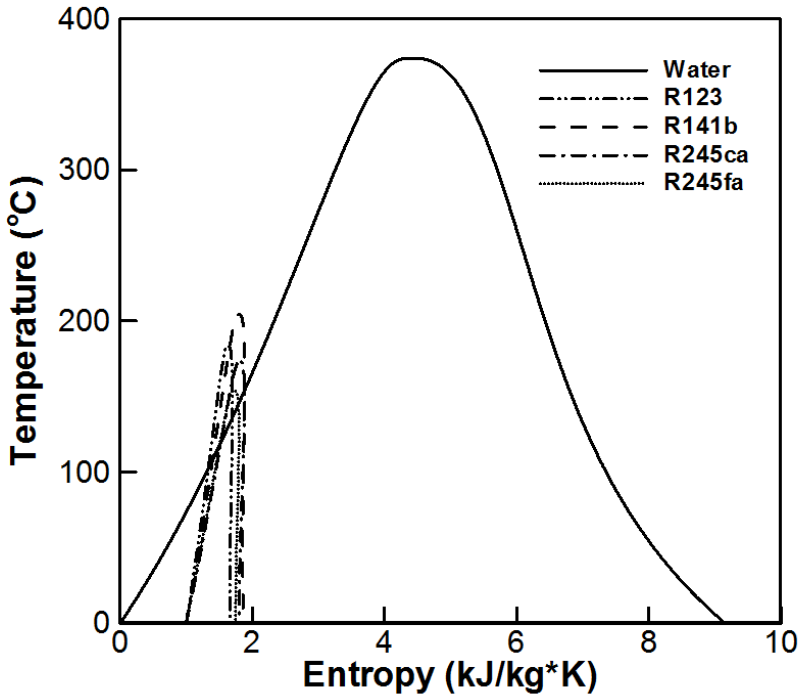

Fig. 1.1 T-s diagrams of water and few organic fluids

evaporation process and the evaporation process takes place at lower temperature and pressure than water. Due to non-negative slope of vapor saturation curve, erosion of expander blades is not concerned. Simple single stage expanders can be used owing to the smaller pressure drop/ratio.

Likewise, the working fluids in the ORC power systems play the most important role to determine the performance and the economic feasibility. Therefore, there are so many sufficient conditions to be the appropriate working fluid of the ORC. In order to lessen the concern of erosion of expander blades, it should have the vapor saturation curve with zero or positive slope. It should have high density of liquid or vapor phase for minimizing the sizes of overall system. It need to have good heat transfer properties such as low viscosity and high thermal conductivity. In order to operate stably at high temperature, it should have good thermal and chemical stability and good compatibility with the conventional materials. For high energetic/exergetic efficiency and good safety characteristics, the working fluid should have high thermodynamic performance and should be non-toxic and non-flammable. Furthermore, because of growing the concern about global climate change and environmental destruction in recent, it should have low ODP and low GWP. The cost and availability should also be considered for selecting the proper working fluid.

In addition, the ORC has been applied to various heat sources and has

shown the possibility to realize in actual field. Especially, in USA, Canada, Italy, Austria, Germany, Netherlands and Sweden, a large number of the ORC power plants have been installed for geothermal heat, solar heat and biomass combustion waste heat. In recent decade, Ocean Thermal Energy Conversion applied to the Earth's oceans as heat source of virtually inexhaustible renewable energy has been intensely investigated as future technology.

1.3 Literature Survey

The researches of the ORC have been conducted actively, since the early 1970's. There have been lots of studies about the ORC applied to low-grade heat sources below 100°C.

Hung et al. [7] analyzed parametrically and compared the efficiencies of the basic ORCs using benzene, ammonia, R11, R12, R134a and R113 as working fluids. The range of evaporation temperature of this study was from 67°C to 287°C and the targeted application was waste heat recovery. They investigated only comparison of first law efficiencies of water and few organic fluids by numerical method.

Maizza et al. [10] investigated the ORCs with one regenerator using R123, R124 as working fluids in realistic operating conditions. The range of vaporization temperature was from 80°C to 110°C and the condensing temperature ranged from 35°C to 60°C. They analyzed the relation of first law efficiencies and some key parameters (e.g. vaporization temperature, condensing temperature) by numerical analysis.

Dai et al. [11] conducted thermodynamic analysis about the effects of parameters on the performance of the ORCs for waste heat recovery systems. Parameter optimizations of the systems with one regenerator were performed with different working fluids (e.g. water and few organic fluids) using a genetic

algorithm. They analyzed and compared the net power outputs of the performance of the ORCs. The evaporating temperature ranged from 80°C to 140°C and condensing temperature was 20°C.

Borsukiewicz-Gozdur et al. [12] conducted the concise survey of simulation of the low-temperature Clasius-Rankine cycle and targeted application was geothermal power station. The range of temperature of heat source was from 80°C to 115°C. They analyzed the possibility of application of different working fluids, both natural and synthetic. The cycle configuration of this study was the basic cycle consisting of pump, evaporator, expander and condenser.

Madhawa et al. [13] conducted the numerical analysis in order to find the cost-effective optimum design criteria for ORCs utilizing low-temperature geothermal heat sources. The cycle configuration was the basic cycle and the temperature of heat source was from 70°C to 90°C. They used the steepest descent method to find the optimum design conditions.

Lemort et al. [14] conducted the experiments to test the performance of the hermetic scroll expander using R245fa as working fluid. The system configuration was the gas cycle operating on vapor region in the whole states. The supply temperature and pressure of expander were 92°C, 12.61 bar, respectively and the range of pressure ratio of expander was from 2.0 to 10.0.

Yue et al. [15] fabricated the low temperature heat recovery ORC system using R245fa and a single-stage axial flow turbine. The cycle configuration was the basic Rankine cycle the range of evaporating and condensing temperature was from 50°C to 100°C and from 20°C to 70°C, respectively. The maximum efficiency of the system was 7.22% and the turbine isentropic efficiency was 56.4%.

Zhao et al. [16] focused on the performance of the hybrid power system consisting of the ORC and Proton Exchange Membrane Fuel Cell (PEMFC). All of the performance analyses of the ORC and Proton Exchange Membrane Fuel Cell were conducted by numerical method. The ORC system configuration was the basic Rankine cycle and used R245fa, R245ca, R236fa, R123 and Isobutane as working fluid. They investigated the effects of some key parameters such as fuel flow rate, fuel cell operating pressure, turbine inlet pressure and turbine back pressure.

Likewise, the previous studies were mainly focused on the selecting appropriate working fluids and numerical method. Therefore, it is necessary to conduct experiments applied to low-grade heat sources below 100°C, in order to provide meaningful experimental data to other researches.

1.4 Motivation and Objective of the Study

Until now, so many researches about the ORC applied to low temperature heat sources have been conducted. However, in the previous studies and commercialization of the ORC, the types of heat sources were mainly geothermal heat, solar heat, biomass combustion waste heat whose temperatures are over 100°C. Although waste heat below 100°C generated from industrial process, engine and fuel cell has a large portion of overall waste heat, it hasn't sufficiently utilized for waste heat recovery. Furthermore, the researches investigating the ORC applied to low temperature heat source below 100°C have been mainly conducted by numerical analysis.

Although the ORC has been investigated actively since 1970's, it hasn't been applied widely until today's growing concern about the declining fossil fuel production and the global climate change. Due to its lower operating temperature than that of the conventional steam Rankine cycle, the ORC can be suitable to recover waste heat from various heat sources. The numerous ORC power plants have already been demonstrated worldwide by the ORC manufacturers and installers. Furthermore, although many companies have recorded data of their machines, there is a lack of exact data to analyze the characteristics and performance of each application. Most of these power plants have also been applied to geothermal heat, solar heat, biomass combustion

waste heat whose temperatures are over 100°C.

In recent, the hybrid power system consisting of the PEMFC and the ORC has been spotlighted as waste heat recovery technology. In order to maintain 60~80°C of the optimal operating temperature of stack, thermal management system is used for only eliminating heat generation of stack where chemical reactions occur. On the other hands, as shown in Fig. 1.2, for using waste heat from stack to produce additional work, the ORC is connected with heat exchanger of thermal management system in the hybrid power system. However, there are only a few studies to investigate this technology by numerical method.

In addition, waste heat generated from industrial process such as steam drying, refrigeration, freezing, sterilization, etc. of food and beverage industry is estimated at 33 TWh, 30% of global waste heat [17]. Low level of temperature (less than 80°C) waste heat has the 54% of total waste heat generated from food and beverage industry. However, although available waste heat below 100°C from industrial process has a large portion of global waste heat, it is hard to find trials to recover waste heat to generate additional power.

Therefore, in this respect, experimental research of the ORC applied to heat sources below 100°C has high usefulness and originality. In this study, the effects of some key parameters (e.g. evaporating pressure, condensing pressure,

mass flow rate, pressure ratio, etc.) and the optimal operating condition which had the maximum generating work were investigated by experiments.

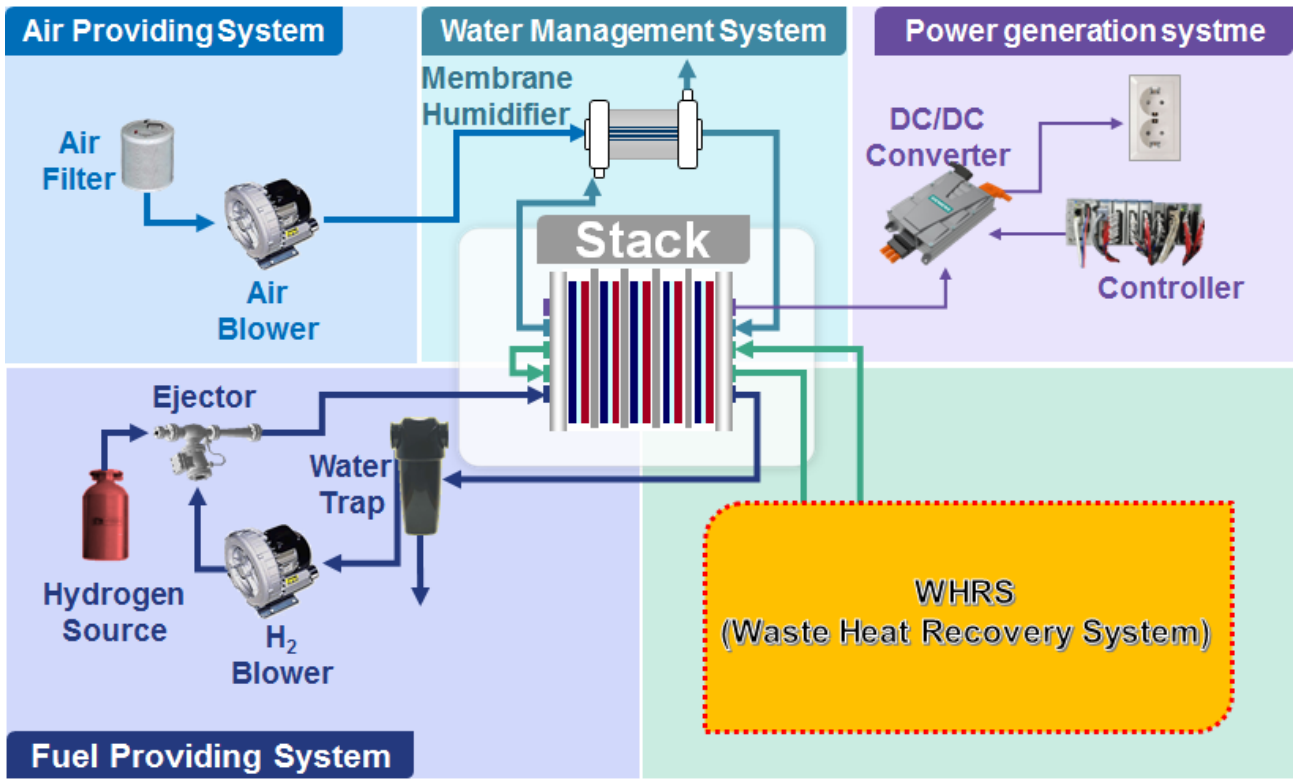

Fig. 1.2 Schematic diagram of PEMFC-ORC hybrid power system

Chapter 2. Experimental Setup and Measurements

2.1 Selection of the Working Fluid

2.1.1 Cycle Analysis

In the ORC researches, the selection of the working fluid is the most important thing to determine the performance of the overall system. Because the working fluid can affect the efficiency of the system, sizes of components, system stability, cost of maintenance and so on. Therefore, in order to find the appropriate working fluid to our experimental system, the working fluid candidates, which were expected to be suitable to the targeted temperature range of heat source, were selected. These candidates were R123, R141b, R245ca and R245fa. According to the previous numerical studies, these fluids were recommended as the most appropriate ones in 50~80^{o}C of evaporating temperature and 25^{o}C of condensing temperature [16, 18]. As shown in Fig. 2.1, the analyzed cycle consisted of pump, evaporator, expander and condenser. Pump and expander's simulation were conducted simply by using the fixed isentropic efficiency. Heat exchangers' modeling was performed by utilizing several heat transfer correlations. The detailed information of the used heat

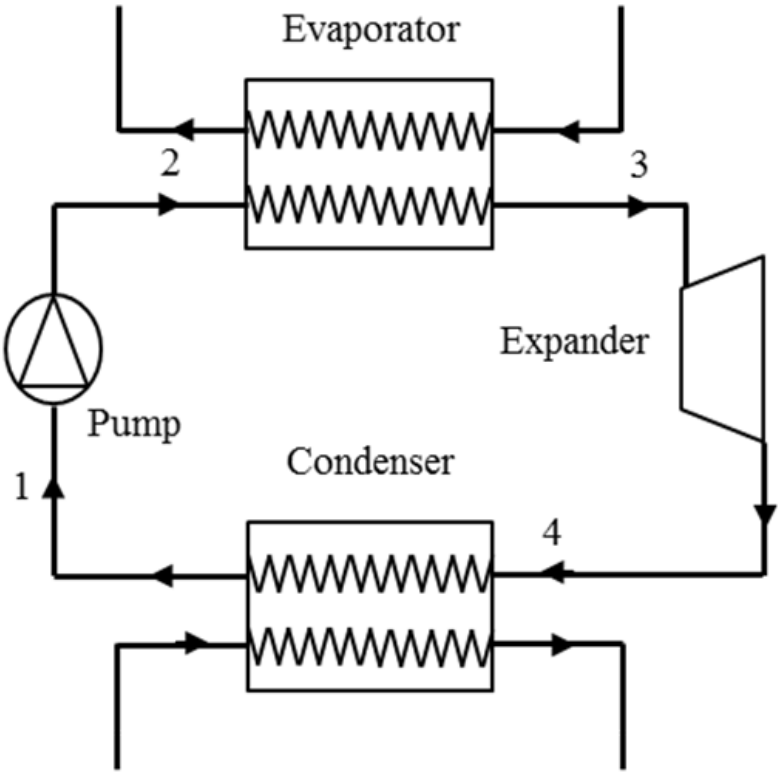

Fig. 2.1 Schematic diagram of the basic organic Rankine cycle

transfer correlations are shown as below:

Single phase region: Dittus-Boelter correlation (1930)

$$\frac{h_r D_h}{k} = 0.023\,\mathrm{Re}^{0.8}\,\mathrm{Pr}^{n}$$

Two phase region in condenser: Chen correlation (1987)

$$\frac{h_r D_h}{k} = 0.018\left(\frac{\mu_v}{\mu_l}\right)^{0.078}\left(\frac{\rho_v}{\rho_l}\right)^{0.39}\mathrm{Re}_l^{0.2}\left(\mathrm{Re}_{lo}-\mathrm{Re}_l\right)^{0.7}\mathrm{Pr}_l^{0.65}$$

Two phase region in evaporator: Gungor-Winterton correlation (1987)

$$h_{tp} = Eh_{sp}$$

$$h_{sp} = \frac{0.023k\,\mathrm{Re}^{0.8}\,\mathrm{Pr}^{0.3}}{D_h}$$

$$E = 1 + 3000Bo^{0.86} + 1.12\left(\frac{x}{1-x}\right)^{0.75}\left(\frac{\rho_l}{\rho_v}\right)^{0.41}$$

$$Bo = \frac{q''}{h_{fg}G}$$

The detailed values of numerical conditions were shown in Table 2.1. In order to reasonably verify and compare the performance of the ORC using each working fluid, the waste heat amount, evaporating temperature and condensing temperature. Because it was important to verify the performance of each case

applied to the same heat source and heat sink. In addition, the evaluation of the pumping and expansion process was conducted by basic thermodynamic concept. All of pumps or expanders were calculated by the same isentropic efficiencies 75%, 60%, respectively. These isentropic efficiencies used by most of the previous analytic researches were used. It assumed that the DSH of inlet/outlet of expander and the DSC of inlet of pump were set to zero. The properties of refrigerants were used from NIST Refprop ver. 9.1 [19].

Table 2.1 Numerical conditions of the cycle analysis

Parameter	Unit	Value
Waste heat amount	kW	5
Evaporating temperature	°C	50 ~ 75
Condensing temperature	°C	25
Isentropic efficiency of pump	%	75
Isentropic efficiency of expander	%	60

2.1.2 Result and Discussion of Cycle Analysis

Fig 2.2 represents the thermal efficiency with different working fluids and evaporating temperature at the same condensing temperature. For all of the working fluids, the thermal efficiencies elevate as the evaporating temperature increases. The reason is that with the increase of pressure difference of evaporator and condenser, the enthalpy difference of the expander elevates. In the given range of evaporating temperature, the minimum thermal efficiency is about 3.5% and the maximum thermal efficiency is about 7.0%. In addition, Result shows that R141b has the highest thermal efficiency and R245fa has a little lower thermal efficiency than that of others. The thermal efficiency difference between R141b and R245fa increases as the evaporating temperature increases. However, this thermal efficiency difference is from 0.1% to 0.5% and it isn't very large.

In this study, although R245fa shows a little lower thermal efficiency than that of others, R245fa was selected as the most appropriate working fluid to our experiment. Because R123 and R141b are classified HCFC refrigerant and the use of HCFC refrigerant was already restricted or will be prohibited by environmental regulations. Furthermore, although R245ca has a good thermodynamic performance and eco-friendly characteristics, it has relatively high flammability.

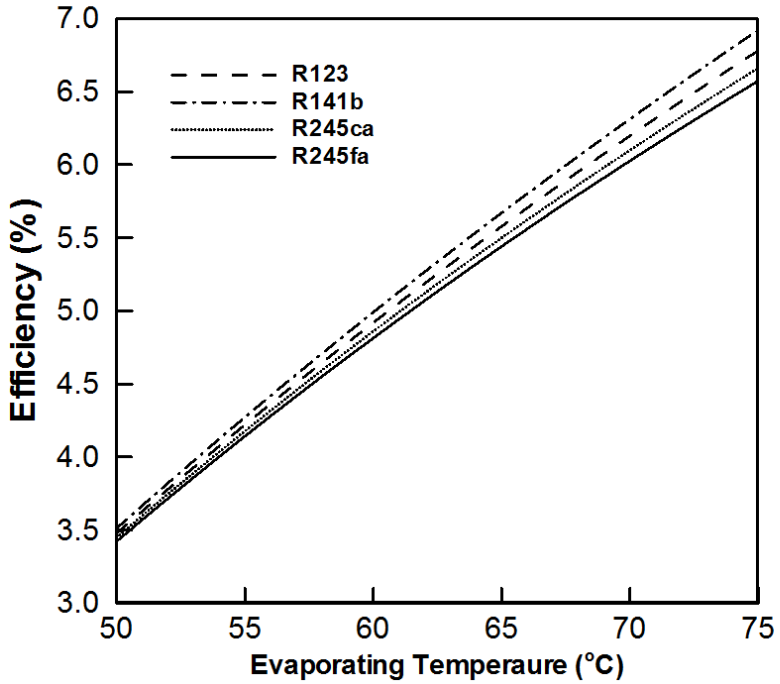

Fig. 2.2 Thermal efficiency variation with various working fluids and evaporating temperature at 25°C of condensing temperature

2.2 Experimental System

The experimental apparatus was fabricated to investigate the ORC applied to low temperature heat source below 100°C. In Fig. 2.3, the schematic diagram of the experimental system are shown. This experimental system consists of gear refrigerant pump, evaporator, scroll expander and condenser as basic Rankine cycle. To supply lubricant to expander, oil ejector and oil separator are built in this system. For preventing cavitation of inlet of pump, customized liquid receiver is used. In addition, in order to measure various parameters of experimental conditions and results such as temperature, pressure, mass flow rate, frictional torque of expander shaft, rotational speed of expander and so on, the appropriate instruments are fabricated. The system consists of one closed loop for R245fa and two closed loop for heating and cooling waters. In order to control temperature and mass flow rate of heating and cooling waters, circulation cycle consisting of water pump, mass flow meter, water tank and electric heater.

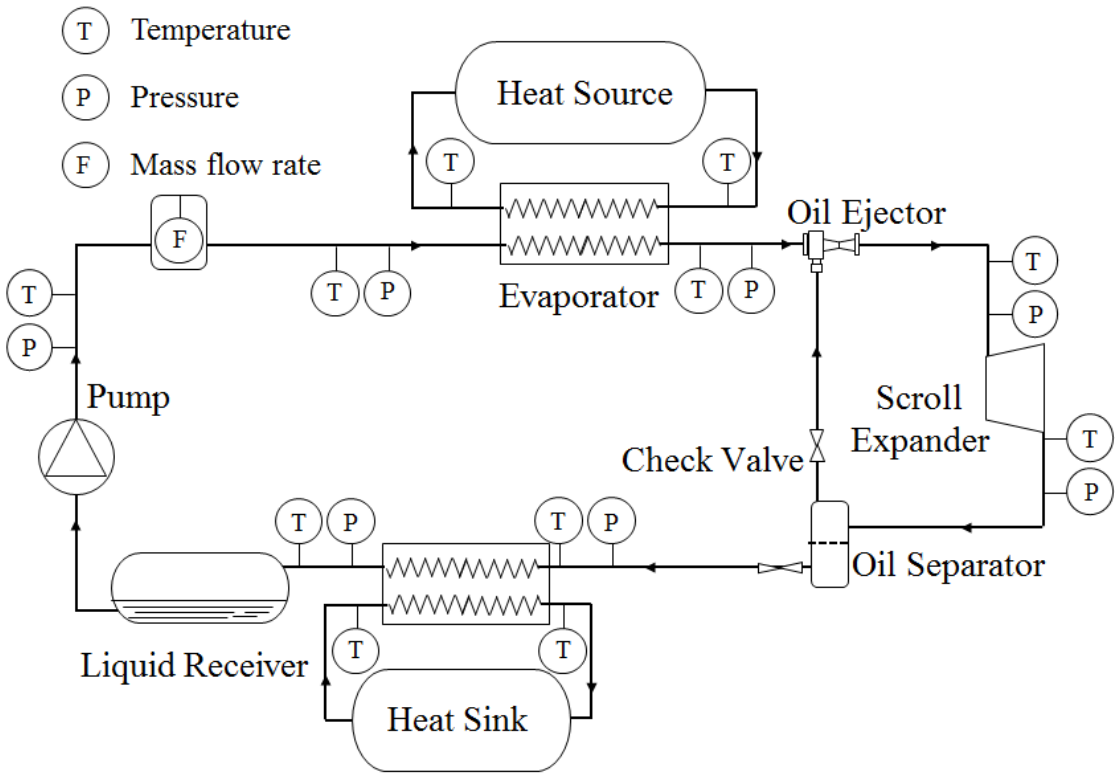

Fig. 2.3 Schematic diagram of the organic Rankine cycle experimental system

2.2.1 Gear Pump

In the ORC power generating system, the selecting of the working fluid pump is also very important. Especially, in small scale systems, pump selection is somewhat difficult owing to unusual operating conditions and sensitivity to surroundings [20]. Generally, centrifugal pumps are improper to operate in this situation.

Therefore, gear pumps, which are positive displacement types, was selected as the most appropriate type of pump due to its ability to stably supply working fluid in low flow rate. In addition, the selecting of the gear pump should be conducted by intensive consideration including leakage losses and friction losses. Considering all of these aspect, the T series refrigerant gear pump made by the Tuthill Company was selected as shown in Fig. 2.4. This gear pump is magnetically coupled to 0.75 kW, 3-phase 380 V motor. Other characteristics of the gear pump are provided in Table 2.2.

Fig. 2.4 Photograph of Tuthill T series gear pump

Table 2.2 Specifications of the gear pump

Parameter	Value
Flow rates	20 ~ 650 GPH
Temperatures	-46 ~ 176ºC
Differential pressures	17.2 bar
Rotational speed	5,000 RPM maximum
Magnet torque	240 ~ 460 in-oz
Metal wetted parts	316 stainless steel, Titanium or Hastelloy C276

2.2.2 Scroll Expander

The scroll expander has the fixed volumetric ratio due to positive displacement machine. When the system pressure ratio doesn't match the optimal pressure ratio corresponding to the fixed volumetric ration of the expander, under or over expansion losses can occur. These two losses can affect considerably the performance of the expander. However, the turbomachines are usually more suitable to high expansion ratio and the piston expanders are more appropriate for operating conditions with large pressure ratio due to their designs optimized for higher internal built-in volumetric ratios [21].

Therefore, the scroll type expander was selected as the most appropriate option to our experimental conditions. Because the pressure ratio between high and low saturation pressures corresponding to expected evaporating and condensing pressure was relatively low. In this research, as shown in Fig. 2.5, the scroll expander, whose rotor was divided from scroll type vapor compressor (Copeland, ZF09K4E-TFD-550), was manufactured for making the scroll rotor to run in reverse. Its specific geometrical data of the scroll expander is shown in Table 2.3.

Fig. 2.5 Photographs of scroll rotor and scroll expander

Table 2.3 Geometrical information of the scroll expander

Parameter	Value
Built-in volumetric ratio	3.1
Basic circle radius	2.1 mm
Wrap height	29.1 mm
Pitch	13.2 mm
Wall thickness	3.3 mm
Suction volume	10.1 cm^3 rev^{-1}

2.2.3 Heat Exchangers

For evaporator and condenser, the plate type heat exchangers were used in experimental system. In order to maximize the heat transfer amount, the directions of the working fluids and the secondary fluids (e.g. heating and cooling water) were made of counter-flow, where the most efficient heat transfer occurs in the available temperature difference.

For evaporator, considering the expected heat addition from heat source and sufficient safety coefficient, the capacity of evaporator was set to 5 RT. Furthermore, in the ORC power system, it is more difficult to reject heat to heat sink in condenser. Therefore, although the heat transfer amount of condenser is smaller than that of evaporator, the capacity of condenser was set to 5 RT. These drawing sheet representing geometrical data is shown in Fig. 2.6.

In this study, in order to replicate heat source and heat sink, water was selected as the secondary fluid of evaporator and condenser. The heating water (i.e. the secondary fluid in evaporator) in evaporator was supplied by the thermostat having 10 kW of heat capacity. The cooling water having constant mass flow rate and temperature was supplied by water pumps, 7.5 RT chiller, heat exchanger, water tank, electric heater and mass flow meter.

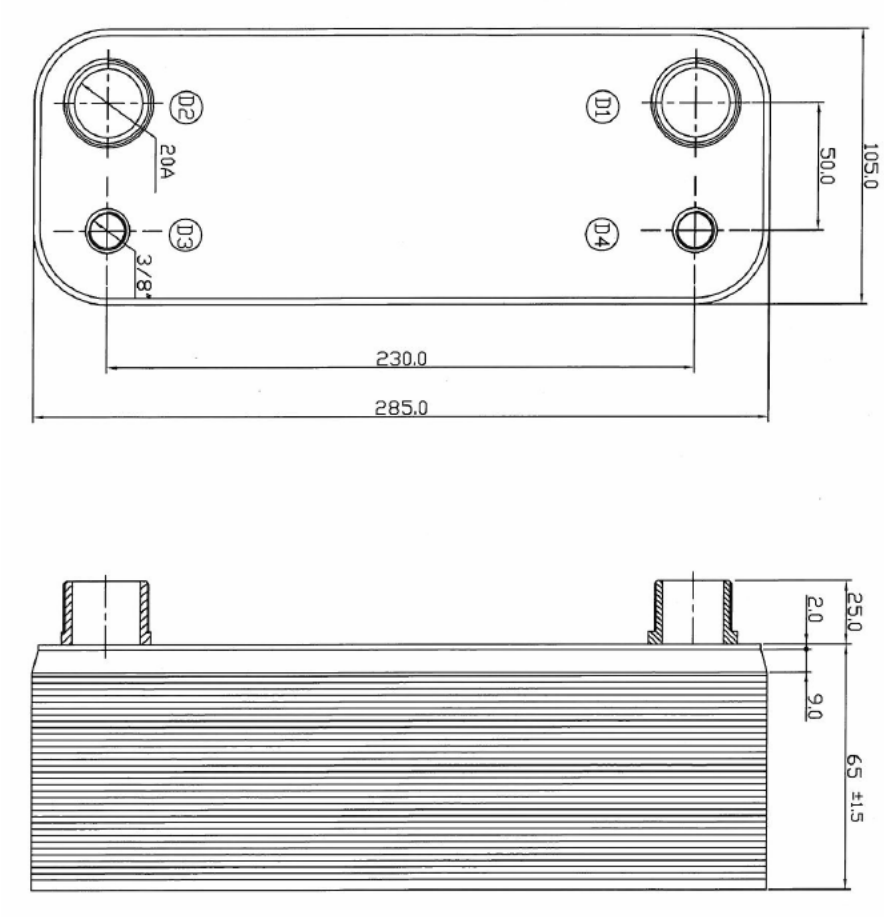

Fig. 2.6 Drawing sheet of evaporator and condenser

2.2.4 Auxiliary Components and Measurements

Oil supplying sub cycle

In order to lubricate the expander, oil supplying sub cycle consisting of oil ejector and oil separator was installed around the expander. By using ventri effect of the oil ejector located in inlet of the expander, the expander could be lubricated sufficiently. The oil ejector was manufactured by Heatech Korea Company. In outlet of the expander, oil passing thorough the expander could be recovered to the oil separator. Considering the capacity of expander, A-W 55877 made by Emerson Company was selected as the proper oil separator. Emkarate RL 100H (POE) was used as the lubricant oil.

Liquid receiver

The liquid receiver was built in inlet of the pump, in order to function as the buffer for refrigerant charge and maintain stable liquid state to prevent cavitation. In this way, it was possible to protect the system from being sensitive to the operating condition changes and the transient load. The liquid receiver was made of a stainless steel and the volume of this component was about 5 L, which was much larger than that of expected system capacity by considering the maximum volume flow rate and the properties of the working fluid in the

targeted operating conditions.

Dynamometer

To measure the frictional torque and the rotational speed of the expander, the expander was coupled with the dynamometer consisting of the torque transducer (SETech, YDNR–1K), RPM meter (Ono Sokki, MP–981) and hysteresis brake (MAGTROL, AHB-5). By using dynamometer, the generating work of the expander could be calculated by the frictional torque and the rotational speed. As shown in Table 2.4, the specific information of these instruments are represented.

Temperature measurement

Temperatures on the pump, evaporator, scroll expander, condenser and the secondary fluid were measured with T-type copper-constantan thermocouple made by the Omega Engineering.

Pressure measurement

Absolute and gauge pressure transducers were installed to acquire pressure data on the experimental system. By the gauge pressure meters (Wikai, A-10), pressures of inlet and outlet of each component could be measured. In addition,

in order to raise the accuracy of pressure data from the gauge pressure transducers, it was calibrated by the absolute pressure meter (DRUCK, PMP 1400). The characteristics of these measurements are provided in Table 2.5.

Mass flow rate measurement

In this experimental system, working fluid mass flow rate was measured with the Bronkhorst's Coriolis type mass flow rate transducer (Bronkhorst, M5X CORI-FLOW) located in outlet of the pump. Heating and cooling water mass flow rate were controlled by using the bypass circuit and were also measured by Coriolis type mass flow rate meters (Oval, CN025C-SS-322K). The specific information of these instruments is represented in Table 2.5.

Consumption work measurement and data collection

The consumption work of the pump was measured with the power meter (Yokogawa, WT-130). The data acquisition instrument (National Instruments, cDAQ-9174) receiving all of output signal from thermocouples, pressure transducers and other measurements was installed. The specifications of these components are shown in Table 2.5.

Table 2.4 Specifications of the dynamometer

Torque transducer (SETech, YDNR-1K)	
Rated capacity	0 ~ 9.807 N m
Rated Output	1.3 mV/V ± 1%
Temperature operating	0 ~ 80°C
RPM meter (Ono Sokki, MP-981)	
Measurement range	1 ~ 20 kHz (1 ~ 20,000 RPM)
Power supply used	DC 12 V ± 2 V
Current consumption	~ 40 mA
Operating temperature range	-10 ~ 70°C
Hysteresis brake (MAGTROL, AHB-5)	
Minimum torque at rated current	5.00 N m
Rated current	380 mA
Maximum rotational speed	15,000 RPM
Rated kinetic power	1,000 W (continuous, with air) 120 W (continuous, without air)

Table 2.5 Specifications of the other measurements

Gauge pressure transducer (Wikai, A-10)	
Measurement range	0 ~ 16 bar
Signal output	4 ~ 20 mA
Accuracy	± 0.l%
Absolute pressure meter (DRUCK, PMP 1400)	
Measurement range	0 ~ 100 bar
Accuracy	± 0.15%
Mass flow rate transducer (Bronkhorst, M5X CORI-FLOW)	
Maximum mass flow rate	600 kg h^{-1}
Minimum mass flow rate	20 kg h^{-1} (liquid) 50 kg h^{-1} (gas)
Accuracy	± 0.2% (liquid) ± 0.5% (gas)
Power meter (Yokogawa, WT-130)	
Measurement range	0 ~ 600 V, 0 ~ 300 A
Accuracy	± 0.2% (voltage) ± 0.3% (current)

Chapter 3. Experimental Results and Discussions

3.1 Experimental Procedure and Conditions

3.1.1 Data Reduction

The heat rate of evaporator and condenser can be evaluated from mass flow rate, the temperature difference and specific heat of the secondary fluids (i.e. water) of heat exchangers. Also, it can be calculated from mass flow rate and the enthalpy difference. Because of stable values and fast response according to changing experimental conditions, it is most reliable to evaluate heat rate from the properties of the secondary fluids. The specific heat and the enthalpy difference of water are calculated based on the measured temperature and pressure by using NIST Refprop ver. 9.1 [19] and the heat rate of heat exchangers is defined as below.

$$\dot{Q}_{eva} = \dot{m}_{w,eva} \cdot C_{p,w} \cdot (T_{in,w} - T_{out,w}) = \dot{m}_{w,eva} \cdot (h_{in,w} - h_{out,w})$$

$$\dot{Q}_{cond} = \dot{m}_{w,cond} \cdot C_{p,w} \cdot (T_{out,w} - T_{in,w}) = \dot{m}_{w,cond} \cdot (h_{out,w} - h_{in,w})$$

The generating work of the expander can be calculated from the frictional torque and the rotational speed of the expander shaft. These values are evaluated based on measured frictional torque and rotational speed by using dynamometer consisting of frictional torque transducer, RPM sensor and hysteresis brake. The equation of the generating work of the expander are shown as below.

$$\dot{W}_{\exp} = 2 \cdot \pi \cdot T_f \cdot RPM_{\exp} / 60$$

The thermal efficiency of the overall system is the ratio between heat input of evaporator and net power of the overall system. The consumption work of the pump was measured by power meter.

$$\eta_{th} = \frac{\dot{W}_{\exp} - \dot{W}_{pump}}{\dot{Q}_{eva}}$$

The degree of super heat (DSH) is defined as the difference of the super-heated vapor's temperature and the saturation temperature corresponding the actual pressure. Likewise, the degree of sub cool (DSC) is also calculated from the difference between sub-cooled liquid's temperature and the saturation

temperature. In this study, DSH of the inlet and outlet of the expander and DSC of the inlet of the pump were calculated from measured temperature and pressure by using NIST Refprop ver. 9.1 [19].

$$DSH = T_{superheat} - T_{sat}$$

$$DSC = T_{sat} - T_{subcool}$$

By the exergy analysis, it is possible to investigate how close the actual performance approaches to the ideal process and the causes of thermodynamic losses. The exergy destruction of each component can be calculated by using the exergy balance of the system at the steady state. The equations of the exergy analysis are defined as below.

$$\dot{E} = \dot{m} \cdot \{h - h_0 - T_0 \cdot (s - s_0)\}$$

$$D_{eva} = (\dot{E}_{in,h,w} - \dot{E}_{out,h,w}) - (\dot{E}_{out,r,eva} - \dot{E}_{in,r,eva})$$

$$D_{cond} = (\dot{E}_{in,c,w} - \dot{E}_{out,c,w}) - (\dot{E}_{out,r,cond} - \dot{E}_{in,r,cond})$$

$$D_{exp} = (\dot{E}_{in,exp} - \dot{E}_{out,exp}) - \dot{W}_{exp}$$

$$D_{pump} = (\dot{E}_{in,pump} - \dot{E}_{out,pump}) + \dot{W}_{pump}$$

$$\eta_{exg} = \frac{\dot{W}_{\exp} - \dot{W}_{pump}}{\dot{E}_{in,h,w} - \dot{E}_{out,h,w}}$$

3.1.2 Experimental Conditions

In this study, the ORC applied to low temperature heat source below 100°C (e.g. waste heat of PEMFC, waste heat of beverage/food industry and so on) was investigated. The range of these waste heat temperature is usually from 60°C to 80°C. Therefore, in order to replicate these low-grade heat source, the inlet temperature of the secondary fluid of evaporator was set to 70°C. To make experimental system to operate stably, the inlet temperature of water of condenser was set to 15°C, which is a little lower than ordinary temperature (i.e. 20°C). Waster was selected as the secondary fluid of evaporator and condenser.

Furthermore, varying refrigerant charge amount of the overall system, preliminary experiments were conducted for finding the optimal charge amount where the maximum generating work occurred. When thermodynamic cycle produces work from heat reservoirs with infinite heat capacity, it is most important to generate the maximum work with low-grade heat source [22]. Fig. 3.1 shows generating work of the expander with respect to refrigerant charge amount. As a result, 8.50 kg was selected as the optimal charge amount.

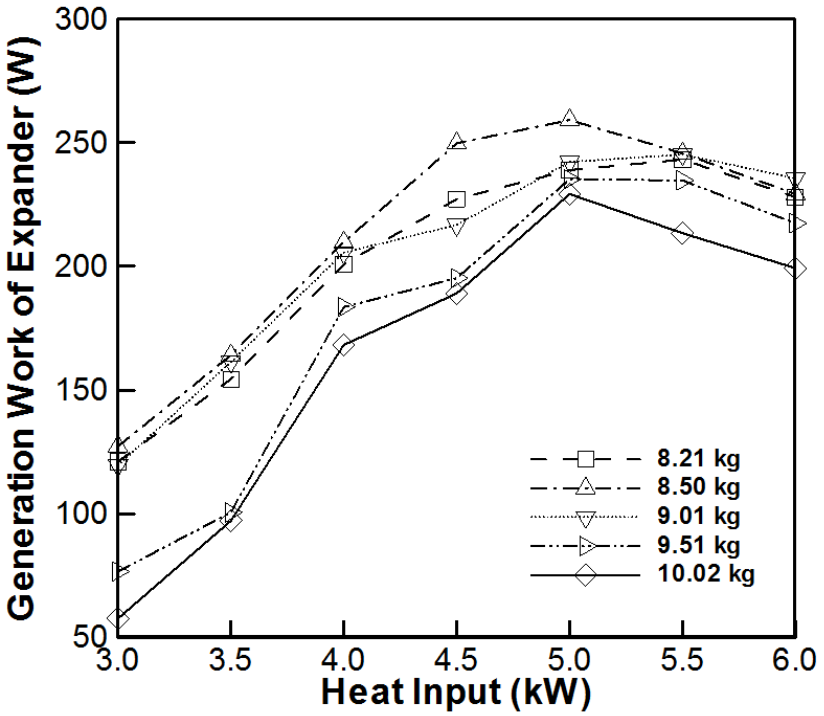

Fig. 3.1 Generating work of the expander with regard to heat input (i.e. heat rate of evaporator) varying refrigerant charge amount

Other experimental parameters were the same values shown in Table 3.1. The experiments were conducted with varying the rotational speed of the gear pump. At the same rotational speed of the pump, increasing the frictional load of the expander shaft by using dynamometer, the performance of the experimental system was investigated.

Table 3.1 Experimental conditions

Parameter	Unit	Value
Inlet temperature of water in evaporator	^{o}C	70
Mass flow rate of water in evaporator	g/s	121.67
Inlet temperature of water in condenser	^{o}C	15
Mass flow rate of water in condenser	g/s	300
Pump frequency	Hz	20~34
Refrigerant charge amount	kg	8.50

3.2 Performance of the Gear Pump

In this study, T-series gear pump made by Tuthill Company was used as the refrigerant pump. This gear pump had been usually used for supplying the lubricant oil or the conventional refrigerant. Therefore, it was necessary to investigate the performance of the gear pump using R245fa as the working fluid. For these objectives, varying the frictional load of the expander, the performance variation with regard to pressure ratio and mass flow rate in the various rotational speed of the gear pump.

Fig. 3.2 shows mass flow rate of the gear pump with regard to pressure ratio and pump frequency. Like the performance of the general pump, the mass flow rate becomes smaller according to pressure ratio is enlarged. In addition, at the same pressure ratio, as the frequency of the pump increases, the mass flow rate increases. Overall, increasing the pump frequency, both of pressure ratio and mass flow rate were enlarged. The mass flow rate ranged from 11 g/s to 35 g/s and the range of the discharge pressure was from 2.8 bar to 4.6 bar. Furthermore, due to lower kinetic viscosity than that of the conventional fluids used to gear pump, the slope of declining mass flow rate with increasing pressure ratio was larger than that of the traditional ones.

The specific pumping work with regard to pressure ratio and pump frequency is presented in Fig. 3.3. The most dominant tendency is that as

pressure ratio increases, the specific consumption work of the pump is enlarged sharply. However, in relatively large pump frequency, the changing aspect of the specific work is alleviated slightly. The maximum specific work of the pump is 5.35 kJ/kg and the minimum specific work is 1.61 kJ/kg.

Fig. 3.4 shows the experimental results of the consumption work of the gear pump with various mass flow rate and pressure ratio. It is confirmed that the pumping work of the system is determined by pressure ratio in relatively low pressure ratio (i.e. less than 2.8). In other words, as the mass flow rate increases, the consumption work of the pump is almost constant. The maximum consumption work of the pump is 130 W and the minimum work is 50 W. Furthermore, the DSC of the inlet of the gear pump was maintained at 7~8^{o}C and the isentropic efficiency of the pump was estimated at 10~20%.

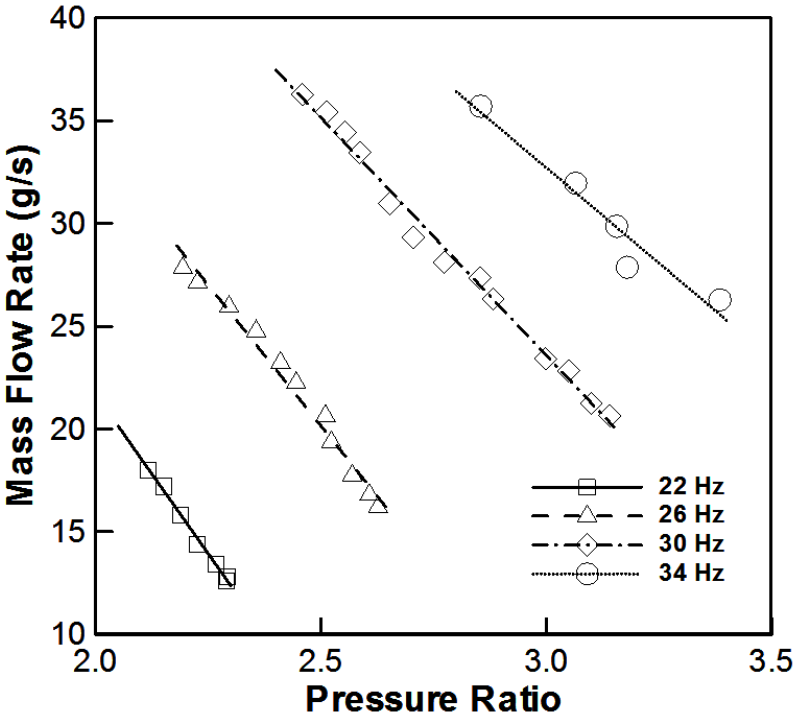

Fig. 3.2 Mass flow rate of the pump
with respect to pressure ratio varying pump frequency

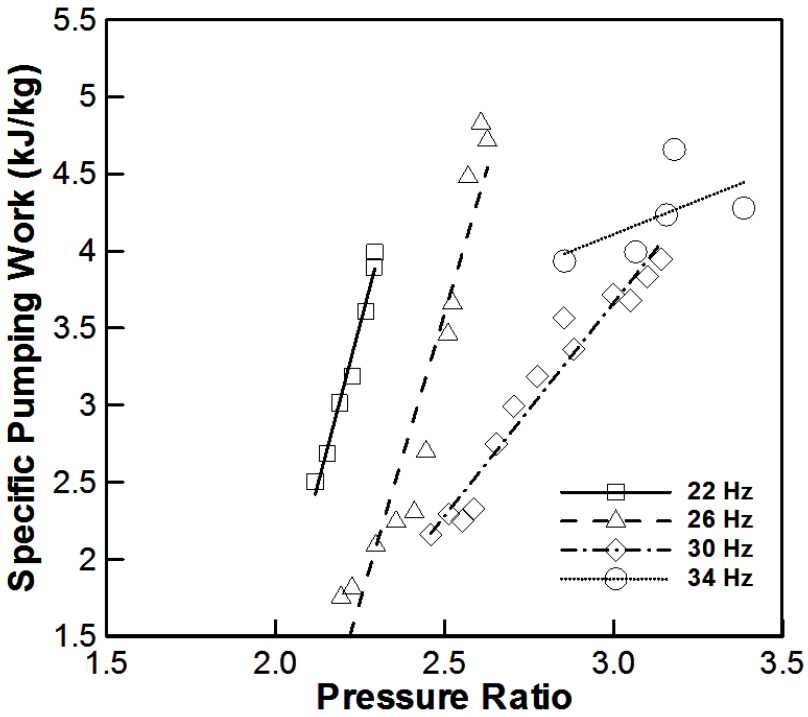

Fig. 3.3 Specific pumping work variation with pressure ratio and pump frequency

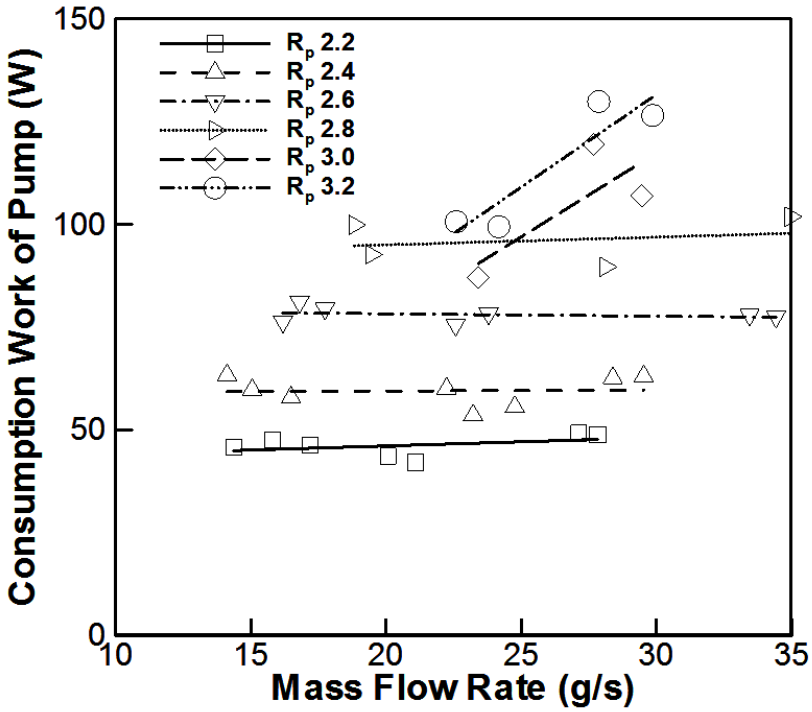

Fig. 3.4 Consumption work of the pump
with regard to mass flow rate and pressure ratio

3.3 Performance of the Scroll Expander

In this study, we produced the scroll expander with scroll rotor divided from vapor scroll compressor, which was used for refrigeration system. Because there hasn't been experimental study about expander applied to low-grade heat source below 70°C and 6 kW, it was essential to make a close investigation of the performance of the scroll expander. By utilizing dynamometer coupled to the expander shaft, we changed the frictional load on the expander and measured the frictional torque and the rotational speed of the expander. Then, the generating work of the expander was calculated by these measured values. In this way, the performance of the expander was examined in the 1000 RPM to 3800 RPM range on the rotational speed of expander.

Fig. 3.5 shows the generating work of the expander with various pressure ratio and the rotational speed of the expander. Generally, it is confirmed that the generating work of the expander is enlarged according to pressure ratio increases. At the same pressure ratio, the general tendency is that as the rotational speed of the expander, the generating work of the expander is elevated. The maximum generating work of the expander is about 360 W at 2400 RPM and pressure ratio 2.6.

These phenomena can be explained by experimental data shown in Fig. 3.6. This picture shows the relation between the rotational speed and frictional

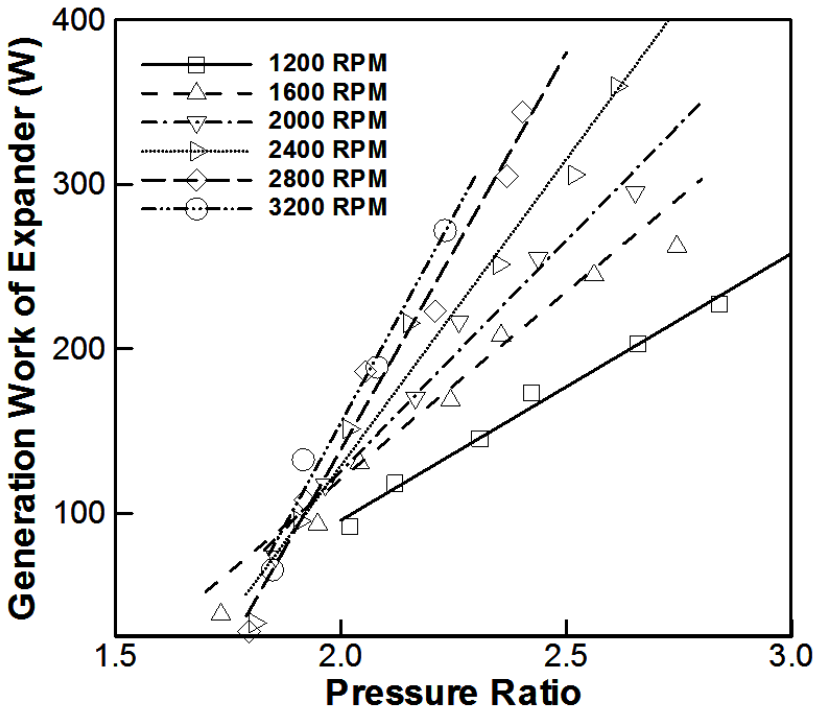

Fig. 3.5 Generating work of the expander with regard to pressure ratio varying rotational speed of the expander

torque of the expander with varying expansion ratio. Generally, as the rotational speed increases, the frictional torque tends to decline slightly. Although, because the generating work of the expander was calculated by multiplying these values, it is possible to exhibit inflection point in the performance curve, the generating work of the expander is enlarged according to the rotational speed increases at the same pressure ratio. Since the decreasing ratio of the frictional torque is relatively lower than increasing ration of the rotational speed.

The results of the generating work of the expander variation with respect to various mass flow rate and pressure ratio are shown in Fig. 3.7. The most evident changing aspect of the generating work is that as the pressure ratio of the expander increases, the variation of the generating work becomes steeper. In addition, at the same pressure ratio, as the mass flow rate increases, the generating work of the expander also increases. Because the specific generating work of the expander tends to be determined by the expansion ratio. However, in low pressure ratio (i.e. pressure ratio 1.8), changing aspect of the generating work opposed to the general tendency is observed. The generating work of the expander deceases slightly according to the mass flow rate is enlarged.

Fig. 3.8 shows the relation between DSH of the inlet of the expander and the generating work of the expander with various heat inputs (i.e. heat capacity of heat source). As the heat capacity of the heat source is enlarged, the variation

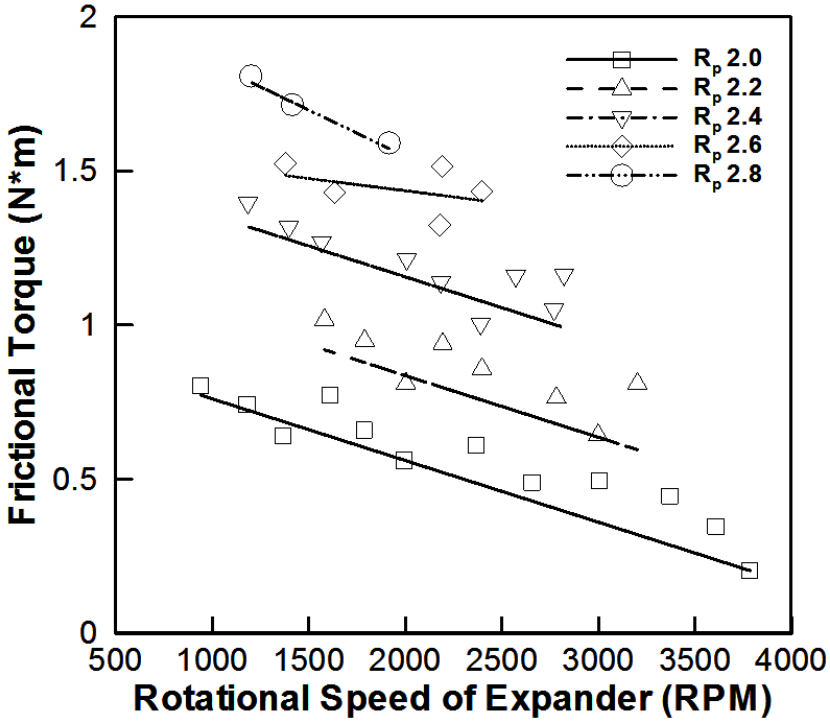

Fig. 3.6 Frictional torque of the expander
with regard to rotational speed and pressure ratio

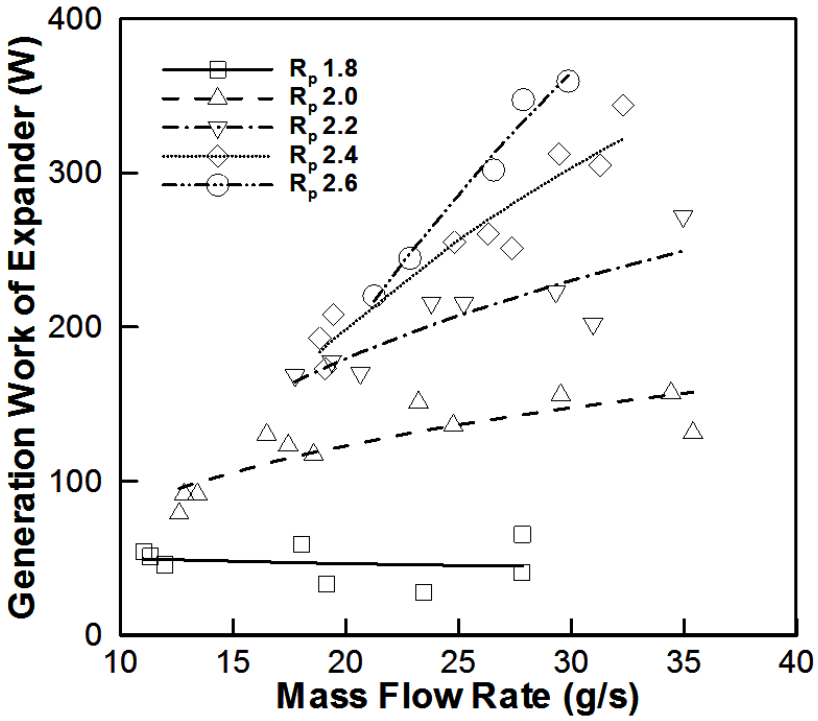

Fig. 3.7 Generating work variation of the expander with mass flow rate and pressure ratio

of the generating work of the expander changes dramatically. In general, it is verified that the lower DSH has the larger generating work of the expander and the small difference of the DSH makes a large change of the generating work.

For the several rotational speed of the expander, we investigated the isentropic efficiency of the expander by using the experimental results and refrigerant properties from NIST Refprop ver. 9.1. Fig. 3.9 shows the variation of the isentropic efficiency of the expander with regard to pressure ratio and rotational speed of the expander. The most significant tendency is that as the pressure ratio increases, the isentropic efficiency becomes large. Especially, in low pressure ratio (less than 2.0), the isentropic efficiency is very low. Which means that mechanical or thermodynamic losses affect considerably the performance of the expander. Because the scroll expander has the optimal pressure ratio corresponding to the fixed built-in volumetric ratio [23]. To be specific, when pressure ratio doesn't match the optimal pressure ratio, over or under expansion losses occur. Furthermore, it is also verified that the higher rotational speed of the expander generally causes the lower isentropic efficiency. Because the higher the rotational speed of the expander, the more the additional losses such as leakage, friction losses and so on [14]. The maximum isentropic efficiency is 68.8% at 2200 RPM and pressure ratio 2.6.

The variation of isentropic efficiency of the expander with various DSH

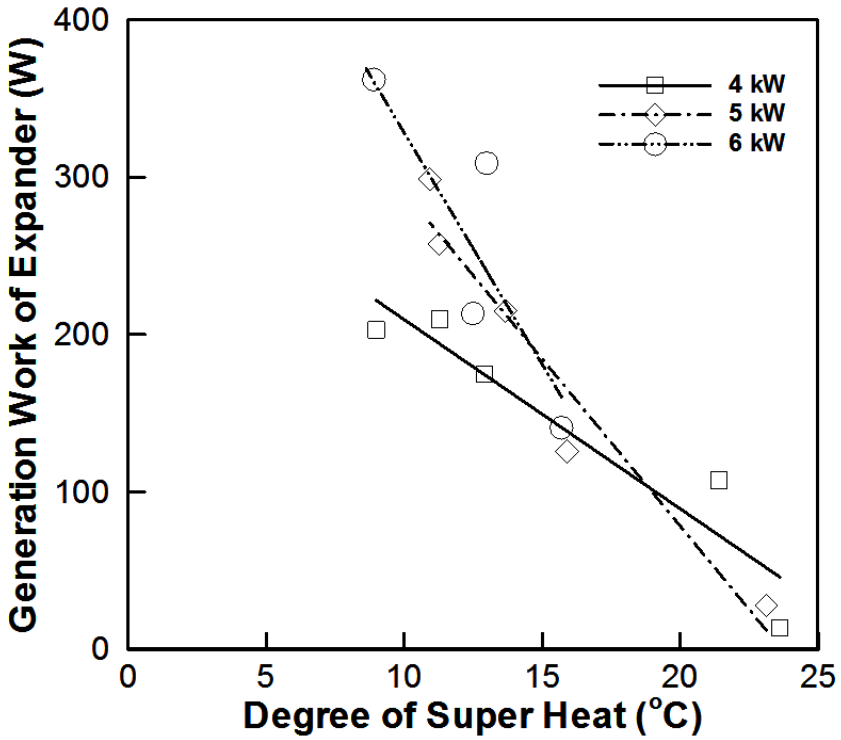

Fig. 3.8 Generating work of the expander with respect to DSH and heat input

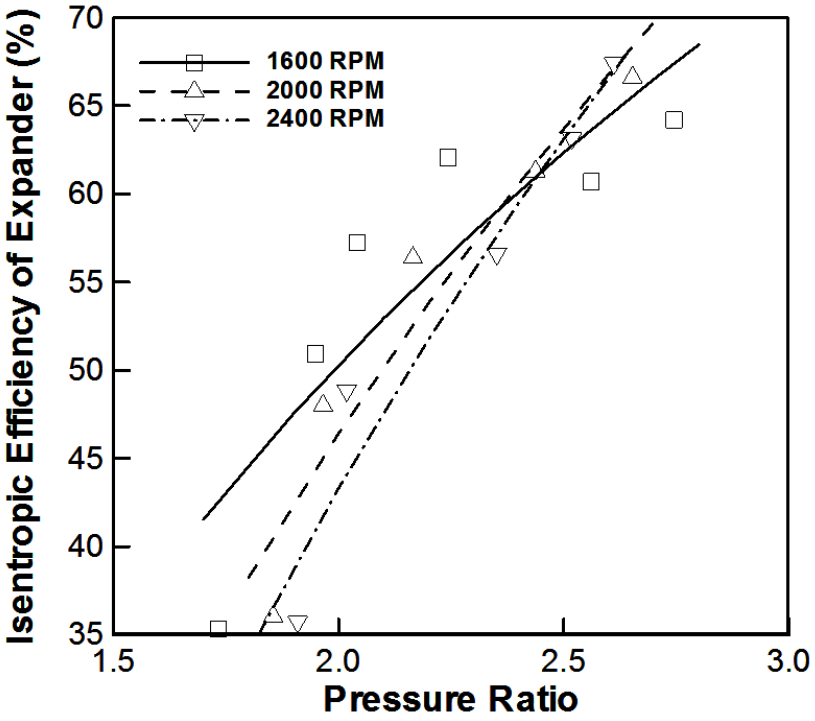

Fig. 3.9 Isentropic efficiency variation of the expander with pressure ratio and rotational speed

and heat inputs is presented in Fig. 3.10. Like the relation of the generating work and DSH, as the heat capacity of the heat source becomes large, the changing aspect of the generating work of the expander occurs significantly. To be specific, it is confirmed that the lower DSH causes efficient operating of the expander and the small difference of the DSH makes a large change of isentropic efficiency of the expander. Therefore, maintaining the low DSH may be significant factor to efficient operating of the expander.

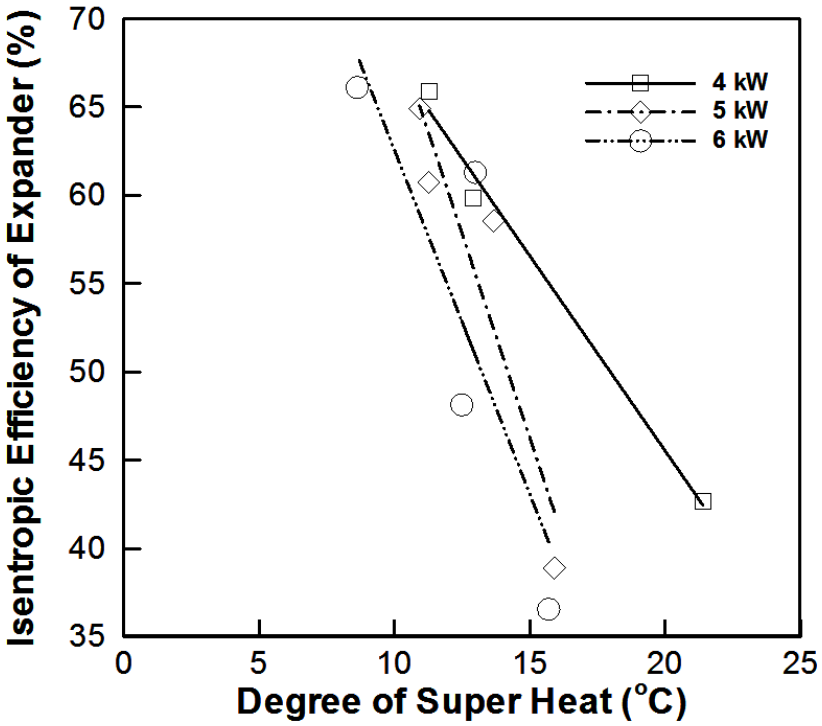

Fig. 3.10 Isentropic efficiency of the expander with respect to DSH and heat input

3.4 Performance of the Overall System

In this part, the performance of the overall system is analyzed by the first and second law of thermodynamics. By using the thermos-physical equations above-mentioned in part 3.1.1, the detailed and complete thermodynamic analysis was conducted.

3.4.1 Energetic Analysis of the Overall System

In all of the thermodynamic cycle studies, the first law analysis is usually the initial basis research viewpoint. The experimental results were investigated, in terms of the effects of some key parameters such as evaporating pressure, condensing pressure, mass flow rate, pump frequency, heat rate of evaporator and so on. These parameters influence the temperature and pressure of the system and the performance of the system is consequently determined by these variables. The performance evaluating factors were mainly the net power and the thermal efficiency of the overall system.

Fig. 3.11 shows the overall system net power with varying evaporating pressure and mass flow rate. Generally, it is verified that as the evaporating pressure increases, the overall system net power tends to be enlarged. In addition, the variations of the net power change more significantly according

to mass flow rate of the system increases. Because as shown in Fig. 3.4 and Fig 3.7, the difference of the consumption work of the pump is usually smaller than that of the generating work of the expander at the same pressure ratio.

The overall system net power variation with various evaporating pressure and pump frequency is presented in Fig. 3.12. The most significant tendency is that the optimal operating condition of each pump frequency exists. Because the generating work curve of the expander exhibits the maximum point which is caused by increase of the frictional torque and decrease of the rotational speed of the expander with respect to elevating evaporating pressure. In addition, in low evaporating pressure region, there are operating conditions which should be avoided to obtain the benefits of operating ORC. The maximum net power is 234.36 W at 34 Hz of pump frequency and 4.4 bar of evaporating pressure.

As shown in Fig. 3.13, there are also the optimal operating conditions of each pump frequency with respect to various heat inputs. As the pump frequency increases, the heat addition rate of evaporator from heat source is generally larger due to the large mass flow rate. The maximum net power is presented at 6.07 kW of heat input.

Fig. 3.14 and Fig. 3.15 show the variation of the overall system net power with respect to evaporating pressure and DSH varying heat inputs, respectively. The common tendency of these results is that the changing aspects of the net

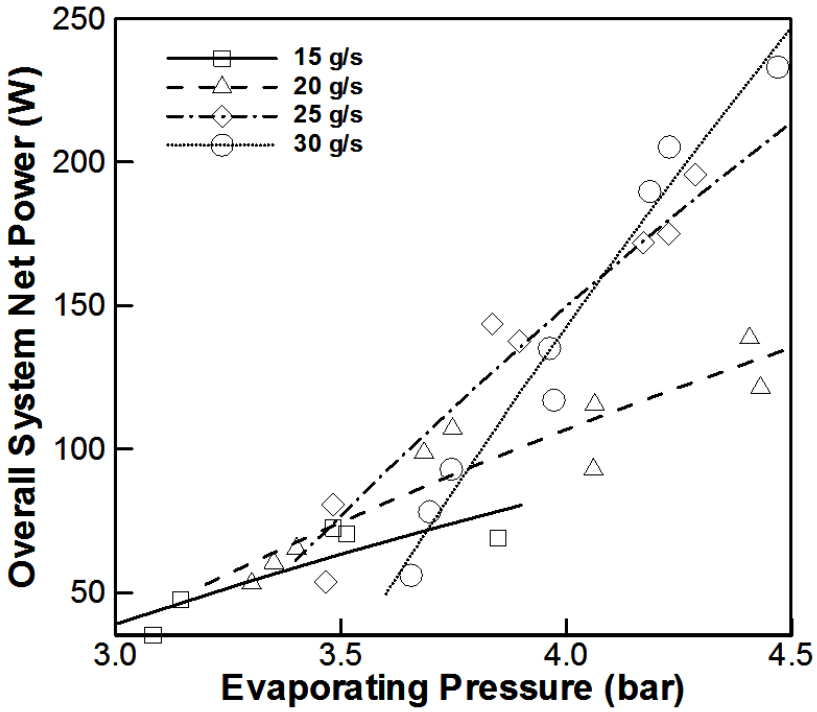

Fig. 3.11 Overall system net power variation with evaporating pressure and mass flow rate

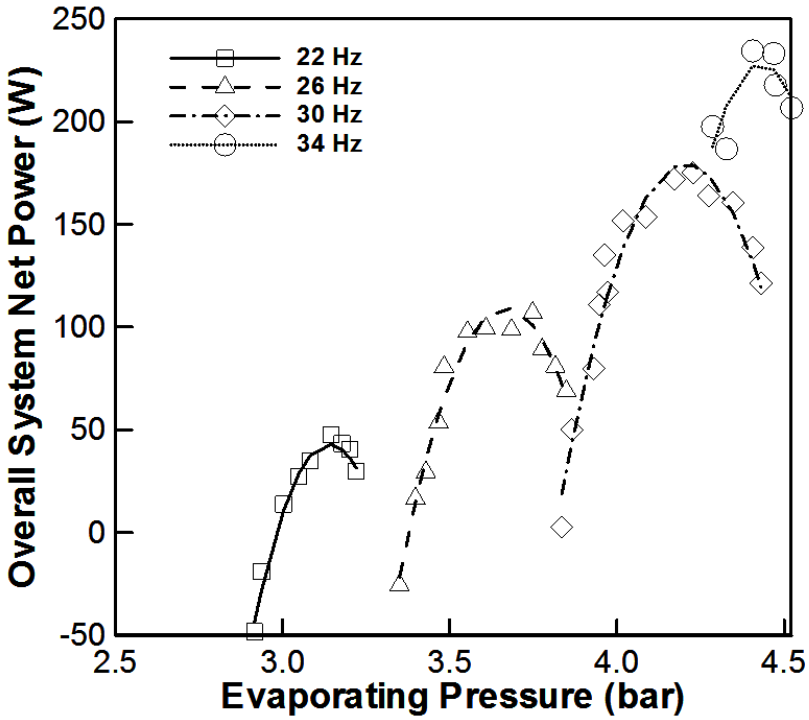

Fig. 3.12 Overall system net power with regard to evaporating pressure varying pump frequency

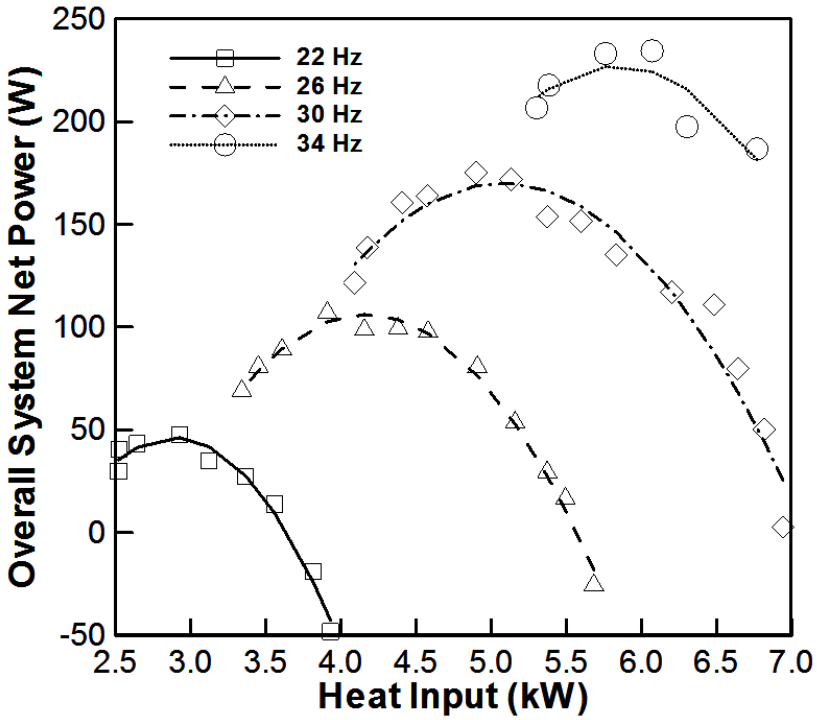

Fig. 3.13 Overall system net power with respect to heat input varying pump frequency

power with regard to evaporating pressure are presented steeper, as heat inputs from heat source increase. However, the effect of each operating parameter to the net power are presented differently. The increase of evaporating pressure causes to increase the overall net power and as the DSH of the inlet of the expander is enlarged, the net power decreases dramatically. Because the generating work and the isentropic efficiency of the expander tend to decline owing to increasing DSH.

The variation of the overall system thermal efficiency with various evaporating pressure and pump frequency is presented in Fig. 3.16. Unlike the general thermodynamic principles, the thermal efficiency is diminished according to the evaporating pressure increases. Because, as referred to earlier in part 3.2 and 3.3, the consumption work of the pump is enlarged as the pressure ration increases and the generating work curve of the expander exhibits the maximum point at a certain operating condition. In addition, like the net power variation, there are region where the thermal efficiency of the overall system is under zero. The maximum thermal efficiency is 4.07% at 4.29 bar of the evaporating pressure and 32 Hz of the pump frequency.

Fig. 3.17 shows the overall thermal efficiency with respect to heat inputs and pump frequency. The changing aspect of the thermal efficiency is similar to the overall system net power variation presented in Fig. 3.13. There are also

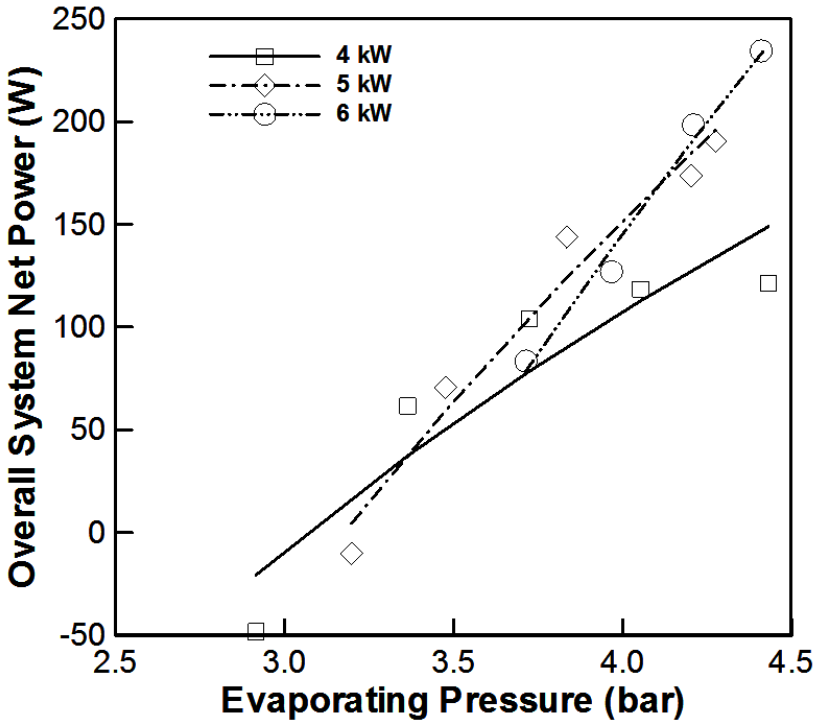

Fig. 3.14 Overall system net power variation with evaporating pressure and heat input

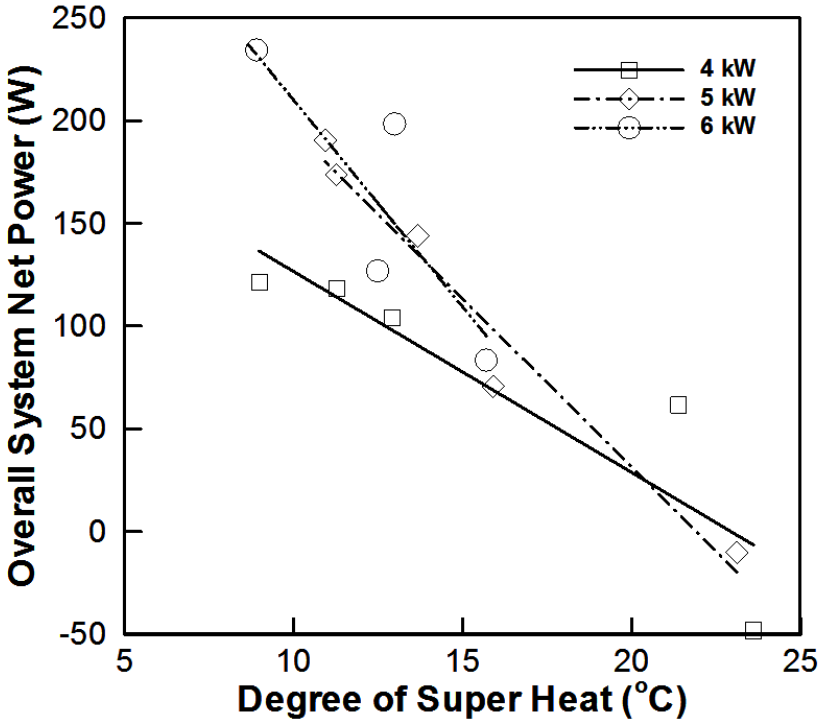

Fig. 3.15 Overall system net power with regard to DSH varying heat input

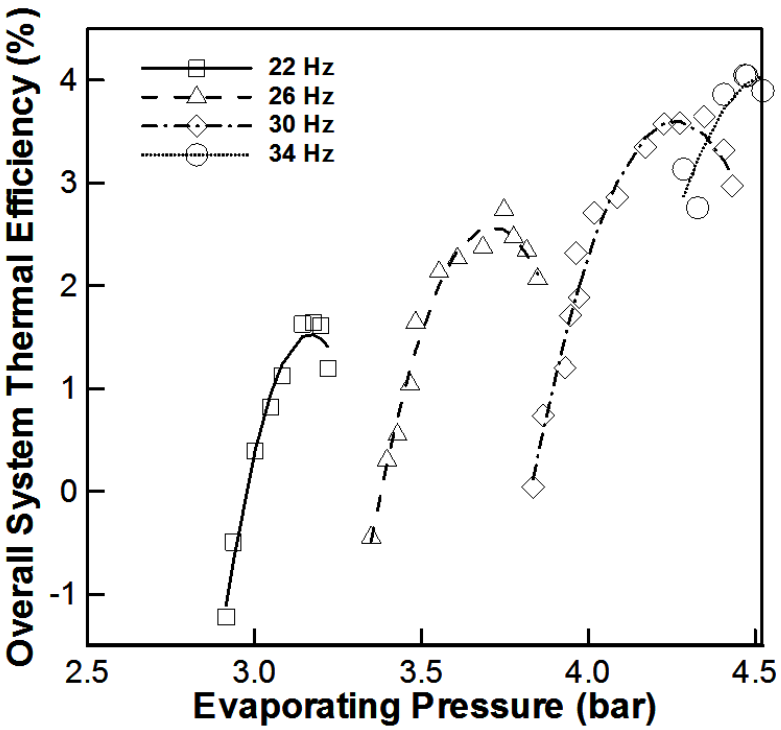

Fig. 3.16 Overall system thermal efficiency variation with evaporating pressure and pump frequency

the optimal operating conditions of each pump frequency with regard to heat inputs. The general tendency is that the heat addition rate of evaporator from heat source is larger according to the pump frequency is enlarged. Unlike the maximum point of the overall net power, the maximum thermal efficiency is presented at 4.80 kW of heat input.

Fig. 3.18 and Fig. 3.19 show the overall system thermal efficiency with regard to evaporating pressure and DSH varying heat inputs, respectively. The general tendency of the thermal efficiency with various evaporating pressure and DSH is considerably similar to that of the overall net power. However, the changing aspect of the thermal efficiency variation rate with respect to evaporating pressure and DSH is presented less steeply than that of the net power variation.

The generating (or consumption) work variation with various evaporating pressure varying heat inputs is shown in Fig. 3.20. Generally, as the evaporating pressure increases, the generating work of the expander and the consuqmption work of the pump are enlarged. Furthermore, the larger the heat addition rate of the evaporator, the larger the generating (or consumption) work of the system components. Because the mass flow rate of the overall system increases according to the heat input is enlarged. In addition, when the heat input is 5 kW, there is the operating region where the net power of the overall system falls to

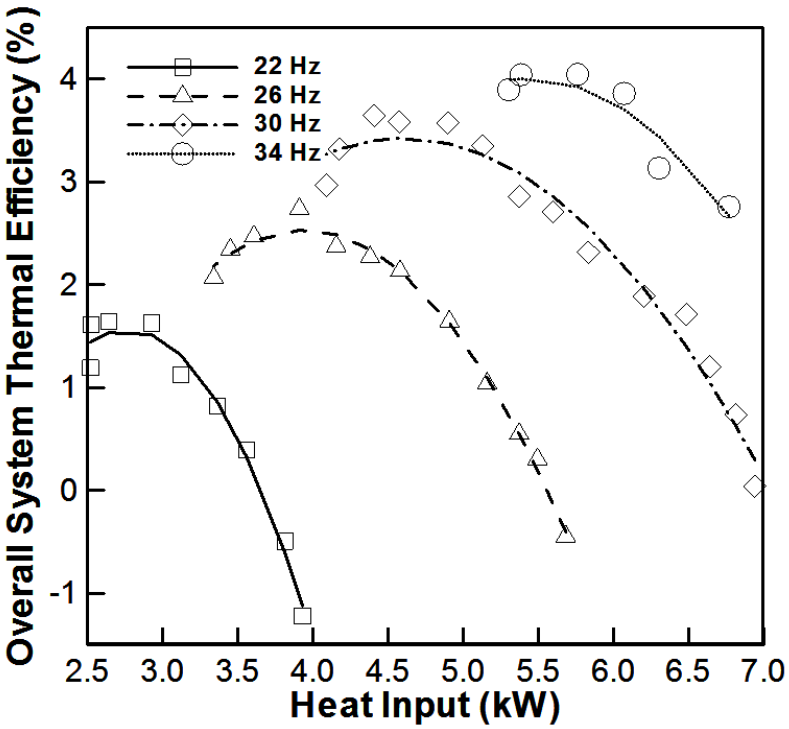

Fig. 3.17 Overall system thermal efficiency
with respect to heat input and pump frequency

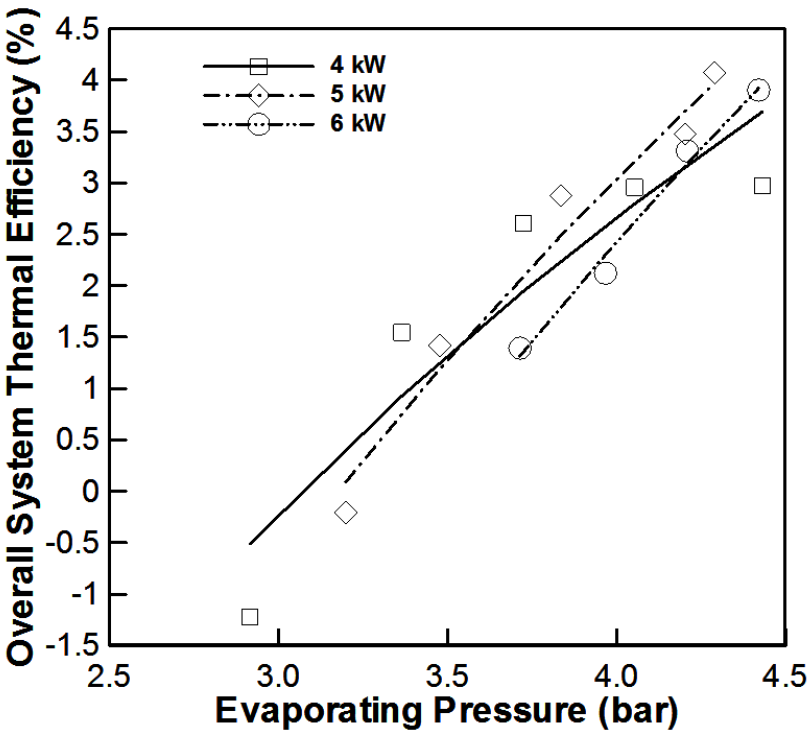

Fig. 3.18 Overall system thermal efficiency variation with evaporating pressure and heat input

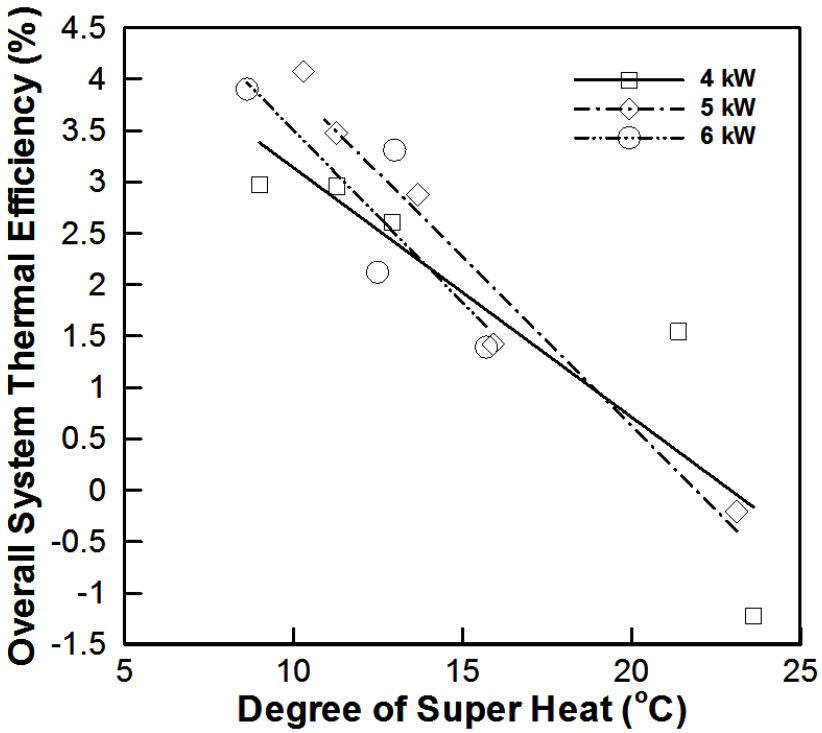

Fig. 3.19 Overall system thermal efficiency
with respect to DSH varying heat input

below zero. However, at 6 kW of the heat input, in all of the operating conditions, it is verified that obtaining the benefits of operating ORC applied to low-grade heat source below 100^{o}C is feasible.

Fig 3.21 and Fig 3.22 show the T-s diagram and the p-h diagram with various heat source capacities. The experimental results used in these diagrams are obtained at the optimal operating conditions where the maximum net powers are under each heat addition rate of the evaporator. The most evident tendency is that the heat source capacity doesn't seem to have relation the condensing temperature (or pressure) and the evaporating temperature (or pressure) increases slightly according to the heat input is enlarged. Because the mass flow rate is determined by only the heat source capacity and the higher evaporating pressure can produce the larger generating work of the expander. The optimal evaporating pressures are 4.08 bar, 4.31 bar and 4.47 bar and the mass flow rates are 18.87 g/s, 25.39 g/s and 31.47 g/s, respectively. The condensing pressures are usually observed at about 1.5 bar. Furthermore, the DSH of the inlet of the expander tends to decrease, as the heat input increases. Since, because of the fixed size of the heat exchangers, as the heat source capacity is enlarged, the mass flow rate increases and the inlet temperature of the expander decreases.

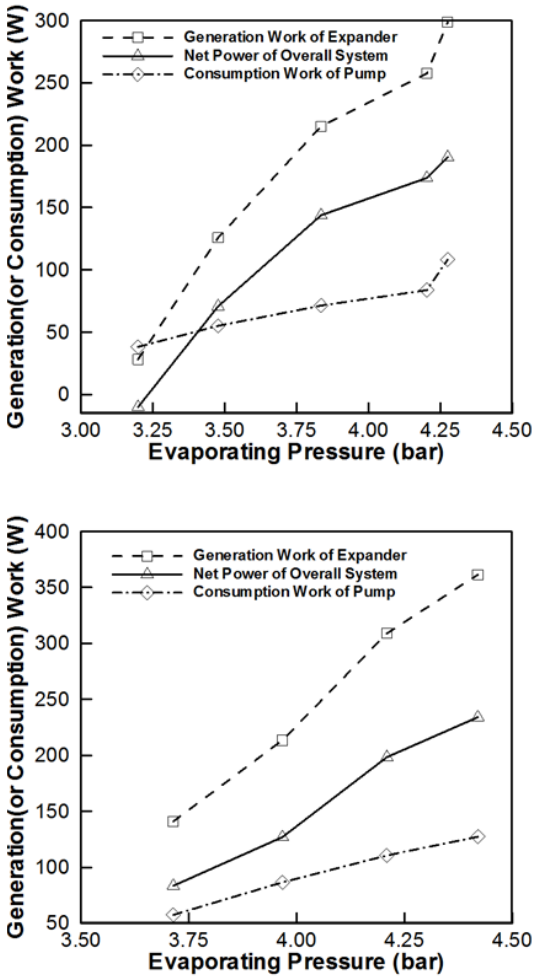

Fig. 3.20 Generation (or consumption) work variation with evaporating pressure varying heat input (5 kW, 6 kW)

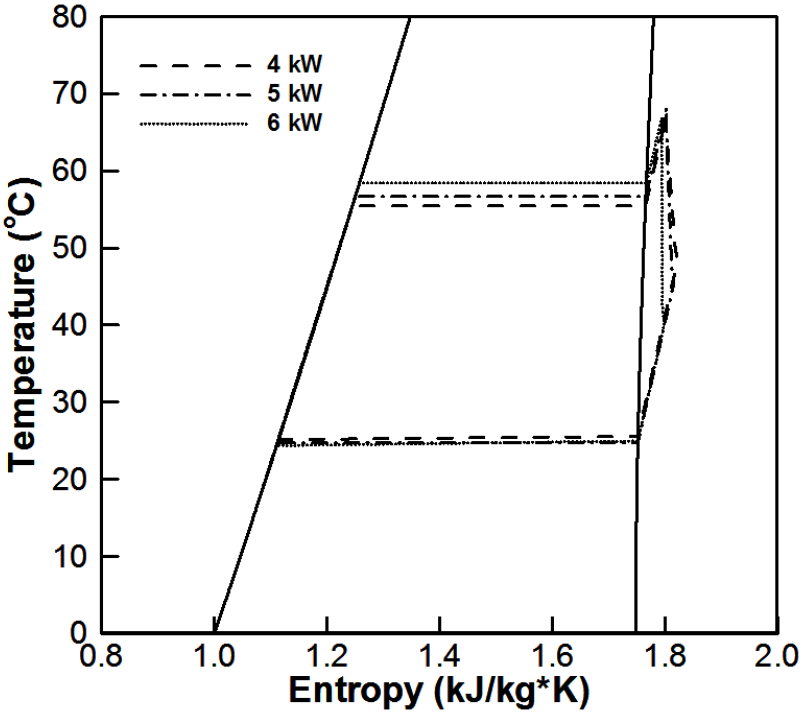

Fig. 3.21 T-s diagram of the organic Rankine cycle with respect to heat input

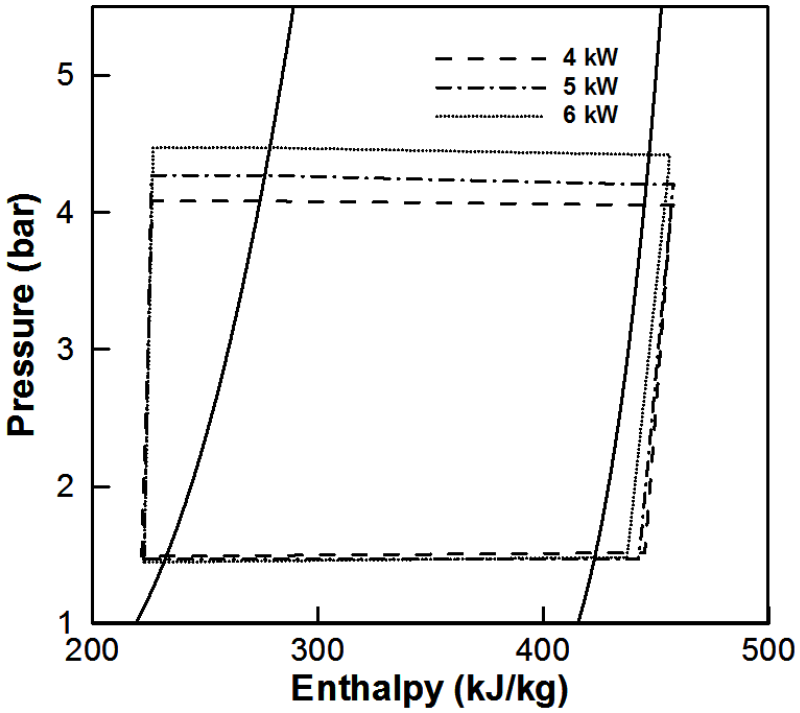

Fig. 3.22 P-h diagram of the organic Rankine cycle with regard to heat input

3.4.2 Exergetic Analysis of the Overall System

In this section, in order to investigate the irreversibility of the system components and the overall system, the exergy efficiency and exergy destruction of the system was calculated. The exergy efficiency means how close the experimental system approaches the ideal system which can produce the maximum useful work obtained from the system reaching equilibrium with the heat reservoir. Furthermore, by using exergy analysis, the thermodynamic losses can be verified more easily than energy analysis.

Fig 3.23 shows the exergy efficiency with respect to the evaporating pressure and heat input. The most general tendency is that the exergy efficiency is enlarged according to the evaporating pressure increases. Since, as shown in Fig. 3.9, due to mismatch between the actual pressure ratio and the optimal pressure ratio, the expander can’t operate efficiently in low pressure ratio. In addition, in all operating conditions, the isentropic efficiencies of the pump are estimated at 10~20%, which means that the pump operated very inefficiently. For these several reasons, it is verified that the overall system can’t operate efficiently in low evaporating pressure and improving the system components is necessary.

The exergy destruction variation of the system components and overall system with various evaporating pressure and heat inputs is shown in Fig. 3.24.

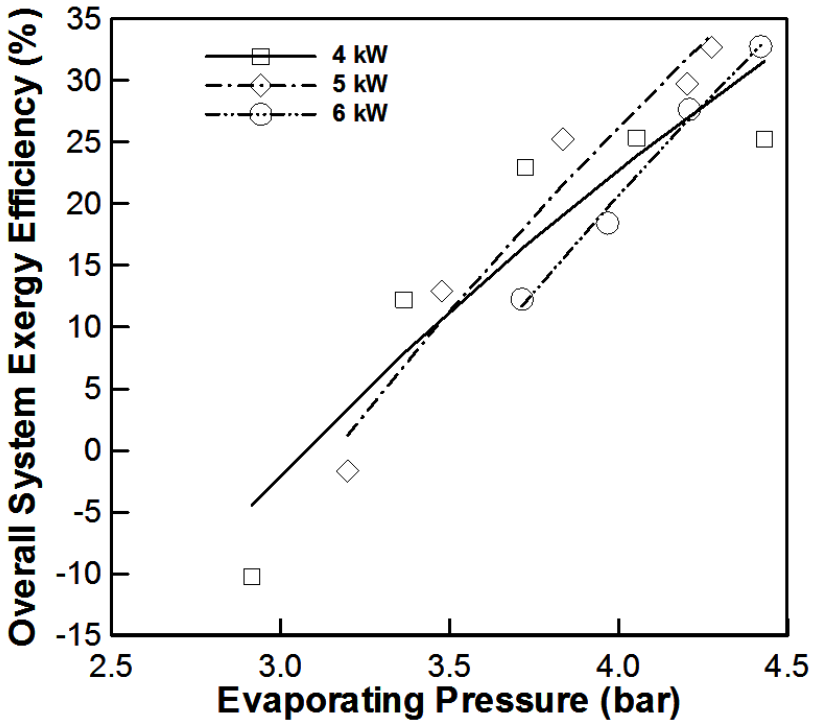

Fig. 3.23 Overall system exergy efficiency variation with evaporating pressure and heat input

Corresponding to the results of the exergy efficiency, the exergy destruction of the overall system tends to decrease according to the evaporating pressure increases. Since, the system components except for the pump can operate more efficiently in high evaporating pressure. Furthermore, in all heat source capacities, the exergy destruction of the expander is the largest, which means that the improvement of the expander is most important for operating ORC applied to low temperature heat source. Especially, compared with other components, the changing aspect of the pump is presented differently. Therefore, in order to improve the performance of the ORC applied to low temperature heat source below 100^{o}C, it is most essential to mitigate the irreversible process of the expander and the pump.

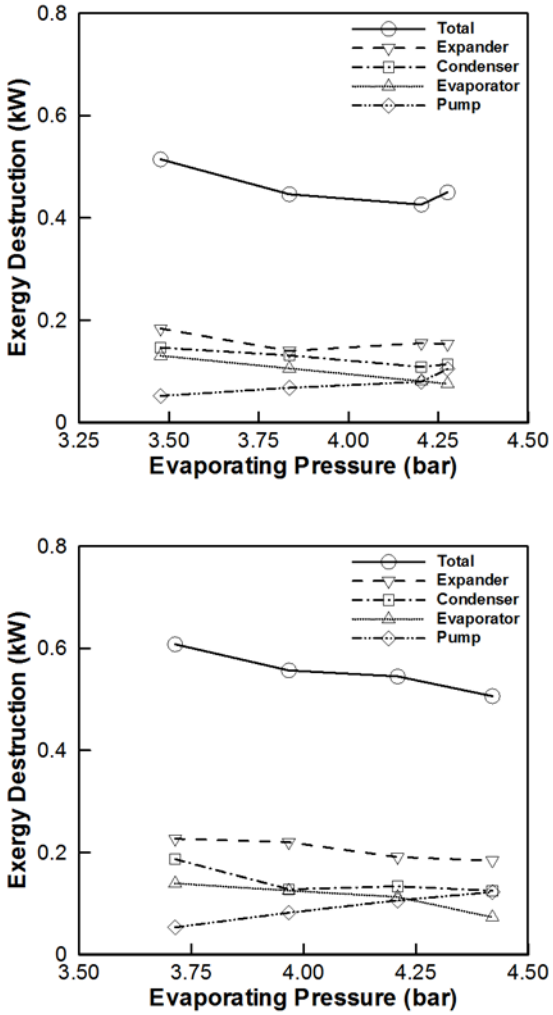

Fig. 3.24 Variation of system components and total exergy destruction with regard to evaporating pressure at different heat inputs (5 kW, 6 kW)

Chapter 4. Conclusion

In this study, in order to provide meaningful information and better understanding on the ORC, the performance of the ORC applied to heat source of 70°C and heat sink of 15°C was investigated.

By conducting the preliminary experiments, the effects of the refrigerant charge amount was investigated for 8.21 kg to 10.02 kg of the charge amount. The generating work curve of the expander variation with regard to refrigerant charge amount exhibited the maximum point at 8.50 kg and this charge amount was selected as the optimal charge amount for this study.

The ORC applied to low temperature heat source below 100°C was analyzed for some key parameters such as evaporating pressure, heat input, DSH and so on. Consequently, the maximum net power of the overall system was 234.36 W at the evaporating pressure of 4.41 bar and heat input of 6.07 kW. The thermal efficiency of this operating condition was 3.86%. Furthermore, at the evaporating pressure 4.29 bar and heat addition rate of 4.80 kW, the maximum thermal efficiency was 4.07%. On the other hands, in low evaporating pressure region, there are operating conditions which should be avoided to obtain the useful work from the system. In addition, due to mismatch between the actual pressure ratio and optimal pressure ratio, the performance reduction of the scroll expander was observed in low evaporating pressure. By conducting exergetic analysis of the ORC, it was verified that the improvement of the

scroll expander was most important for operating the ORC applied to low-grade heat source. In conclusion, it was confirmed that obtaining the benefits of operating ORC applied to low temperature heat source below 100^{o}C is feasible.

References

[1] United Nations Population Division. World population prospects: the 2012 revision. New York, United States. 2013.

[2] International Energy Egency. World energy outlook 2014. Paris, France. 2014.

[3] International Energy Egency. CO_2 emissions from fuel combustion. Paris, France. 2015.

[4] World Energy Council. 2015 World energy issues monitor. London, United Kingdom. 2015.

[5] International Energy Egency. Linking heat and electricity systems: co-generation and district heating and cooling solutions for a clean energy future. Paris, France. 2014.

[6] Tchanche BF, Lambrinos Gr, Frangoudakis A, Papadikis G. Low-grade heat conversion into power using organinc Rankine cycles – A review of various applications. Renewable and Sustatinable Energy Reviews 2011;15(8):3963-3979.

[7] Hung TC, Shai TY, Wang SK. A review of organic Rankine cycles (ORCs) for the recovery low-grade waste heat. Energy 1997;15(8):3963-3979.

[8] Imran M, Park BS, Kim HJ, Usman M. Economic assessment of greenhouse gas reduction through low-grade waste heat recovery using organic Rankine cycle (ORC). Journal of Mechanical Science and Technology 2015;29;835-843.

[9] Wali E. Optimum working fluids for solar powered Rankine cycle cooling of buildings. Solar Energy 1980;25:235-241.

[10] Maizza V, Maizza A. Unconventional working fluids in organic Rankine-cycles for waste heat recvoery. Applied Thermal Engineering 2001;21(3):381-390.

[11] Dai Y, Wang J, Gao J. Parametric optimization and comparative study of organic Rankine cycle (ORC) for low grade waste heat recovery. Energy Conversion and Management 2009;50(3):576-582.

[12] Borsukiewicz-Gozdur A, Nowak W. Comparative analysis of natural and synthetic refrigerants in application to low temperature Clausius-Rankine cycle. Energy 2007;32(4):344-352.

[13] Madhawa Hettiarachchi HD, Golubovic M, Worek WM, Ikegami Y. Optimum design criteria for an organic Rankine cycle using low-temperature geothermal heat sources. Engery 2007;32(9):1698-1706.

[14] Lemort V, Devlaye S, Quoilin S. Experimental characterization of a hermetic scroll expander for use in a micro-scale Rankine cycle.

Proceedings of the Institution of Mechanical Engineers, Part A: Journal of Power and Energy 2012;226(1):126-136.

[15] Yue C, Huang Y, Wu Y. Experimental study of low-temperature organic Rankine cycle with axial flow turbine. International Conference on Applied Energy 2015;75:1583-1589.

[16] Zhao P, Wang J, Gao L, Dai Y. Parametric analysis of a hybrid power system using organic Rankine cycle to recover waste heat from proton exchange membrane fuel cell. International Journal of Hydrogen Energy 2012;37:3382-3391.

[17] Centre d'études et de recherches économiques sur l'énergie (CEREN). Potentiel de récupération de chaleur à partir des effluents industriels. Paris, France. 2011.

[18] Wang D, Ling X, Peng H. Performance analysis of double organic Rankine cycle for discontinuous low temperature waste heat recovery. Applied Thermal Engineering 2012;48:63-71.

[19] Lemmon EW, Huber ML, McLinden MO. Refprop: reference fluid thermodynamic and transport properties, NIST standard reference database 23, version 9.1. National Institute of Standards and Technology, Gaithersburg, Maryland, USA. 2013.

[20] Muhammad U, Imran M, Lee DH, Park BS. Design and experimental investigation of a 1 kW organinc Rankine cycle system usign R245fa as working fluid for low-grade waste heat recovery from steam. Energy Conversion and Managament 2015;103:1089-1100.

[21] Quoilin S. Sustainable energy conversion through the use of organic Rankine cycles for waste heat recovery and solar applications. PhD thesis. University of Liège, Belgium; 2011.

[22] Baik YJ, Kim M, Chang KC, Lee YS, Ra HS. Power maximization of a heat engine between the heat source and sink with finite heat capacity rates. Korean Journal of Air-Conditioning and Refrigeration Engineering 2011;23:556-561.

[23] Declaye S, Quoilin S, Guillaume L, Lemort V. Experimental study on an open-drive scroll expander integrated into an ORC (Organinc Rankine Cycle) system with R245fa as working fluid. Energy 2013;55:173-183.

국 문 초 록

최근 수 십여 년간 전지구적 에너지 위기와 기후 변화가 큰 화제로 대두되고 있다. 이를 해결하기 위해, 기존 발전 시스템의 효율 향상, 새로운 형태의 발전 시스템 개발, 신 재생 에너지, 대체에너지와 같은 새로운 유형의 에너지원에 대해 연구되고 있으며, 그 중에서도 폐열 회수를 통한 발전 시스템 효율 향상에 대한 연구가 활발히 진행되고 있다. 250°C 이상의 중·고온 폐열 발전에 대해서 기존 스팀 사이클을 이용하여 실제 발전 산업 현장에서 폐열이 원활히 회수되고 있지만, 물의 비교적 높은 비등점으로 인해 저온 폐열은 충분히 활용되지 못하고 있다. 이러한 배경에서 유기 냉매를 작동 유체로 이용함으로써 저온 열원에 적합하게 구성된 것이 유기 랭킨 사이클이며, 지난 수 십 년간 연구가 진행되었다. 하지만 기존에 수행된 유기 랭킨 사이클에 대한 연구마저도 150~350°C 의 지열, 태양열, 바이오매스 연소 폐열 등의 열원에 집중되어 있다.

따라서 본 연구는 전체 폐열원의 상당 부분을 차지하나 온도가 낮아 이용가능성이 떨어지는 100°C 이하의 열원에 적용된 유기 랭킨 사이클에 대한 실험을 수행하였다. 그 중에서도 전체 산업 폐열의 약 30%를 차지하며 그 중 54%가 80°C 이하인 식품 및 섬유 산업의 폐열과 앞으로 차량용, 소규모 발전용 등으로 이용될 것으로 예상되는 60~80°C 의 연료전지 폐열에 주안점을 두었다. 이에 대한 실험적 연구를 진행하기 위해 기어 펌프, 스크롤 팽창기, 증발기, 응축기 등으로 구성된 기본 랭킨 사이클을 구성하고, 작동유체를 간단한 사이클 해석을 통해 R245fa 로 선정하여 실험장치를 구성하였다. 이를 통해 증발압력, 응축압력, 질량유량, 폐열량, 냉매 충전량 등의 변수를 변화시켜가며 다양한 작동 조건에서의 유기 랭킨 사이클의 성능을 분석하였다.

냉매 충전량 실험을 통해 시스템이 최대 출력을 내는 최적 냉매 충전량은 8.50 kg 인 것을 확인하여 이를 냉매 충전량으로 고정하고, 고온열원과 저온열원의 온도를 각각 70°C, 15°C 로 설정하고 3~6 kW 로 변화시켜가며 실험을 진행하였다. 그 결과, 최대 출력은 증발압력 4.40 bar, 열원 크기 6.07 kW 에서 약 234 W 로, 최대 열효율은 증발압력 4.29 bar, 열원 크기 4.80 kW 에서 4.07%로 확인되었다. 또한, 스크롤 팽창기의 고정된 built-in volumetric ratio 에 의한 성능 저하에 대한 현상도 확인할 수 있었다.

본 연구를 통해 유기 랭킨 사이클이 100°C 이하의 열원에도 적용 가능함을 확인하였고, 다양한 운전 조건에서의 성능을 면밀히 파악할 수 있었다.

주요어: 유기 랭킨 사이클, 스크롤 팽창기, 폐열 회수, 저온열원, 산업 폐열, 고분자 전해질막 연료 전지 폐열, R-245fa

학 번: 2013-23833

공학석사 학위논문

100°C 이하 저온 열원에 적용된 유기 랭킨 사이클의 성능에 관한 연구

Studies on the Performance of Organic Rankine Cycle Applied to Low Temperature Heat Source below 100°C

2016년 2월

서울대학교 대학원

기계항공공학부

이 지 성

100°C 이하 저온 열원에 적용된
유기 랭킨 사이클의 성능에 관한 연구

Studies on the Performance of
Organic Rankine Cycle Applied to Low Temperature
Heat Source below 100°C

지도교수 김 민 수

이 논문을 공학석사 학위논문으로 제출함

2015년 11월

서울대학교 대학원
기계항공공학부
이 지 성

이지성의 공학석사 학위논문을 인준함
2015년 12월

위 원 장 _____ (인)

부위원장 _____ (인)

위 원 _____ (인)

Abstract

Studies on the Performance of Organic Rankine Cycle Applied to Low Temperature Heat Source below 100ºC

Ji Sung Lee
Department of Mechanical and Aerospace Engineering
The Graduate School
Seoul National University

In this study, the performance of Organic Rankine Cycle (ORC) applied to low temperature heat source was investigated to provide meaningful information and better understanding on ORC. In previous studies of ORC, the types of heat source were mainly geothermal heat, solar heat, biomass combustion waste heat whose temperatures range from 150ºC to 350ºC. However, although waste heat below 100ºC generated from industrial process (e.g. food, beverage, fiber industry) and PEM fuel cell has a large portion of overall waste heat, it isn't sufficiently utilized for waste heat recovery.

Therefore, it is necessary to investigate operating characteristics of ORC using waste heat from heat source under 100°C. In order to verify the performance of ORC applied to heat source below 100°C, experiment was conducted to investigate the effects of some key parameters (e.g. evaporation pressure, condensation pressure, mass flow rate, etc.) and the optimal operating condition which has maximum generation work. Results show that the maximum generation work was about 234 W and the thermal efficiency of ORC was about 4%, when the range of heat input was from 3 kW to 6 kW. By experiment of ORC applied to low temperature heat source, it was confirmed that ORC can obtain the additional generating power from waste heat under 100°C.

Keywords: Organic Rankine Cycle, Scroll Expander, Waste Heat Recovery, Low Temperature Heat Source, Industrial Waste Heat, PEM fuel cell Waste Heat, R-245fa

***Identification Number*: 2013-23833**

Contents

List of Figures

List of Tables

Nomenclature

P_c	Critical pressure (MPa)
T_c	Critical temperature (^oC)
T_{bp}	Boiling point temperature (^oC)
PEMFC	Proton Exchange Membrane Fuel Cell
ORC	Organic Rankine Cycle
ODP	Ozone Depletion Potential relative to R11
GWP	Global Warming Potential relative to CO_2
h	Heat transfer coefficient (W m^{-2} K^{-1})
D_h	Hydrauric diameter (m)
k	Thermal conductivity (W m^{-1} K^{-1})
Re	Reynolds number
Pr	Prandtl number
μ	Dynamic viscosity (Pa s^{-1})
ρ	Density (kg m^{-3})
x	Quality
Bo	Boiling number
q"	Heat flux (W m^{-2})
G	Mass flux (kg m^{-2} s^{-1})
DSH	Degree of Super Heating (^oC)
DSC	Degree of Sub Cooling (^oC)
GPH	Gallon per hour (Gal h^{-1})

RPM	Revolution per minute (rev min^{-1})
cps	Centi poise (g cm^{-1} s^{-1})
RT	Refrigeration tons (=3.52 kW)
E	Exergy (W)
Q	Heat (J)
W	Work (J)
T_f	Frictional torque (N m)
η	Efficiency
D	Exergy destruction (W)
R_p	Pressure ratio

Subscript

r	Refrigerant
v	Saturated vapor
l	Saturated liquid
tp	Two phase
sp	Single phase
cell	Fuel cell
w	Water
eva	Evaporator
cond	Condenser
exp	Expander
th	Thermal

sat	Saturation
0	Dead state
h	Hot
r	Refrigerant
exg	Exergy
0	Dead state

Chapter 1. Introduction

1.1 Background of the Study

In recent decades, global energy crisis and global warming problem have been great issues. By 2035, the world's population is expected to reach 8.7 billion and the primary energy consumption is projected to increase by 37% between 2013 and 2035 [1, 2]. The growing fossil fuel use for transportation and industry, the decreasing crude oil production, and the political and social unrest of major oil supplying countries has accelerated the global energy crisis. Furthermore, due to increasing carbon dioxide emissions which have the largest portion of the overall anthropogenic greenhouse gas emissions, the global land-ocean temperature has been increasing steadily and the abnormal climate has been occurring more frequently. Especially, the 42% of the global carbon dioxide emissions comes from the primary energy consumption for generating electricity [3]. Therefore, in order to overcome these problems, it is most important to improve the efficiency of the conventional or novel power generation systems and find new type of energy sources such as renewable energy, alternative energy and so on.

Considering the feasibility of application and the impact to the energy and

climate problem, it is most essential to increase the conversion efficiencies of the utilization of available energy sources [4]. Because improving energy efficiency plays a key role towards planning to make energy security and fulfilling climate and environmental regulations. There are several ways to increase conversion efficiencies of generating electricity such as co-generation using waste heat, developing new type of power generation cycle and so on. Among these ways, recovering waste heat from conventional power cycle or engine exhaust and industrial waste heat sources has been evaluated as most effective method. Because roughly two-thirds of the fuel used to generate power is lost as waste heat during fossil-fuelled power generation [5]. Waste heat sources are classified according to the temperature rage as: high temperature (>650^{o}C), medium temperature (230~650^{o}C), low temperature or low-grade (<230^{o}C) [6]. According to statistical information, the low temperature waste heat sources accounts for 50% of overall heat generated from industry [7]. In this respect, organic Rankine cycle (ORC) has been spotlighted as the viable technology to produce electrical power from low-grade heat sources due to lower ebullition temperature and pressure, simpler structure, and lower cost of maintenance compared to conventional steam cycle. Furthermore, the ORC applied to waste heat recovery is expected to be helpful to the reduction of greenhouse gas emissions which would have been produced if

fossil fuel was to be used for the conventional power generation system [8].

Likewise, the ORC has several benefits and potentials for applying to waste heat recovery. In this study, in order to provide meaningful information and better understanding on the ORC, the performance of the ORC applied to low temperature heat source was investigated. Especially, unlike the previous studies on the ORC, the experiments was conducted to investigate the characteristics of the ORC utilizing waste heat below 100^{o}C.

1.2 Overview on the Organic Rankine Cycle

The steam Rankine cycle has been used for transforming on large scale thermal energy into electrical power as the most important method. By using water as working fluid, it is possible to lessen the concerns about toxicity, flammability, consumption work of the pump, thermal/chemical stability, cost, and so on. However, when steam cycle is used as small and medium scale power plant, there are many disadvantages such as need of superheating to prevent condensation during expansion process, risk of erosion of turbine blades, excess pressure in evaporator, and complex and expensive turbines [9].

With this background, in order to overcome these problems, it was necessary to partially mitigate the limitations of water by selecting an alternative working fluid. As shown in Table 1.1 and Fig. 1.1, Organic fluids having higher molecular mass and lower boiling point/critical temperature than water have been proposed in so called “organic Rankine cycle”.

Due to the same fundamentals of operating of both of the ORC and the conventional steam cycle, these cycles have few similarities about cycle configurations, components and applications. However, because these cycles use different working fluids, the characteristics of these cycles appear differently depending on situations. The ORC has several advantages over traditional steam Rankine cycle. For example, less heat is needed during the

Table 1.1 Properties of water and organic fluids

Substance	**Molecular mass (kg/kmol)**	**P_c (MPa)**	**T_c (°C)**	**T_{bp} (°C)**
Water	18.02	22.06	373.95	99.974
R245fa	134.05	3.64	154.05	14.90
R245ca	134.05	3.93	174.42	25.13
R11	137.37	4.408	197.96	23.71
R113	187.38	3.392	214.06	47.59
R114	170.92	3.257	145.68	3.49
R123	152.93	3.662	183.68	27.82
R134a	102.03	4.06	101.03	-26.07
R141b	116.95	4.25	204.50	32.05

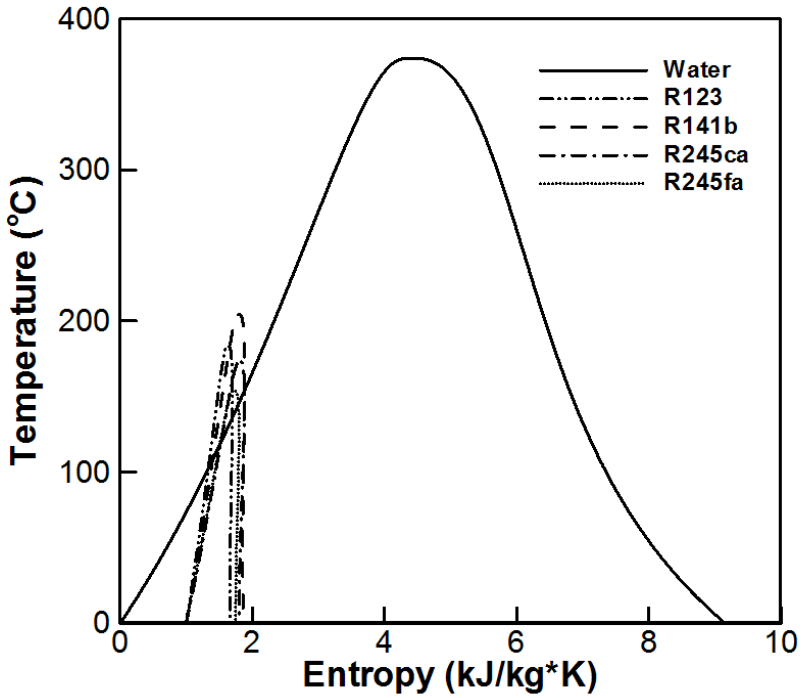

Fig. 1.1 T-s diagrams of water and few organic fluids

evaporation process and the evaporation process takes place at lower temperature and pressure than water. Due to non-negative slope of vapor saturation curve, erosion of expander blades is not concerned. Simple single stage expanders can be used owing to the smaller pressure drop/ratio.

Likewise, the working fluids in the ORC power systems play the most important role to determine the performance and the economic feasibility. Therefore, there are so many sufficient conditions to be the appropriate working fluid of the ORC. In order to lessen the concern of erosion of expander blades, it should have the vapor saturation curve with zero or positive slope. It should have high density of liquid or vapor phase for minimizing the sizes of overall system. It need to have good heat transfer properties such as low viscosity and high thermal conductivity. In order to operate stably at high temperature, it should have good thermal and chemical stability and good compatibility with the conventional materials. For high energetic/exergetic efficiency and good safety characteristics, the working fluid should have high thermodynamic performance and should be non-toxic and non-flammable. Furthermore, because of growing the concern about global climate change and environmental destruction in recent, it should have low ODP and low GWP. The cost and availability should also be considered for selecting the proper working fluid.

In addition, the ORC has been applied to various heat sources and has

shown the possibility to realize in actual field. Especially, in USA, Canada, Italy, Austria, Germany, Netherlands and Sweden, a large number of the ORC power plants have been installed for geothermal heat, solar heat and biomass combustion waste heat. In recent decade, Ocean Thermal Energy Conversion applied to the Earth's oceans as heat source of virtually inexhaustible renewable energy has been intensely investigated as future technology.

1.3 Literature Survey

The researches of the ORC have been conducted actively, since the early 1970's. There have been lots of studies about the ORC applied to low-grade heat sources below 100°C.

Hung et al. [7] analyzed parametrically and compared the efficiencies of the basic ORCs using benzene, ammonia, R11, R12, R134a and R113 as working fluids. The range of evaporation temperature of this study was from 67°C to 287°C and the targeted application was waste heat recovery. They investigated only comparison of first law efficiencies of water and few organic fluids by numerical method.

Maizza et al. [10] investigated the ORCs with one regenerator using R123, R124 as working fluids in realistic operating conditions. The range of vaporization temperature was from 80°C to 110°C and the condensing temperature ranged from 35°C to 60°C. They analyzed the relation of first law efficiencies and some key parameters (e.g. vaporization temperature, condensing temperature) by numerical analysis.

Dai et al. [11] conducted thermodynamic analysis about the effects of parameters on the performance of the ORCs for waste heat recovery systems. Parameter optimizations of the systems with one regenerator were performed with different working fluids (e.g. water and few organic fluids) using a genetic

algorithm. They analyzed and compared the net power outputs of the performance of the ORCs. The evaporating temperature ranged from 80°C to 140°C and condensing temperature was 20°C.

Borsukiewicz-Gozdur et al. [12] conducted the concise survey of simulation of the low-temperature Clasius-Rankine cycle and targeted application was geothermal power station. The range of temperature of heat source was from 80°C to 115°C. They analyzed the possibility of application of different working fluids, both natural and synthetic. The cycle configuration of this study was the basic cycle consisting of pump, evaporator, expander and condenser.

Madhawa et al. [13] conducted the numerical analysis in order to find the cost-effective optimum design criteria for ORCs utilizing low-temperature geothermal heat sources. The cycle configuration was the basic cycle and the temperature of heat source was from 70°C to 90°C. They used the steepest descent method to find the optimum design conditions.

Lemort et al. [14] conducted the experiments to test the performance of the hermetic scroll expander using R245fa as working fluid. The system configuration was the gas cycle operating on vapor region in the whole states. The supply temperature and pressure of expander were 92°C, 12.61 bar, respectively and the range of pressure ratio of expander was from 2.0 to 10.0.

Yue et al. [15] fabricated the low temperature heat recovery ORC system using R245fa and a single-stage axial flow turbine. The cycle configuration was the basic Rankine cycle the range of evaporating and condensing temperature was from 50°C to 100°C and from 20°C to 70°C, respectively. The maximum efficiency of the system was 7.22% and the turbine isentropic efficiency was 56.4%.

Zhao et al. [16] focused on the performance of the hybrid power system consisting of the ORC and Proton Exchange Membrane Fuel Cell (PEMFC). All of the performance analyses of the ORC and Proton Exchange Membrane Fuel Cell were conducted by numerical method. The ORC system configuration was the basic Rankine cycle and used R245fa, R245ca, R236fa, R123 and Isobutane as working fluid. They investigated the effects of some key parameters such as fuel flow rate, fuel cell operating pressure, turbine inlet pressure and turbine back pressure.

Likewise, the previous studies were mainly focused on the selecting appropriate working fluids and numerical method. Therefore, it is necessary to conduct experiments applied to low-grade heat sources below 100°C, in order to provide meaningful experimental data to other researches.

1.4 Motivation and Objective of the Study

Until now, so many researches about the ORC applied to low temperature heat sources have been conducted. However, in the previous studies and commercialization of the ORC, the types of heat sources were mainly geothermal heat, solar heat, biomass combustion waste heat whose temperatures are over 100°C. Although waste heat below 100°C generated from industrial process, engine and fuel cell has a large portion of overall waste heat, it hasn't sufficiently utilized for waste heat recovery. Furthermore, the researches investigating the ORC applied to low temperature heat source below 100°C have been mainly conducted by numerical analysis.

Although the ORC has been investigated actively since 1970's, it hasn't been applied widely until today's growing concern about the declining fossil fuel production and the global climate change. Due to its lower operating temperature than that of the conventional steam Rankine cycle, the ORC can be suitable to recover waste heat from various heat sources. The numerous ORC power plants have already been demonstrated worldwide by the ORC manufacturers and installers. Furthermore, although many companies have recorded data of their machines, there is a lack of exact data to analyze the characteristics and performance of each application. Most of these power plants have also been applied to geothermal heat, solar heat, biomass combustion

waste heat whose temperatures are over 100°C.

In recent, the hybrid power system consisting of the PEMFC and the ORC has been spotlighted as waste heat recovery technology. In order to maintain 60~80°C of the optimal operating temperature of stack, thermal management system is used for only eliminating heat generation of stack where chemical reactions occur. On the other hands, as shown in Fig. 1.2, for using waste heat from stack to produce additional work, the ORC is connected with heat exchanger of thermal management system in the hybrid power system. However, there are only a few studies to investigate this technology by numerical method.

In addition, waste heat generated from industrial process such as steam drying, refrigeration, freezing, sterilization, etc. of food and beverage industry is estimated at 33 TWh, 30% of global waste heat [17]. Low level of temperature (less than 80°C) waste heat has the 54% of total waste heat generated from food and beverage industry. However, although available waste heat below 100°C from industrial process has a large portion of global waste heat, it is hard to find trials to recover waste heat to generate additional power.

Therefore, in this respect, experimental research of the ORC applied to heat sources below 100°C has high usefulness and originality. In this study, the effects of some key parameters (e.g. evaporating pressure, condensing pressure,

mass flow rate, pressure ratio, etc.) and the optimal operating condition which had the maximum generating work were investigated by experiments.

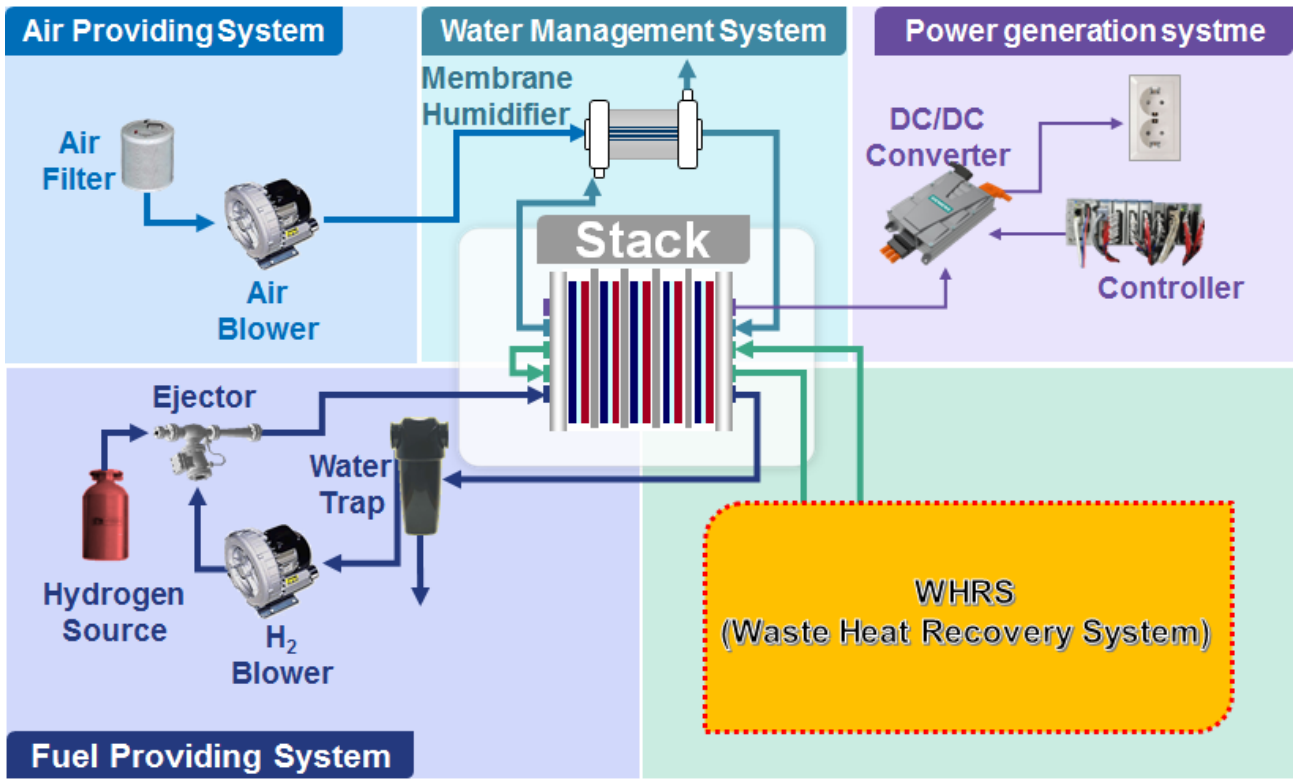

Fig. 1.2 Schematic diagram of PEMFC-ORC hybrid power system

Chapter 2. Experimental Setup and Measurements

2.1 Selection of the Working Fluid

2.1.1 Cycle Analysis

In the ORC researches, the selection of the working fluid is the most important thing to determine the performance of the overall system. Because the working fluid can affect the efficiency of the system, sizes of components, system stability, cost of maintenance and so on. Therefore, in order to find the appropriate working fluid to our experimental system, the working fluid candidates, which were expected to be suitable to the targeted temperature range of heat source, were selected. These candidates were R123, R141b, R245ca and R245fa. According to the previous numerical studies, these fluids were recommended as the most appropriate ones in 50~80^{o}C of evaporating temperature and 25^{o}C of condensing temperature [16, 18]. As shown in Fig. 2.1, the analyzed cycle consisted of pump, evaporator, expander and condenser. Pump and expander's simulation were conducted simply by using the fixed isentropic efficiency. Heat exchangers' modeling was performed by utilizing several heat transfer correlations. The detailed information of the used heat

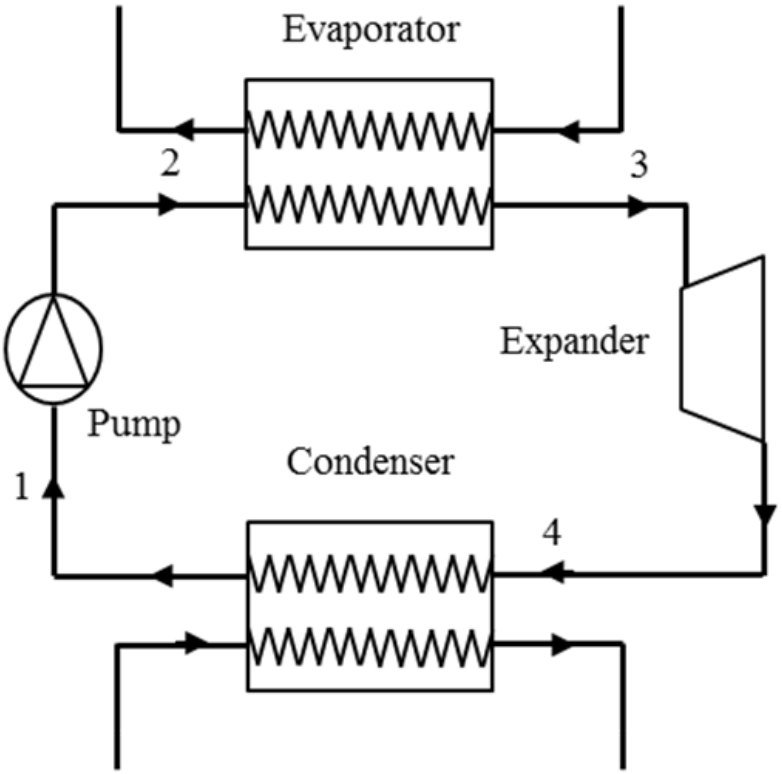

Fig. 2.1 Schematic diagram of the basic organic Rankine cycle

transfer correlations are shown as below:

Single phase region: Dittus-Boelter correlation (1930)

$$\frac{h_r D_h}{k} = 0.023\,\mathrm{Re}^{0.8}\,\mathrm{Pr}^{n}$$

Two phase region in condenser: Chen correlation (1987)

$$\frac{h_r D_h}{k} = 0.018\left(\frac{\mu_v}{\mu_l}\right)^{0.078}\left(\frac{\rho_v}{\rho_l}\right)^{0.39}\mathrm{Re}_l^{0.2}\left(\mathrm{Re}_{lo}-\mathrm{Re}_l\right)^{0.7}\mathrm{Pr}_l^{0.65}$$

Two phase region in evaporator: Gungor-Winterton correlation (1987)

$$h_{tp} = Eh_{sp}$$

$$h_{sp} = \frac{0.023k\,\mathrm{Re}^{0.8}\,\mathrm{Pr}^{0.3}}{D_h}$$

$$E = 1 + 3000Bo^{0.86} + 1.12\left(\frac{x}{1-x}\right)^{0.75}\left(\frac{\rho_l}{\rho_v}\right)^{0.41}$$

$$Bo = \frac{q''}{h_{fg}G}$$

The detailed values of numerical conditions were shown in Table 2.1. In order to reasonably verify and compare the performance of the ORC using each working fluid, the waste heat amount, evaporating temperature and condensing temperature. Because it was important to verify the performance of each case

applied to the same heat source and heat sink. In addition, the evaluation of the pumping and expansion process was conducted by basic thermodynamic concept. All of pumps or expanders were calculated by the same isentropic efficiencies 75%, 60%, respectively. These isentropic efficiencies used by most of the previous analytic researches were used. It assumed that the DSH of inlet/outlet of expander and the DSC of inlet of pump were set to zero. The properties of refrigerants were used from NIST Refprop ver. 9.1 [19].

Table 2.1 Numerical conditions of the cycle analysis

Parameter	Unit	Value
Waste heat amount	kW	5
Evaporating temperature	°C	50 ~ 75
Condensing temperature	°C	25
Isentropic efficiency of pump	%	75
Isentropic efficiency of expander	%	60

2.1.2 Result and Discussion of Cycle Analysis

Fig 2.2 represents the thermal efficiency with different working fluids and evaporating temperature at the same condensing temperature. For all of the working fluids, the thermal efficiencies elevate as the evaporating temperature increases. The reason is that with the increase of pressure difference of evaporator and condenser, the enthalpy difference of the expander elevates. In the given range of evaporating temperature, the minimum thermal efficiency is about 3.5% and the maximum thermal efficiency is about 7.0%. In addition, Result shows that R141b has the highest thermal efficiency and R245fa has a little lower thermal efficiency than that of others. The thermal efficiency difference between R141b and R245fa increases as the evaporating temperature increases. However, this thermal efficiency difference is from 0.1% to 0.5% and it isn't very large.

In this study, although R245fa shows a little lower thermal efficiency than that of others, R245fa was selected as the most appropriate working fluid to our experiment. Because R123 and R141b are classified HCFC refrigerant and the use of HCFC refrigerant was already restricted or will be prohibited by environmental regulations. Furthermore, although R245ca has a good thermodynamic performance and eco-friendly characteristics, it has relatively high flammability.

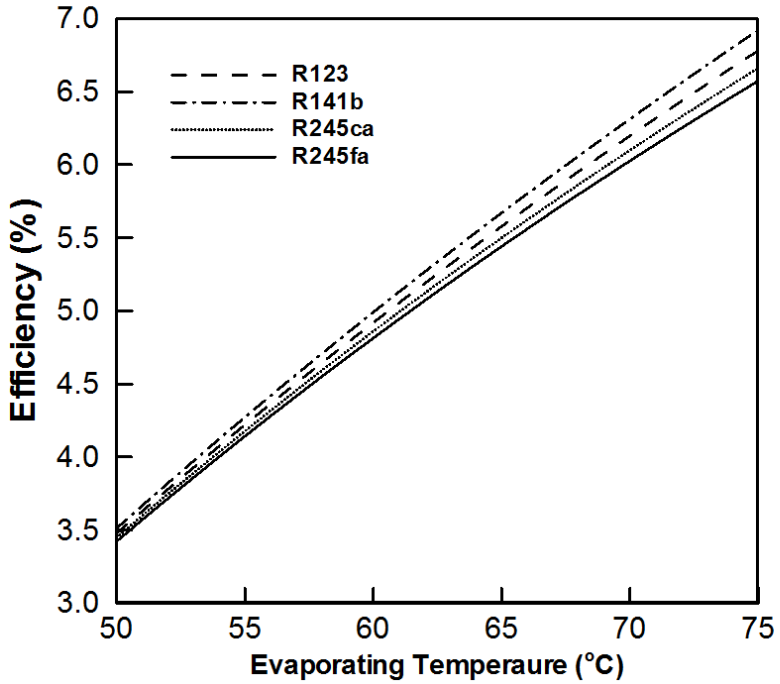

Fig. 2.2 Thermal efficiency variation with various working fluids and evaporating temperature at 25°C of condensing temperature

2.2 Experimental System

The experimental apparatus was fabricated to investigate the ORC applied to low temperature heat source below 100°C. In Fig. 2.3, the schematic diagram of the experimental system are shown. This experimental system consists of gear refrigerant pump, evaporator, scroll expander and condenser as basic Rankine cycle. To supply lubricant to expander, oil ejector and oil separator are built in this system. For preventing cavitation of inlet of pump, customized liquid receiver is used. In addition, in order to measure various parameters of experimental conditions and results such as temperature, pressure, mass flow rate, frictional torque of expander shaft, rotational speed of expander and so on, the appropriate instruments are fabricated. The system consists of one closed loop for R245fa and two closed loop for heating and cooling waters. In order to control temperature and mass flow rate of heating and cooling waters, circulation cycle consisting of water pump, mass flow meter, water tank and electric heater.

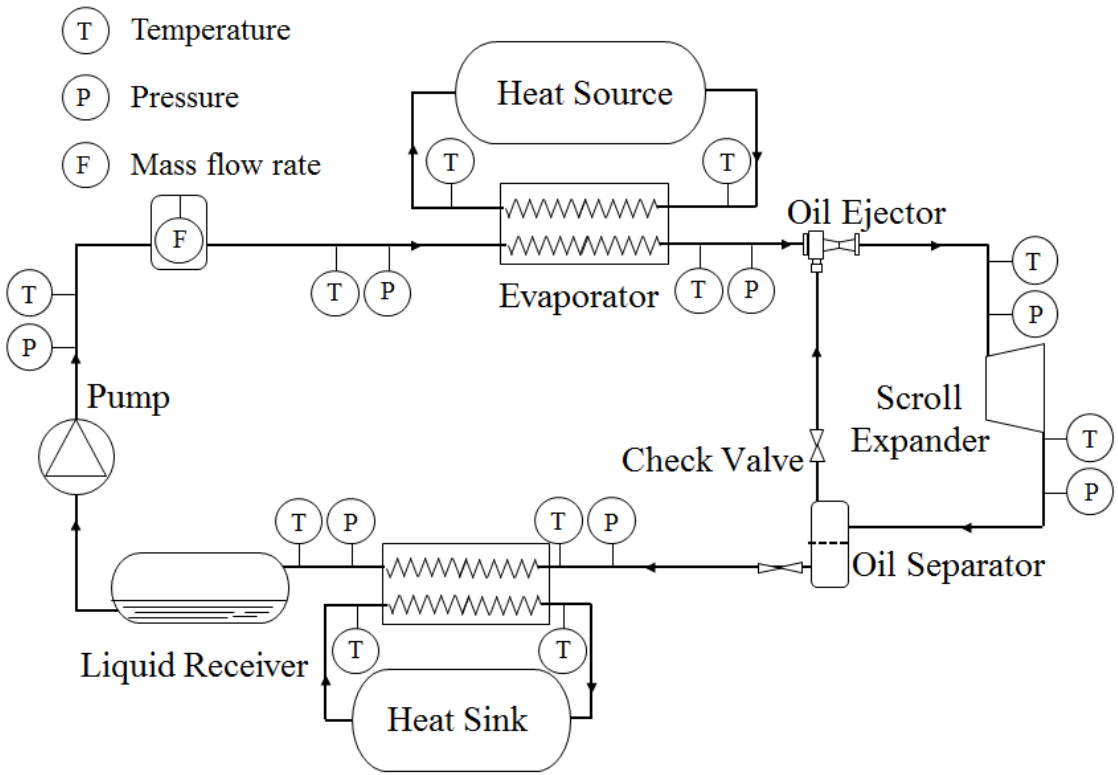

Fig. 2.3 Schematic diagram of the organic Rankine cycle experimental system

2.2.1 Gear Pump

In the ORC power generating system, the selecting of the working fluid pump is also very important. Especially, in small scale systems, pump selection is somewhat difficult owing to unusual operating conditions and sensitivity to surroundings [20]. Generally, centrifugal pumps are improper to operate in this situation.

Therefore, gear pumps, which are positive displacement types, was selected as the most appropriate type of pump due to its ability to stably supply working fluid in low flow rate. In addition, the selecting of the gear pump should be conducted by intensive consideration including leakage losses and friction losses. Considering all of these aspect, the T series refrigerant gear pump made by the Tuthill Company was selected as shown in Fig. 2.4. This gear pump is magnetically coupled to 0.75 kW, 3-phase 380 V motor. Other characteristics of the gear pump are provided in Table 2.2.

Fig. 2.4 Photograph of Tuthill T series gear pump

Table 2.2 Specifications of the gear pump

Parameter	Value
Flow rates	20 ~ 650 GPH
Temperatures	-46 ~ 176ºC
Differential pressures	17.2 bar
Rotational speed	5,000 RPM maximum
Magnet torque	240 ~ 460 in-oz
Metal wetted parts	316 stainless steel, Titanium or Hastelloy C276

2.2.2 Scroll Expander

The scroll expander has the fixed volumetric ratio due to positive displacement machine. When the system pressure ratio doesn't match the optimal pressure ratio corresponding to the fixed volumetric ration of the expander, under or over expansion losses can occur. These two losses can affect considerably the performance of the expander. However, the turbomachines are usually more suitable to high expansion ratio and the piston expanders are more appropriate for operating conditions with large pressure ratio due to their designs optimized for higher internal built-in volumetric ratios [21].

Therefore, the scroll type expander was selected as the most appropriate option to our experimental conditions. Because the pressure ratio between high and low saturation pressures corresponding to expected evaporating and condensing pressure was relatively low. In this research, as shown in Fig. 2.5, the scroll expander, whose rotor was divided from scroll type vapor compressor (Copeland, ZF09K4E-TFD-550), was manufactured for making the scroll rotor to run in reverse. Its specific geometrical data of the scroll expander is shown in Table 2.3.

Fig. 2.5 Photographs of scroll rotor and scroll expander

Table 2.3 Geometrical information of the scroll expander

Parameter	Value
Built-in volumetric ratio	3.1
Basic circle radius	2.1 mm
Wrap height	29.1 mm
Pitch	13.2 mm
Wall thickness	3.3 mm
Suction volume	10.1 cm^3 rev^{-1}

2.2.3 Heat Exchangers

For evaporator and condenser, the plate type heat exchangers were used in experimental system. In order to maximize the heat transfer amount, the directions of the working fluids and the secondary fluids (e.g. heating and cooling water) were made of counter-flow, where the most efficient heat transfer occurs in the available temperature difference.

For evaporator, considering the expected heat addition from heat source and sufficient safety coefficient, the capacity of evaporator was set to 5 RT. Furthermore, in the ORC power system, it is more difficult to reject heat to heat sink in condenser. Therefore, although the heat transfer amount of condenser is smaller than that of evaporator, the capacity of condenser was set to 5 RT. These drawing sheet representing geometrical data is shown in Fig. 2.6.

In this study, in order to replicate heat source and heat sink, water was selected as the secondary fluid of evaporator and condenser. The heating water (i.e. the secondary fluid in evaporator) in evaporator was supplied by the thermostat having 10 kW of heat capacity. The cooling water having constant mass flow rate and temperature was supplied by water pumps, 7.5 RT chiller, heat exchanger, water tank, electric heater and mass flow meter.

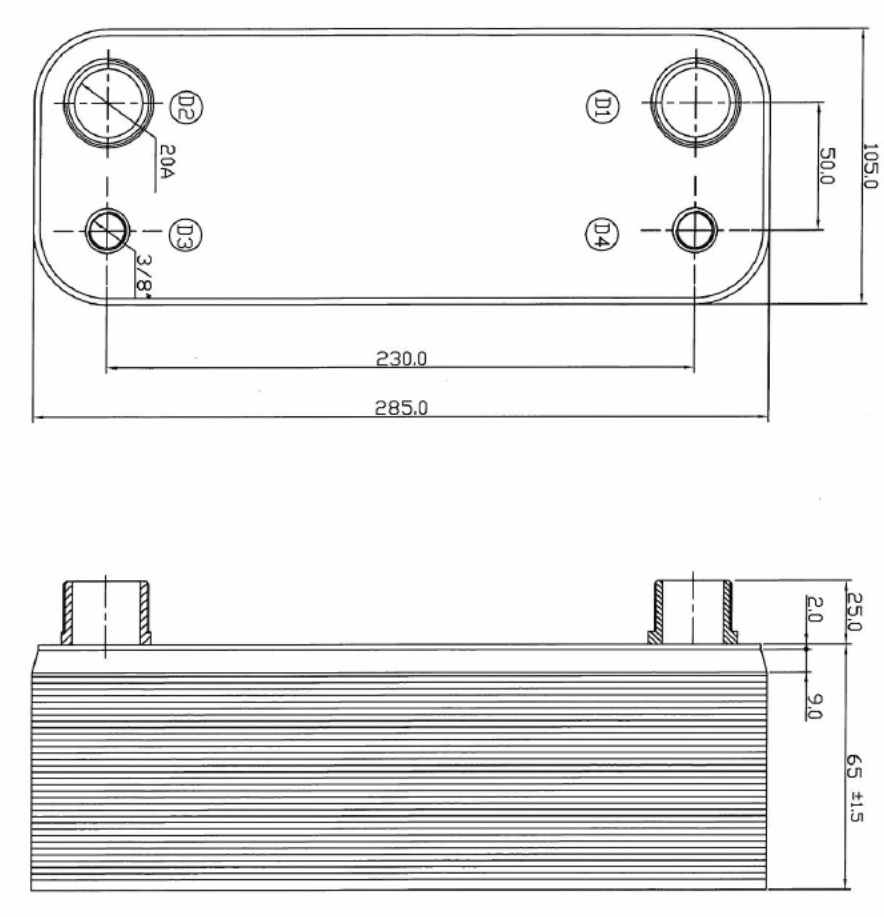

Fig. 2.6 Drawing sheet of evaporator and condenser

2.2.4 Auxiliary Components and Measurements

Oil supplying sub cycle

In order to lubricate the expander, oil supplying sub cycle consisting of oil ejector and oil separator was installed around the expander. By using ventri effect of the oil ejector located in inlet of the expander, the expander could be lubricated sufficiently. The oil ejector was manufactured by Heatech Korea Company. In outlet of the expander, oil passing thorough the expander could be recovered to the oil separator. Considering the capacity of expander, A-W 55877 made by Emerson Company was selected as the proper oil separator. Emkarate RL 100H (POE) was used as the lubricant oil.

Liquid receiver

The liquid receiver was built in inlet of the pump, in order to function as the buffer for refrigerant charge and maintain stable liquid state to prevent cavitation. In this way, it was possible to protect the system from being sensitive to the operating condition changes and the transient load. The liquid receiver was made of a stainless steel and the volume of this component was about 5 L, which was much larger than that of expected system capacity by considering the maximum volume flow rate and the properties of the working fluid in the

targeted operating conditions.

Dynamometer

To measure the frictional torque and the rotational speed of the expander, the expander was coupled with the dynamometer consisting of the torque transducer (SETech, YDNR–1K), RPM meter (Ono Sokki, MP–981) and hysteresis brake (MAGTROL, AHB-5). By using dynamometer, the generating work of the expander could be calculated by the frictional torque and the rotational speed. As shown in Table 2.4, the specific information of these instruments are represented.

Temperature measurement

Temperatures on the pump, evaporator, scroll expander, condenser and the secondary fluid were measured with T-type copper-constantan thermocouple made by the Omega Engineering.

Pressure measurement

Absolute and gauge pressure transducers were installed to acquire pressure data on the experimental system. By the gauge pressure meters (Wikai, A-10), pressures of inlet and outlet of each component could be measured. In addition,

in order to raise the accuracy of pressure data from the gauge pressure transducers, it was calibrated by the absolute pressure meter (DRUCK, PMP 1400). The characteristics of these measurements are provided in Table 2.5.

Mass flow rate measurement

In this experimental system, working fluid mass flow rate was measured with the Bronkhorst's Coriolis type mass flow rate transducer (Bronkhorst, M5X CORI-FLOW) located in outlet of the pump. Heating and cooling water mass flow rate were controlled by using the bypass circuit and were also measured by Coriolis type mass flow rate meters (Oval, CN025C-SS-322K). The specific information of these instruments is represented in Table 2.5.

Consumption work measurement and data collection

The consumption work of the pump was measured with the power meter (Yokogawa, WT-130). The data acquisition instrument (National Instruments, cDAQ-9174) receiving all of output signal from thermocouples, pressure transducers and other measurements was installed. The specifications of these components are shown in Table 2.5.

Table 2.4 Specifications of the dynamometer

Torque transducer (SETech, YDNR-1K)	
Rated capacity	0 ~ 9.807 N m
Rated Output	1.3 mV/V ± 1%
Temperature operating	0 ~ 80°C
RPM meter (Ono Sokki, MP-981)	
Measurement range	1 ~ 20 kHz (1 ~ 20,000 RPM)
Power supply used	DC 12 V ± 2 V
Current consumption	~ 40 mA
Operating temperature range	-10 ~ 70°C
Hysteresis brake (MAGTROL, AHB-5)	
Minimum torque at rated current	5.00 N m
Rated current	380 mA
Maximum rotational speed	15,000 RPM
Rated kinetic power	1,000 W (continuous, with air) 120 W (continuous, without air)

Table 2.5 Specifications of the other measurements

Gauge pressure transducer (Wikai, A-10)	
Measurement range	0 ~ 16 bar
Signal output	4 ~ 20 mA
Accuracy	± 0.l%
Absolute pressure meter (DRUCK, PMP 1400)	
Measurement range	0 ~ 100 bar
Accuracy	± 0.15%
Mass flow rate transducer (Bronkhorst, M5X CORI-FLOW)	
Maximum mass flow rate	600 kg h^{-1}
Minimum mass flow rate	20 kg h^{-1} (liquid) 50 kg h^{-1} (gas)
Accuracy	± 0.2% (liquid) ± 0.5% (gas)
Power meter (Yokogawa, WT-130)	
Measurement range	0 ~ 600 V, 0 ~ 300 A
Accuracy	± 0.2% (voltage) ± 0.3% (current)

Chapter 3. Experimental Results and Discussions

3.1 Experimental Procedure and Conditions

3.1.1 Data Reduction

The heat rate of evaporator and condenser can be evaluated from mass flow rate, the temperature difference and specific heat of the secondary fluids (i.e. water) of heat exchangers. Also, it can be calculated from mass flow rate and the enthalpy difference. Because of stable values and fast response according to changing experimental conditions, it is most reliable to evaluate heat rate from the properties of the secondary fluids. The specific heat and the enthalpy difference of water are calculated based on the measured temperature and pressure by using NIST Refprop ver. 9.1 [19] and the heat rate of heat exchangers is defined as below.

$$\dot{Q}_{eva} = \dot{m}_{w,eva} \cdot C_{p,w} \cdot (T_{in,w} - T_{out,w}) = \dot{m}_{w,eva} \cdot (h_{in,w} - h_{out,w})$$

$$\dot{Q}_{cond} = \dot{m}_{w,cond} \cdot C_{p,w} \cdot (T_{out,w} - T_{in,w}) = \dot{m}_{w,cond} \cdot (h_{out,w} - h_{in,w})$$

The generating work of the expander can be calculated from the frictional torque and the rotational speed of the expander shaft. These values are evaluated based on measured frictional torque and rotational speed by using dynamometer consisting of frictional torque transducer, RPM sensor and hysteresis brake. The equation of the generating work of the expander are shown as below.

$$\dot{W}_{\exp} = 2 \cdot \pi \cdot T_f \cdot RPM_{\exp} / 60$$

The thermal efficiency of the overall system is the ratio between heat input of evaporator and net power of the overall system. The consumption work of the pump was measured by power meter.

$$\eta_{th} = \frac{\dot{W}_{\exp} - \dot{W}_{pump}}{\dot{Q}_{eva}}$$

The degree of super heat (DSH) is defined as the difference of the super-heated vapor's temperature and the saturation temperature corresponding the actual pressure. Likewise, the degree of sub cool (DSC) is also calculated from the difference between sub-cooled liquid's temperature and the saturation

temperature. In this study, DSH of the inlet and outlet of the expander and DSC of the inlet of the pump were calculated from measured temperature and pressure by using NIST Refprop ver. 9.1 [19].

$$DSH = T_{superheat} - T_{sat}$$

$$DSC = T_{sat} - T_{subcool}$$

By the exergy analysis, it is possible to investigate how close the actual performance approaches to the ideal process and the causes of thermodynamic losses. The exergy destruction of each component can be calculated by using the exergy balance of the system at the steady state. The equations of the exergy analysis are defined as below.

$$\dot{E} = \dot{m} \cdot \{h - h_0 - T_0 \cdot (s - s_0)\}$$

$$D_{eva} = (\dot{E}_{in,h,w} - \dot{E}_{out,h,w}) - (\dot{E}_{out,r,eva} - \dot{E}_{in,r,eva})$$

$$D_{cond} = (\dot{E}_{in,c,w} - \dot{E}_{out,c,w}) - (\dot{E}_{out,r,cond} - \dot{E}_{in,r,cond})$$

$$D_{exp} = (\dot{E}_{in,exp} - \dot{E}_{out,exp}) - \dot{W}_{exp}$$

$$D_{pump} = (\dot{E}_{in,pump} - \dot{E}_{out,pump}) + \dot{W}_{pump}$$

$$\eta_{exg} = \frac{\dot{W}_{\exp} - \dot{W}_{pump}}{\dot{E}_{in,h,w} - \dot{E}_{out,h,w}}$$

3.1.2 Experimental Conditions

In this study, the ORC applied to low temperature heat source below 100°C (e.g. waste heat of PEMFC, waste heat of beverage/food industry and so on) was investigated. The range of these waste heat temperature is usually from 60°C to 80°C. Therefore, in order to replicate these low-grade heat source, the inlet temperature of the secondary fluid of evaporator was set to 70°C. To make experimental system to operate stably, the inlet temperature of water of condenser was set to 15°C, which is a little lower than ordinary temperature (i.e. 20°C). Waster was selected as the secondary fluid of evaporator and condenser.

Furthermore, varying refrigerant charge amount of the overall system, preliminary experiments were conducted for finding the optimal charge amount where the maximum generating work occurred. When thermodynamic cycle produces work from heat reservoirs with infinite heat capacity, it is most important to generate the maximum work with low-grade heat source [22]. Fig. 3.1 shows generating work of the expander with respect to refrigerant charge amount. As a result, 8.50 kg was selected as the optimal charge amount.

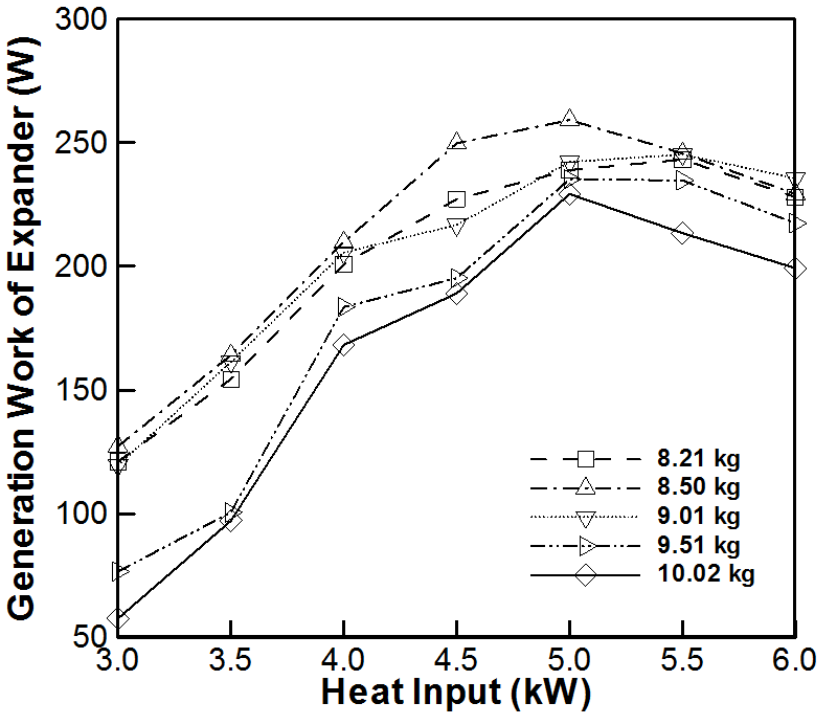

Fig. 3.1 Generating work of the expander with regard to heat input (i.e. heat rate of evaporator) varying refrigerant charge amount

Other experimental parameters were the same values shown in Table 3.1. The experiments were conducted with varying the rotational speed of the gear pump. At the same rotational speed of the pump, increasing the frictional load of the expander shaft by using dynamometer, the performance of the experimental system was investigated.

Table 3.1 Experimental conditions

Parameter	Unit	Value
Inlet temperature of water in evaporator	^{o}C	70
Mass flow rate of water in evaporator	g/s	121.67
Inlet temperature of water in condenser	^{o}C	15
Mass flow rate of water in condenser	g/s	300
Pump frequency	Hz	20~34
Refrigerant charge amount	kg	8.50

3.2 Performance of the Gear Pump

In this study, T-series gear pump made by Tuthill Company was used as the refrigerant pump. This gear pump had been usually used for supplying the lubricant oil or the conventional refrigerant. Therefore, it was necessary to investigate the performance of the gear pump using R245fa as the working fluid. For these objectives, varying the frictional load of the expander, the performance variation with regard to pressure ratio and mass flow rate in the various rotational speed of the gear pump.

Fig. 3.2 shows mass flow rate of the gear pump with regard to pressure ratio and pump frequency. Like the performance of the general pump, the mass flow rate becomes smaller according to pressure ratio is enlarged. In addition, at the same pressure ratio, as the frequency of the pump increases, the mass flow rate increases. Overall, increasing the pump frequency, both of pressure ratio and mass flow rate were enlarged. The mass flow rate ranged from 11 g/s to 35 g/s and the range of the discharge pressure was from 2.8 bar to 4.6 bar. Furthermore, due to lower kinetic viscosity than that of the conventional fluids used to gear pump, the slope of declining mass flow rate with increasing pressure ratio was larger than that of the traditional ones.

The specific pumping work with regard to pressure ratio and pump frequency is presented in Fig. 3.3. The most dominant tendency is that as

pressure ratio increases, the specific consumption work of the pump is enlarged sharply. However, in relatively large pump frequency, the changing aspect of the specific work is alleviated slightly. The maximum specific work of the pump is 5.35 kJ/kg and the minimum specific work is 1.61 kJ/kg.

Fig. 3.4 shows the experimental results of the consumption work of the gear pump with various mass flow rate and pressure ratio. It is confirmed that the pumping work of the system is determined by pressure ratio in relatively low pressure ratio (i.e. less than 2.8). In other words, as the mass flow rate increases, the consumption work of the pump is almost constant. The maximum consumption work of the pump is 130 W and the minimum work is 50 W. Furthermore, the DSC of the inlet of the gear pump was maintained at 7~8^{o}C and the isentropic efficiency of the pump was estimated at 10~20%.

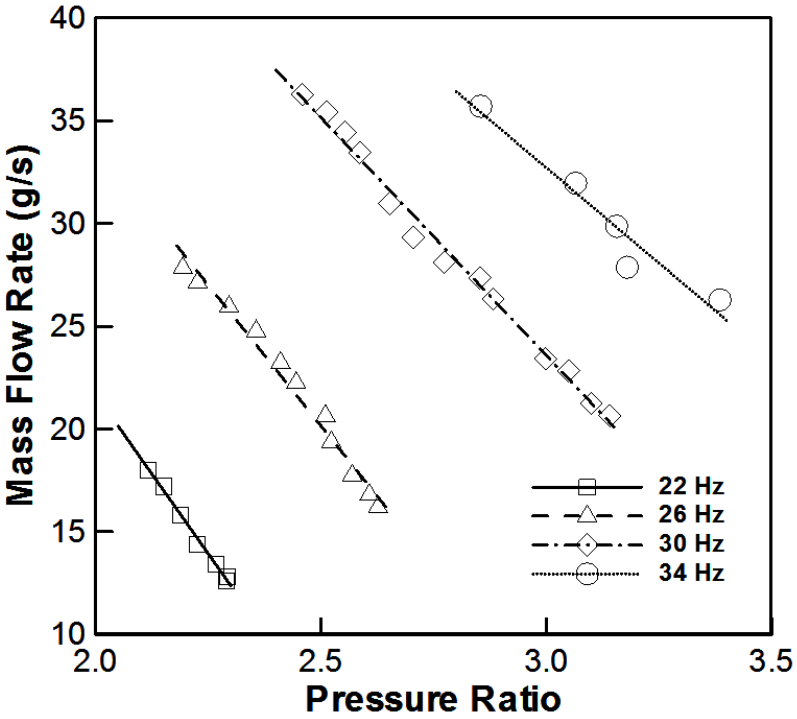

Fig. 3.2 Mass flow rate of the pump
with respect to pressure ratio varying pump frequency

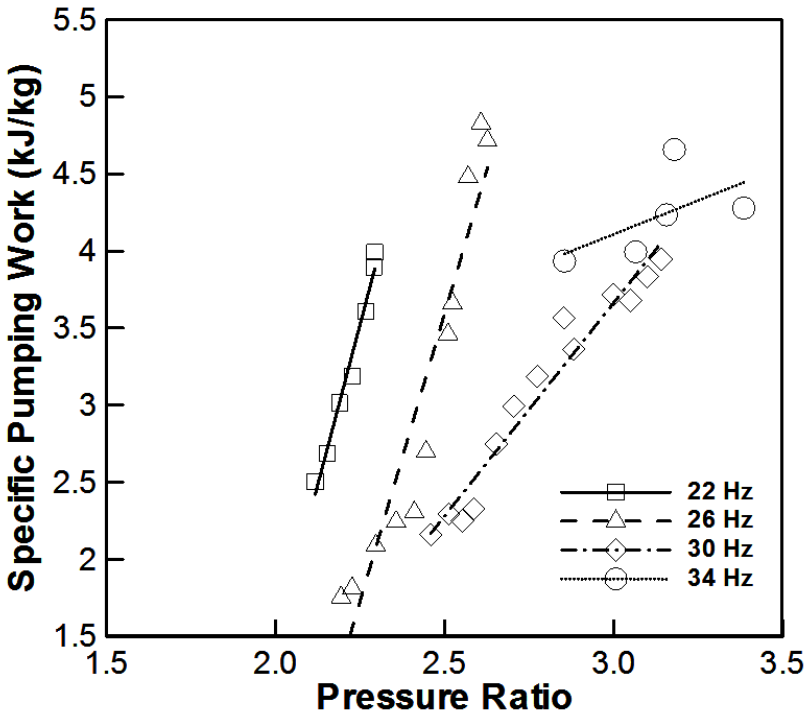

Fig. 3.3 Specific pumping work variation with pressure ratio and pump frequency

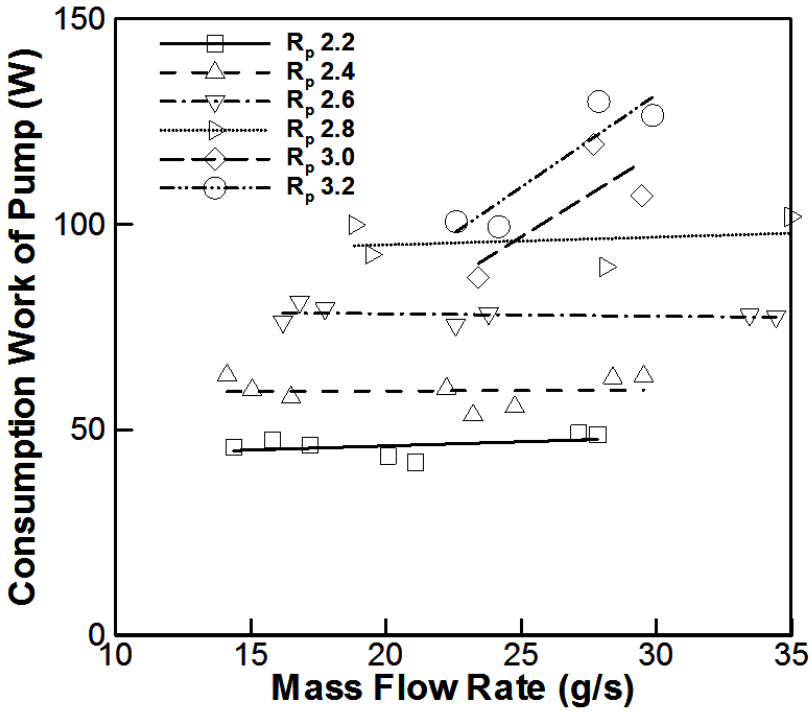

Fig. 3.4 Consumption work of the pump
with regard to mass flow rate and pressure ratio

3.3 Performance of the Scroll Expander

In this study, we produced the scroll expander with scroll rotor divided from vapor scroll compressor, which was used for refrigeration system. Because there hasn't been experimental study about expander applied to low-grade heat source below 70°C and 6 kW, it was essential to make a close investigation of the performance of the scroll expander. By utilizing dynamometer coupled to the expander shaft, we changed the frictional load on the expander and measured the frictional torque and the rotational speed of the expander. Then, the generating work of the expander was calculated by these measured values. In this way, the performance of the expander was examined in the 1000 RPM to 3800 RPM range on the rotational speed of expander.

Fig. 3.5 shows the generating work of the expander with various pressure ratio and the rotational speed of the expander. Generally, it is confirmed that the generating work of the expander is enlarged according to pressure ratio increases. At the same pressure ratio, the general tendency is that as the rotational speed of the expander, the generating work of the expander is elevated. The maximum generating work of the expander is about 360 W at 2400 RPM and pressure ratio 2.6.

These phenomena can be explained by experimental data shown in Fig. 3.6. This picture shows the relation between the rotational speed and frictional

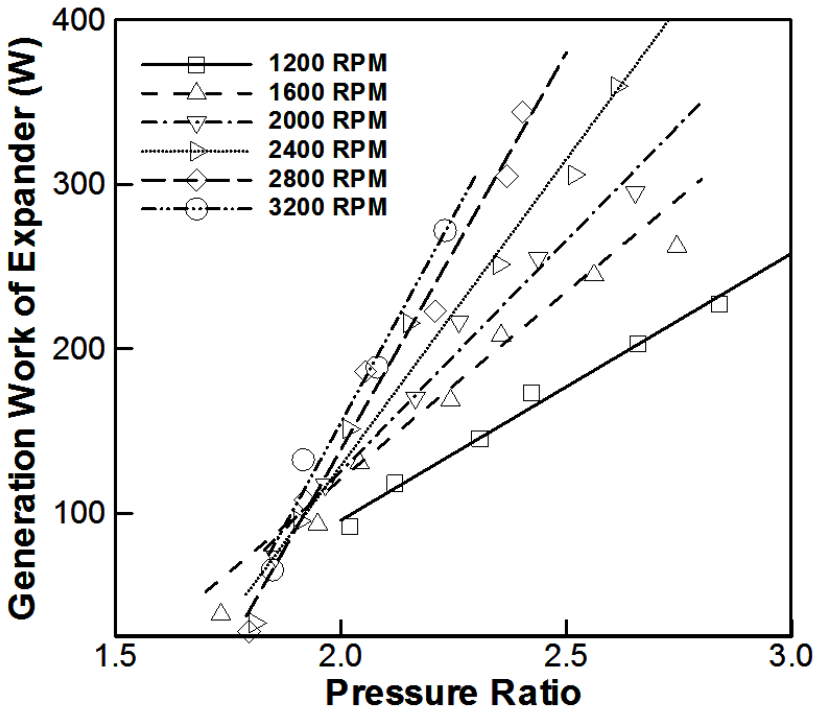

Fig. 3.5 Generating work of the expander with regard to pressure ratio varying rotational speed of the expander

torque of the expander with varying expansion ratio. Generally, as the rotational speed increases, the frictional torque tends to decline slightly. Although, because the generating work of the expander was calculated by multiplying these values, it is possible to exhibit inflection point in the performance curve, the generating work of the expander is enlarged according to the rotational speed increases at the same pressure ratio. Since the decreasing ratio of the frictional torque is relatively lower than increasing ration of the rotational speed.

The results of the generating work of the expander variation with respect to various mass flow rate and pressure ratio are shown in Fig. 3.7. The most evident changing aspect of the generating work is that as the pressure ratio of the expander increases, the variation of the generating work becomes steeper. In addition, at the same pressure ratio, as the mass flow rate increases, the generating work of the expander also increases. Because the specific generating work of the expander tends to be determined by the expansion ratio. However, in low pressure ratio (i.e. pressure ratio 1.8), changing aspect of the generating work opposed to the general tendency is observed. The generating work of the expander deceases slightly according to the mass flow rate is enlarged.

Fig. 3.8 shows the relation between DSH of the inlet of the expander and the generating work of the expander with various heat inputs (i.e. heat capacity of heat source). As the heat capacity of the heat source is enlarged, the variation

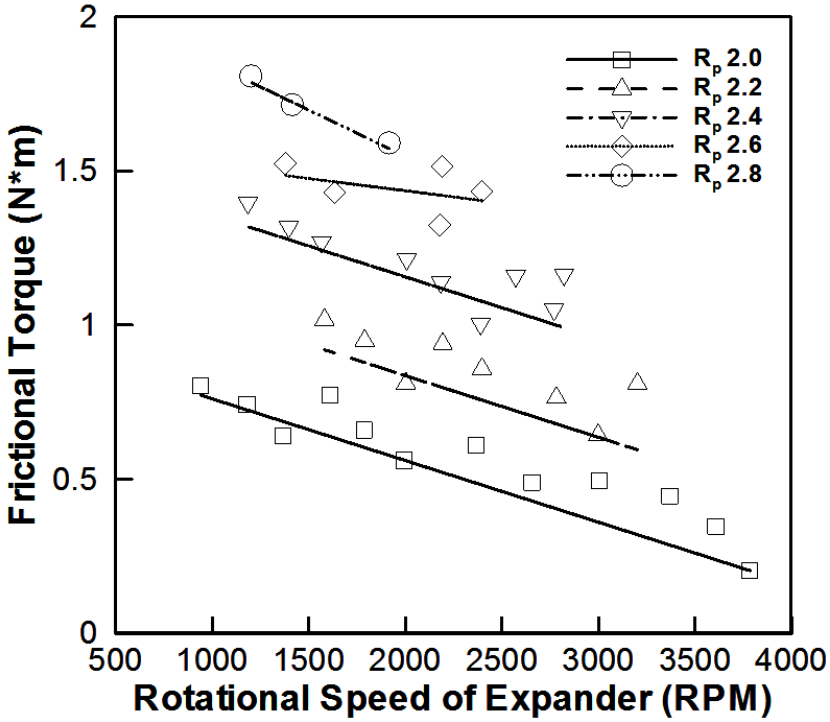

Fig. 3.6 Frictional torque of the expander
with regard to rotational speed and pressure ratio

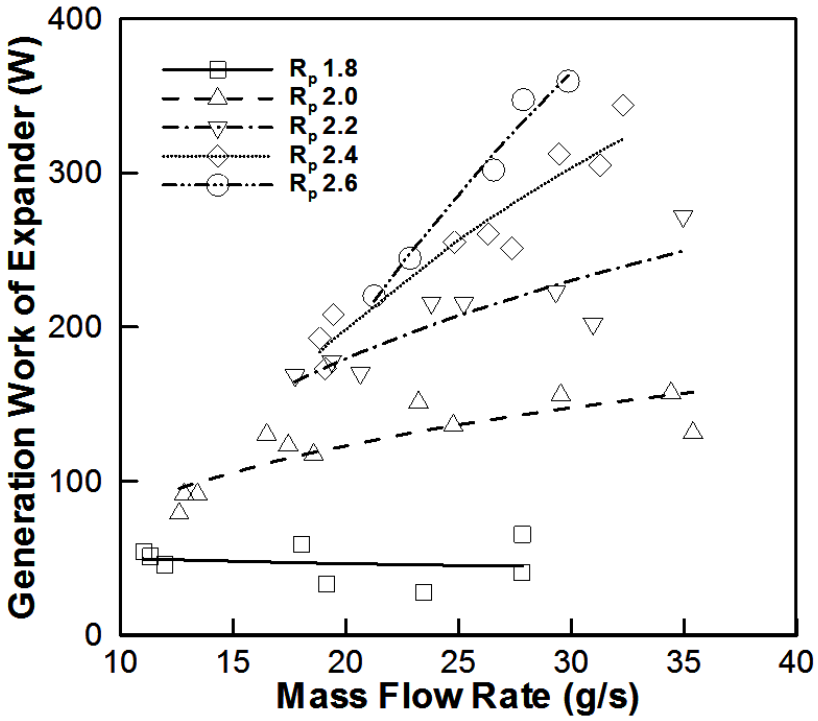

Fig. 3.7 Generating work variation of the expander with mass flow rate and pressure ratio

of the generating work of the expander changes dramatically. In general, it is verified that the lower DSH has the larger generating work of the expander and the small difference of the DSH makes a large change of the generating work.

For the several rotational speed of the expander, we investigated the isentropic efficiency of the expander by using the experimental results and refrigerant properties from NIST Refprop ver. 9.1. Fig. 3.9 shows the variation of the isentropic efficiency of the expander with regard to pressure ratio and rotational speed of the expander. The most significant tendency is that as the pressure ratio increases, the isentropic efficiency becomes large. Especially, in low pressure ratio (less than 2.0), the isentropic efficiency is very low. Which means that mechanical or thermodynamic losses affect considerably the performance of the expander. Because the scroll expander has the optimal pressure ratio corresponding to the fixed built-in volumetric ratio [23]. To be specific, when pressure ratio doesn't match the optimal pressure ratio, over or under expansion losses occur. Furthermore, it is also verified that the higher rotational speed of the expander generally causes the lower isentropic efficiency. Because the higher the rotational speed of the expander, the more the additional losses such as leakage, friction losses and so on [14]. The maximum isentropic efficiency is 68.8% at 2200 RPM and pressure ratio 2.6.

The variation of isentropic efficiency of the expander with various DSH

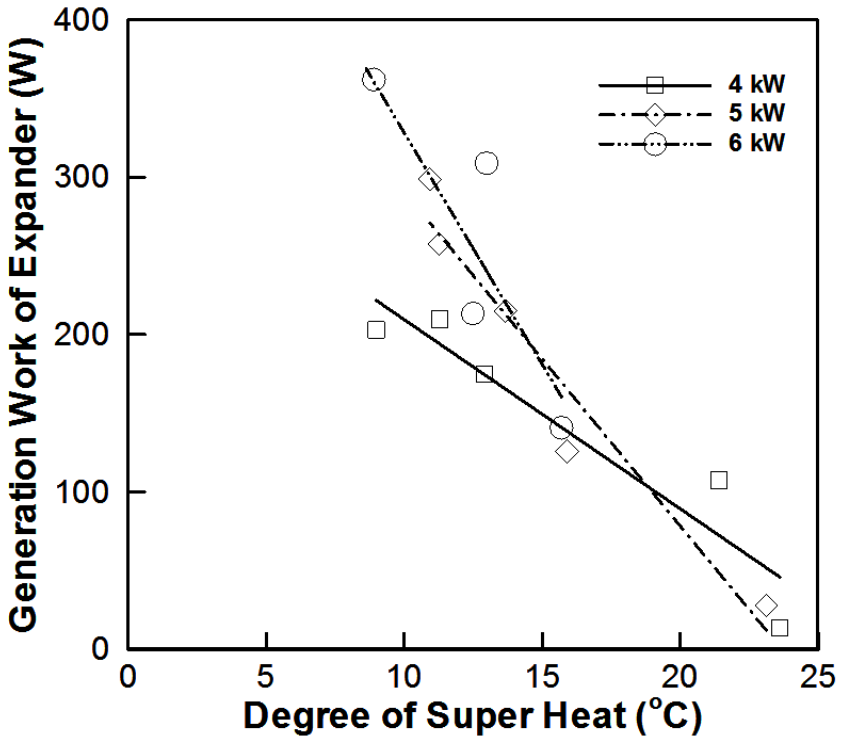

Fig. 3.8 Generating work of the expander with respect to DSH and heat input

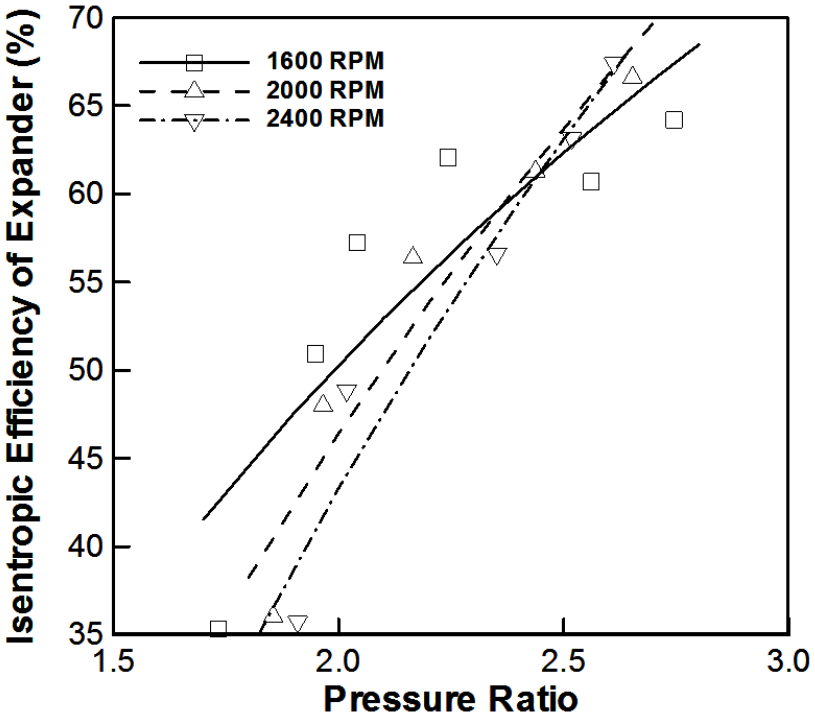

Fig. 3.9 Isentropic efficiency variation of the expander with pressure ratio and rotational speed

and heat inputs is presented in Fig. 3.10. Like the relation of the generating work and DSH, as the heat capacity of the heat source becomes large, the changing aspect of the generating work of the expander occurs significantly. To be specific, it is confirmed that the lower DSH causes efficient operating of the expander and the small difference of the DSH makes a large change of isentropic efficiency of the expander. Therefore, maintaining the low DSH may be significant factor to efficient operating of the expander.

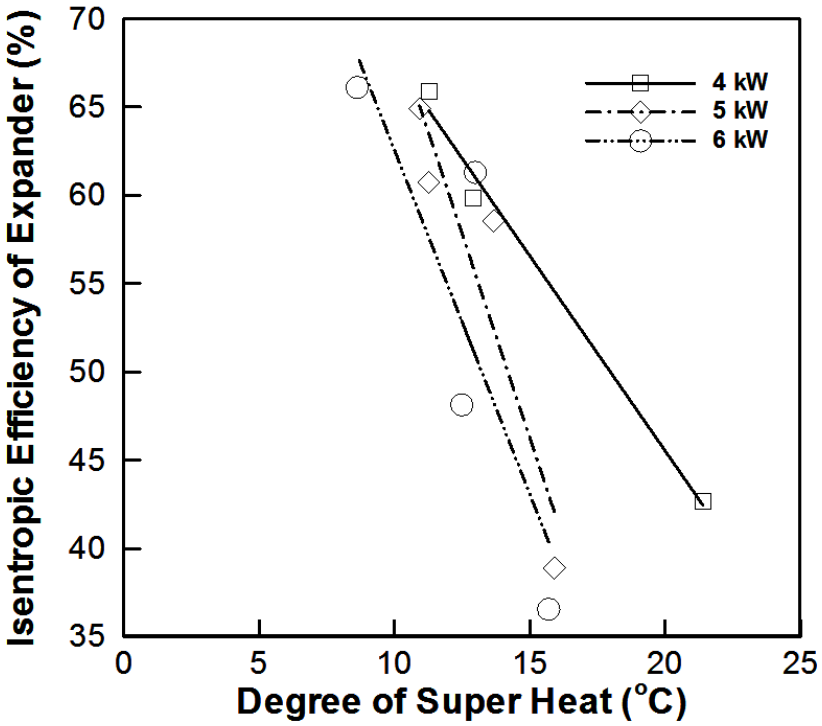

Fig. 3.10 Isentropic efficiency of the expander with respect to DSH and heat input

3.4 Performance of the Overall System

In this part, the performance of the overall system is analyzed by the first and second law of thermodynamics. By using the thermos-physical equations above-mentioned in part 3.1.1, the detailed and complete thermodynamic analysis was conducted.

3.4.1 Energetic Analysis of the Overall System

In all of the thermodynamic cycle studies, the first law analysis is usually the initial basis research viewpoint. The experimental results were investigated, in terms of the effects of some key parameters such as evaporating pressure, condensing pressure, mass flow rate, pump frequency, heat rate of evaporator and so on. These parameters influence the temperature and pressure of the system and the performance of the system is consequently determined by these variables. The performance evaluating factors were mainly the net power and the thermal efficiency of the overall system.

Fig. 3.11 shows the overall system net power with varying evaporating pressure and mass flow rate. Generally, it is verified that as the evaporating pressure increases, the overall system net power tends to be enlarged. In addition, the variations of the net power change more significantly according

to mass flow rate of the system increases. Because as shown in Fig. 3.4 and Fig 3.7, the difference of the consumption work of the pump is usually smaller than that of the generating work of the expander at the same pressure ratio.

The overall system net power variation with various evaporating pressure and pump frequency is presented in Fig. 3.12. The most significant tendency is that the optimal operating condition of each pump frequency exists. Because the generating work curve of the expander exhibits the maximum point which is caused by increase of the frictional torque and decrease of the rotational speed of the expander with respect to elevating evaporating pressure. In addition, in low evaporating pressure region, there are operating conditions which should be avoided to obtain the benefits of operating ORC. The maximum net power is 234.36 W at 34 Hz of pump frequency and 4.4 bar of evaporating pressure.

As shown in Fig. 3.13, there are also the optimal operating conditions of each pump frequency with respect to various heat inputs. As the pump frequency increases, the heat addition rate of evaporator from heat source is generally larger due to the large mass flow rate. The maximum net power is presented at 6.07 kW of heat input.

Fig. 3.14 and Fig. 3.15 show the variation of the overall system net power with respect to evaporating pressure and DSH varying heat inputs, respectively. The common tendency of these results is that the changing aspects of the net

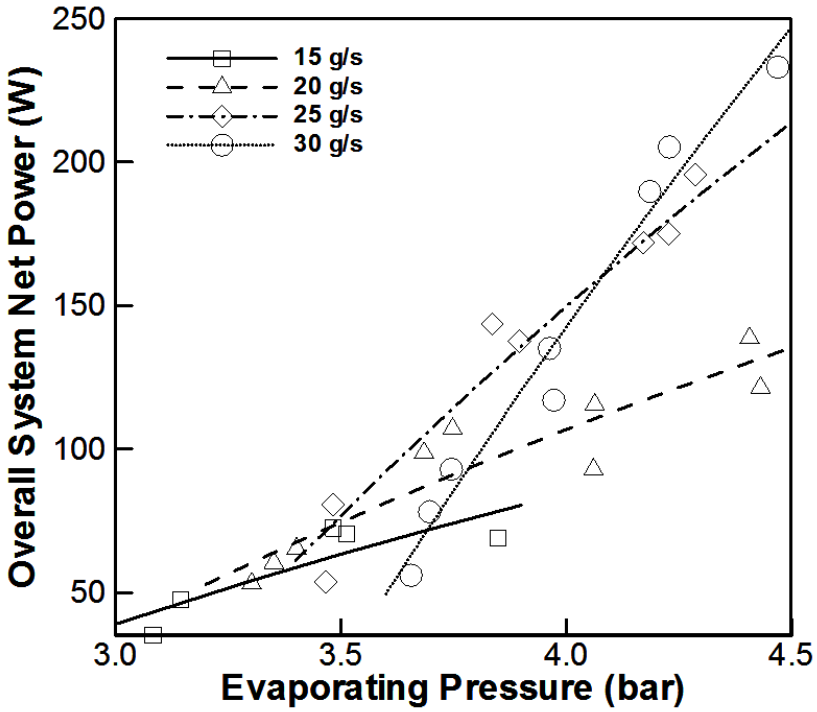

Fig. 3.11 Overall system net power variation with evaporating pressure and mass flow rate

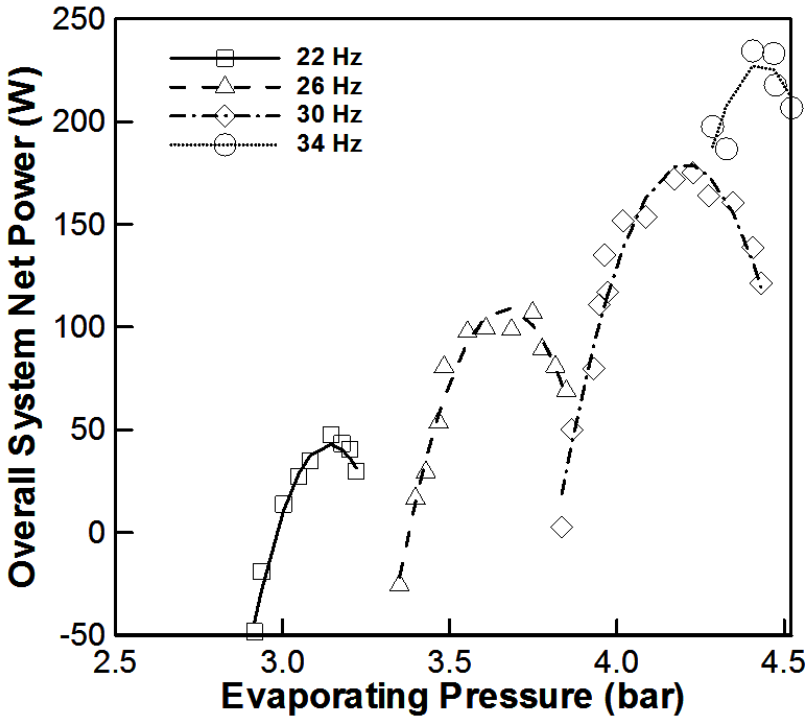

Fig. 3.12 Overall system net power with regard to evaporating pressure varying pump frequency

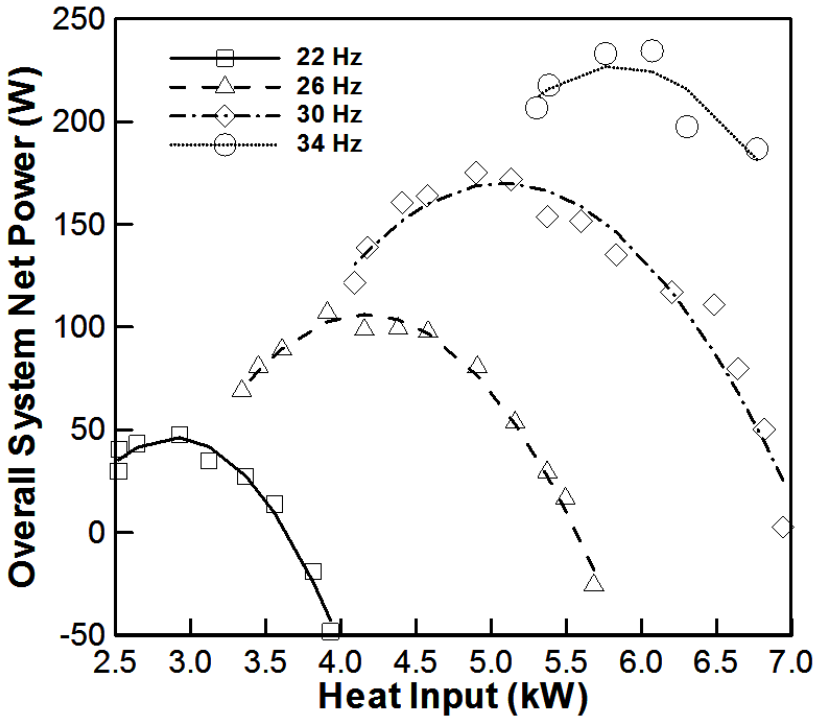

Fig. 3.13 Overall system net power with respect to heat input varying pump frequency

power with regard to evaporating pressure are presented steeper, as heat inputs from heat source increase. However, the effect of each operating parameter to the net power are presented differently. The increase of evaporating pressure causes to increase the overall net power and as the DSH of the inlet of the expander is enlarged, the net power decreases dramatically. Because the generating work and the isentropic efficiency of the expander tend to decline owing to increasing DSH.

The variation of the overall system thermal efficiency with various evaporating pressure and pump frequency is presented in Fig. 3.16. Unlike the general thermodynamic principles, the thermal efficiency is diminished according to the evaporating pressure increases. Because, as referred to earlier in part 3.2 and 3.3, the consumption work of the pump is enlarged as the pressure ration increases and the generating work curve of the expander exhibits the maximum point at a certain operating condition. In addition, like the net power variation, there are region where the thermal efficiency of the overall system is under zero. The maximum thermal efficiency is 4.07% at 4.29 bar of the evaporating pressure and 32 Hz of the pump frequency.

Fig. 3.17 shows the overall thermal efficiency with respect to heat inputs and pump frequency. The changing aspect of the thermal efficiency is similar to the overall system net power variation presented in Fig. 3.13. There are also

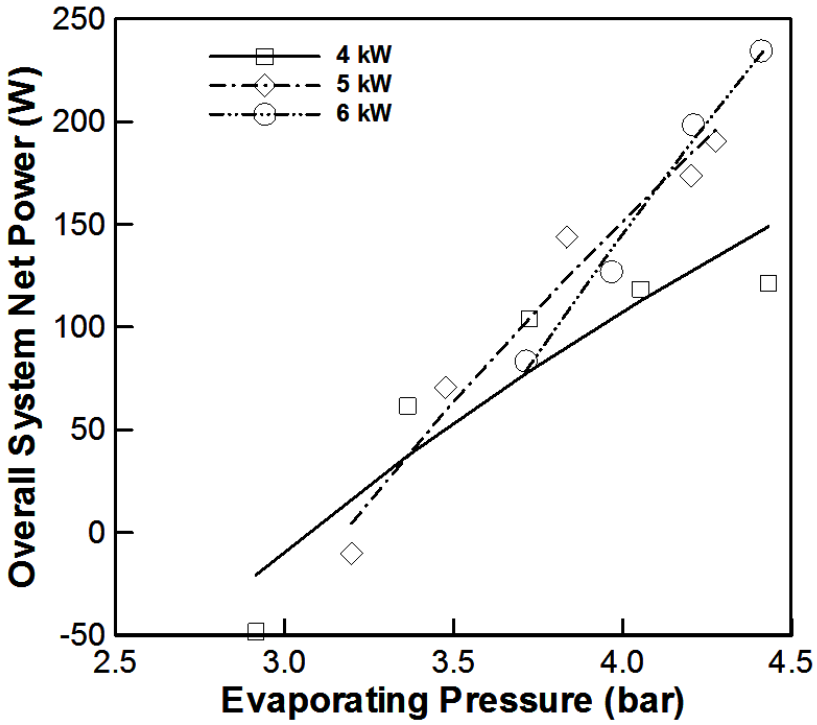

Fig. 3.14 Overall system net power variation with evaporating pressure and heat input

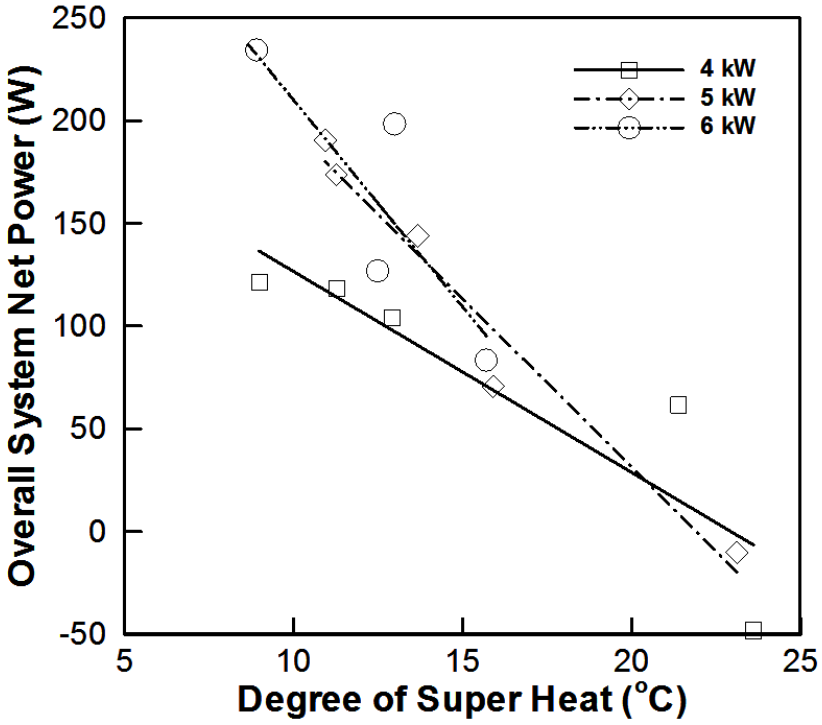

Fig. 3.15 Overall system net power with regard to DSH varying heat input

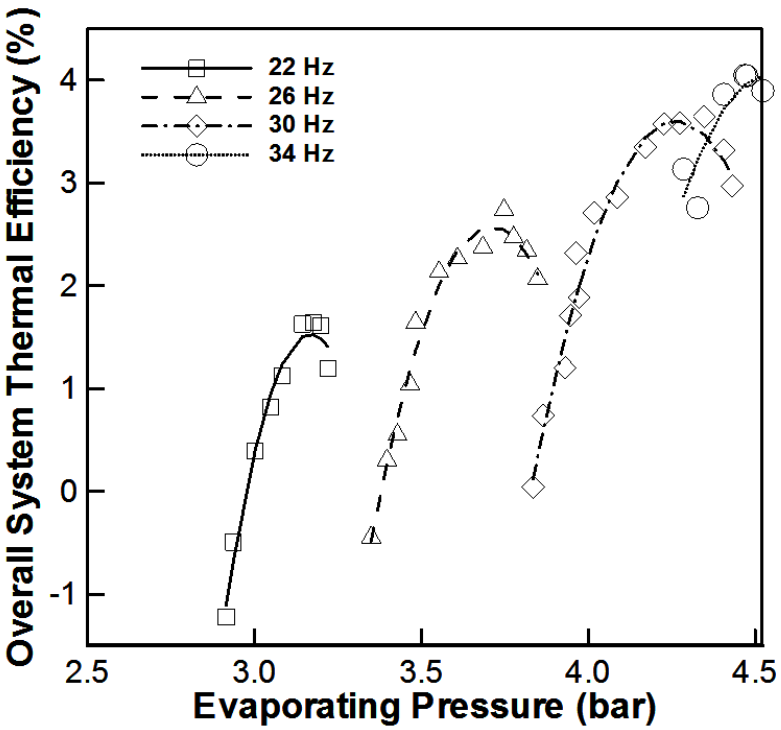

Fig. 3.16 Overall system thermal efficiency variation with evaporating pressure and pump frequency

the optimal operating conditions of each pump frequency with regard to heat inputs. The general tendency is that the heat addition rate of evaporator from heat source is larger according to the pump frequency is enlarged. Unlike the maximum point of the overall net power, the maximum thermal efficiency is presented at 4.80 kW of heat input.

Fig. 3.18 and Fig. 3.19 show the overall system thermal efficiency with regard to evaporating pressure and DSH varying heat inputs, respectively. The general tendency of the thermal efficiency with various evaporating pressure and DSH is considerably similar to that of the overall net power. However, the changing aspect of the thermal efficiency variation rate with respect to evaporating pressure and DSH is presented less steeply than that of the net power variation.

The generating (or consumption) work variation with various evaporating pressure varying heat inputs is shown in Fig. 3.20. Generally, as the evaporating pressure increases, the generating work of the expander and the consuqmption work of the pump are enlarged. Furthermore, the larger the heat addition rate of the evaporator, the larger the generating (or consumption) work of the system components. Because the mass flow rate of the overall system increases according to the heat input is enlarged. In addition, when the heat input is 5 kW, there is the operating region where the net power of the overall system falls to

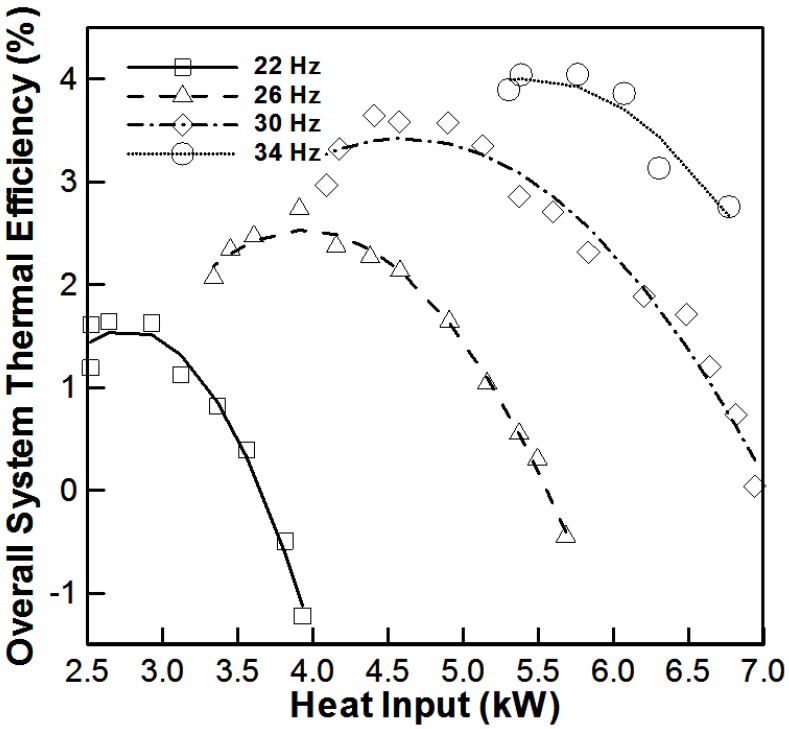

Fig. 3.17 Overall system thermal efficiency
with respect to heat input and pump frequency

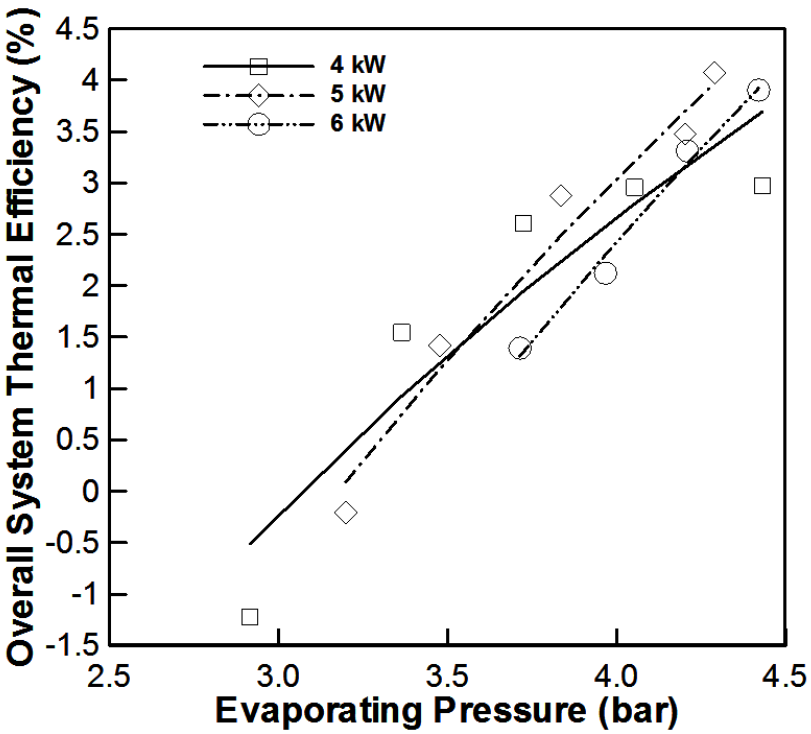

Fig. 3.18 Overall system thermal efficiency variation with evaporating pressure and heat input

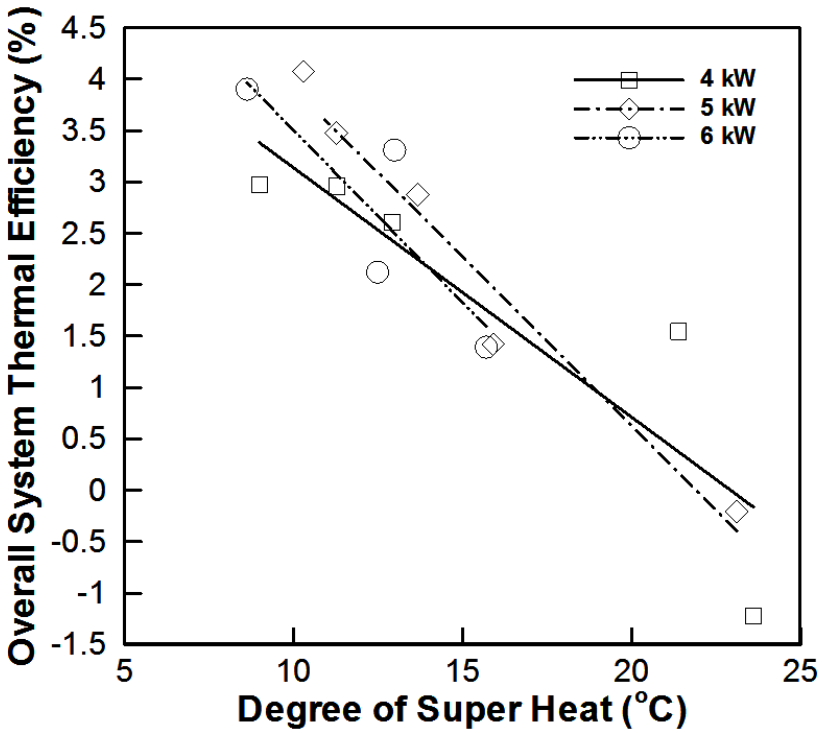

Fig. 3.19 Overall system thermal efficiency
with respect to DSH varying heat input

below zero. However, at 6 kW of the heat input, in all of the operating conditions, it is verified that obtaining the benefits of operating ORC applied to low-grade heat source below 100^{o}C is feasible.

Fig 3.21 and Fig 3.22 show the T-s diagram and the p-h diagram with various heat source capacities. The experimental results used in these diagrams are obtained at the optimal operating conditions where the maximum net powers are under each heat addition rate of the evaporator. The most evident tendency is that the heat source capacity doesn't seem to have relation the condensing temperature (or pressure) and the evaporating temperature (or pressure) increases slightly according to the heat input is enlarged. Because the mass flow rate is determined by only the heat source capacity and the higher evaporating pressure can produce the larger generating work of the expander. The optimal evaporating pressures are 4.08 bar, 4.31 bar and 4.47 bar and the mass flow rates are 18.87 g/s, 25.39 g/s and 31.47 g/s, respectively. The condensing pressures are usually observed at about 1.5 bar. Furthermore, the DSH of the inlet of the expander tends to decrease, as the heat input increases. Since, because of the fixed size of the heat exchangers, as the heat source capacity is enlarged, the mass flow rate increases and the inlet temperature of the expander decreases.

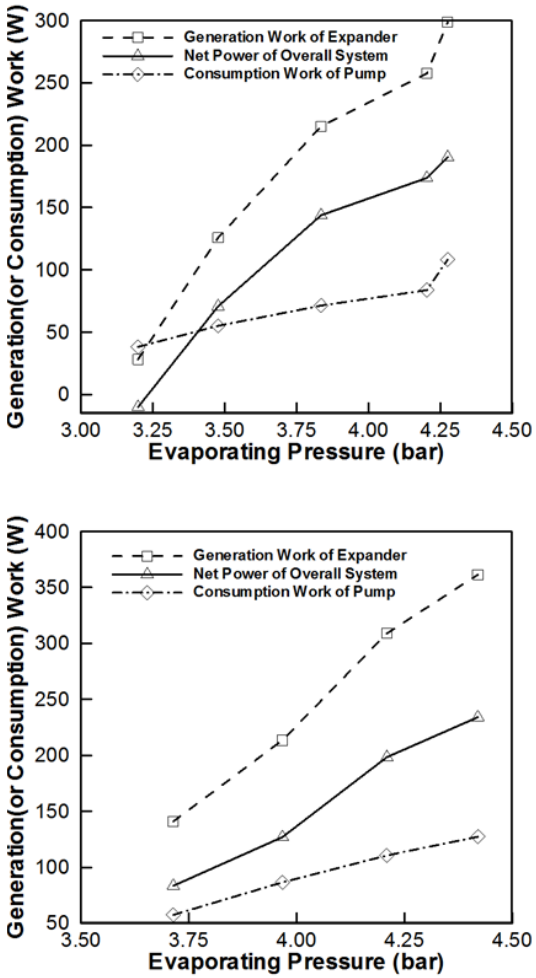

Fig. 3.20 Generation (or consumption) work variation with evaporating pressure varying heat input (5 kW, 6 kW)

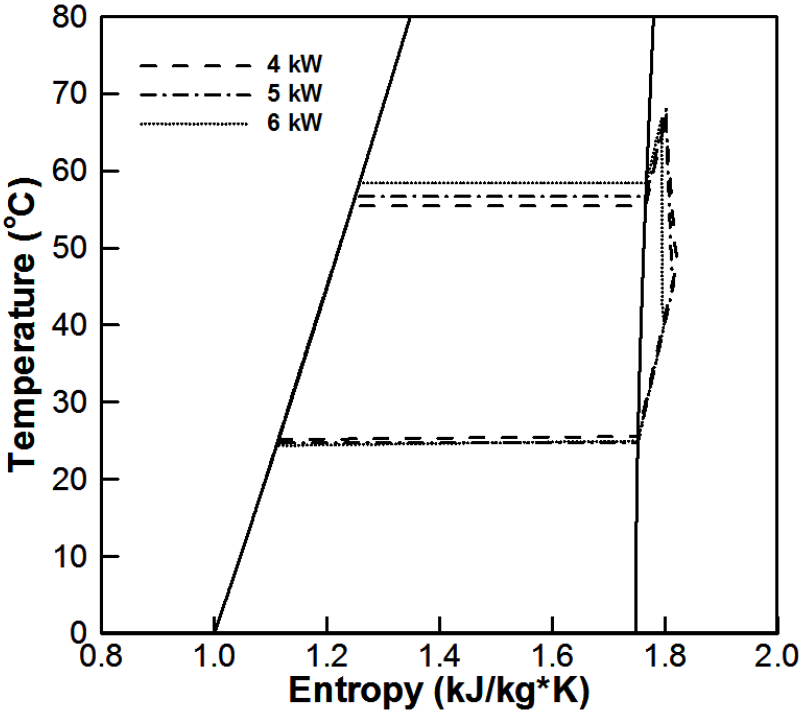

Fig. 3.21 T-s diagram of the organic Rankine cycle with respect to heat input

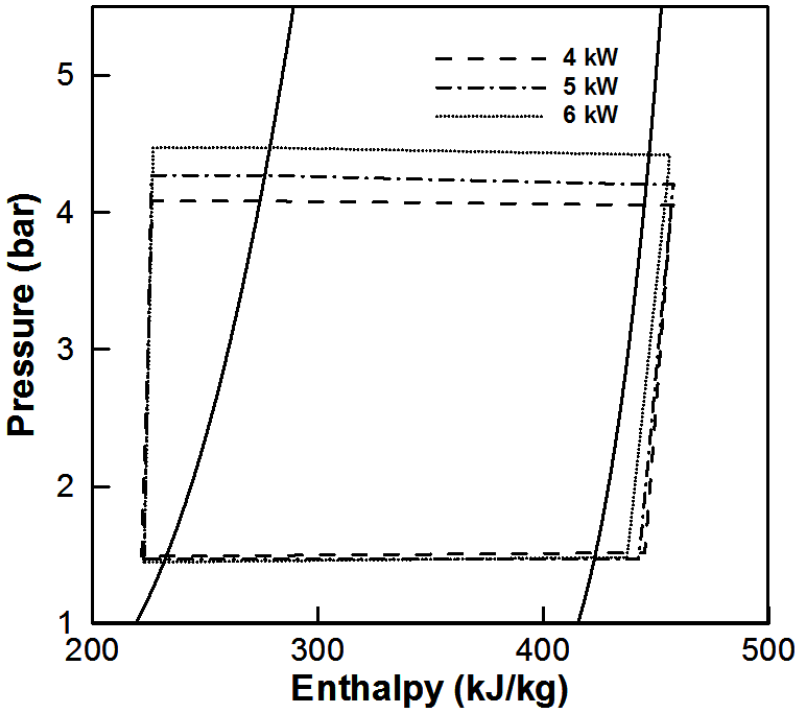

Fig. 3.22 P-h diagram of the organic Rankine cycle with regard to heat input

3.4.2 Exergetic Analysis of the Overall System

In this section, in order to investigate the irreversibility of the system components and the overall system, the exergy efficiency and exergy destruction of the system was calculated. The exergy efficiency means how close the experimental system approaches the ideal system which can produce the maximum useful work obtained from the system reaching equilibrium with the heat reservoir. Furthermore, by using exergy analysis, the thermodynamic losses can be verified more easily than energy analysis.

Fig 3.23 shows the exergy efficiency with respect to the evaporating pressure and heat input. The most general tendency is that the exergy efficiency is enlarged according to the evaporating pressure increases. Since, as shown in Fig. 3.9, due to mismatch between the actual pressure ratio and the optimal pressure ratio, the expander can’t operate efficiently in low pressure ratio. In addition, in all operating conditions, the isentropic efficiencies of the pump are estimated at 10~20%, which means that the pump operated very inefficiently. For these several reasons, it is verified that the overall system can’t operate efficiently in low evaporating pressure and improving the system components is necessary.

The exergy destruction variation of the system components and overall system with various evaporating pressure and heat inputs is shown in Fig. 3.24.

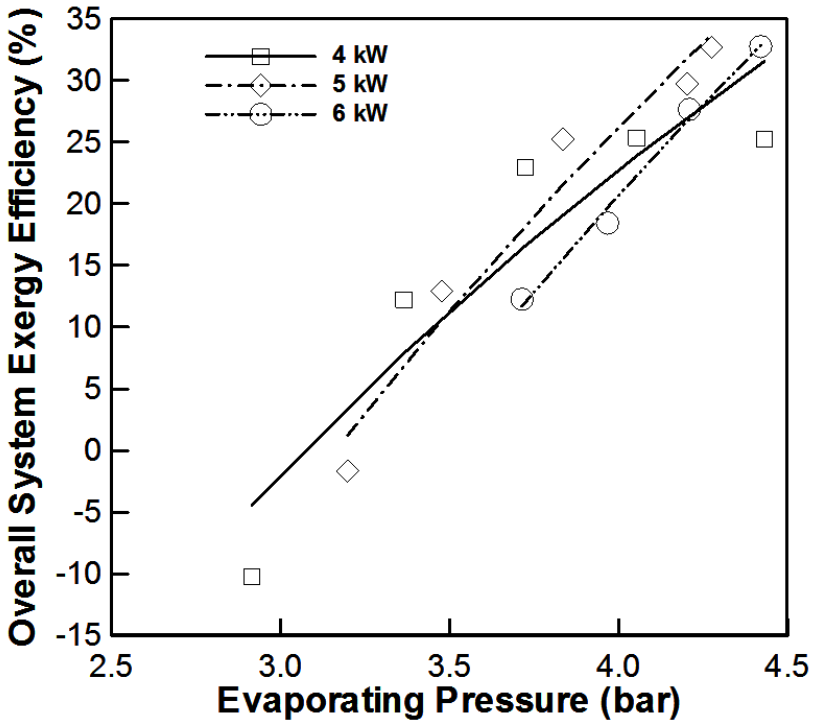

Fig. 3.23 Overall system exergy efficiency variation with evaporating pressure and heat input

Corresponding to the results of the exergy efficiency, the exergy destruction of the overall system tends to decrease according to the evaporating pressure increases. Since, the system components except for the pump can operate more efficiently in high evaporating pressure. Furthermore, in all heat source capacities, the exergy destruction of the expander is the largest, which means that the improvement of the expander is most important for operating ORC applied to low temperature heat source. Especially, compared with other components, the changing aspect of the pump is presented differently. Therefore, in order to improve the performance of the ORC applied to low temperature heat source below 100^{o}C, it is most essential to mitigate the irreversible process of the expander and the pump.

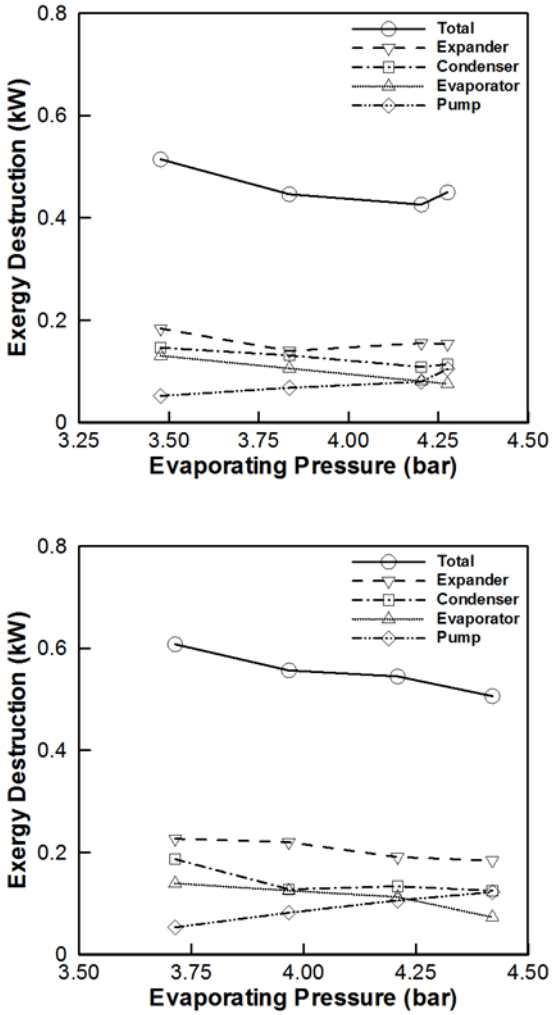

Fig. 3.24 Variation of system components and total exergy destruction with regard to evaporating pressure at different heat inputs (5 kW, 6 kW)

Chapter 4. Conclusion

In this study, in order to provide meaningful information and better understanding on the ORC, the performance of the ORC applied to heat source of 70°C and heat sink of 15°C was investigated.

By conducting the preliminary experiments, the effects of the refrigerant charge amount was investigated for 8.21 kg to 10.02 kg of the charge amount. The generating work curve of the expander variation with regard to refrigerant charge amount exhibited the maximum point at 8.50 kg and this charge amount was selected as the optimal charge amount for this study.

The ORC applied to low temperature heat source below 100°C was analyzed for some key parameters such as evaporating pressure, heat input, DSH and so on. Consequently, the maximum net power of the overall system was 234.36 W at the evaporating pressure of 4.41 bar and heat input of 6.07 kW. The thermal efficiency of this operating condition was 3.86%. Furthermore, at the evaporating pressure 4.29 bar and heat addition rate of 4.80 kW, the maximum thermal efficiency was 4.07%. On the other hands, in low evaporating pressure region, there are operating conditions which should be avoided to obtain the useful work from the system. In addition, due to mismatch between the actual pressure ratio and optimal pressure ratio, the performance reduction of the scroll expander was observed in low evaporating pressure. By conducting exergetic analysis of the ORC, it was verified that the improvement of the

scroll expander was most important for operating the ORC applied to low-grade heat source. In conclusion, it was confirmed that obtaining the benefits of operating ORC applied to low temperature heat source below 100^{o}C is feasible.

References

[1] United Nations Population Division. World population prospects: the 2012 revision. New York, United States. 2013.

[2] International Energy Egency. World energy outlook 2014. Paris, France. 2014.

[3] International Energy Egency. CO_2 emissions from fuel combustion. Paris, France. 2015.

[4] World Energy Council. 2015 World energy issues monitor. London, United Kingdom. 2015.

[5] International Energy Egency. Linking heat and electricity systems: co-generation and district heating and cooling solutions for a clean energy future. Paris, France. 2014.

[6] Tchanche BF, Lambrinos Gr, Frangoudakis A, Papadikis G. Low-grade heat conversion into power using organinc Rankine cycles – A review of various applications. Renewable and Sustatinable Energy Reviews 2011;15(8):3963-3979.

[7] Hung TC, Shai TY, Wang SK. A review of organic Rankine cycles (ORCs) for the recovery low-grade waste heat. Energy 1997;15(8):3963-3979.

[8] Imran M, Park BS, Kim HJ, Usman M. Economic assessment of greenhouse gas reduction through low-grade waste heat recovery using organic Rankine cycle (ORC). Journal of Mechanical Science and Technology 2015;29;835-843.

[9] Wali E. Optimum working fluids for solar powered Rankine cycle cooling of buildings. Solar Energy 1980;25:235-241.

[10] Maizza V, Maizza A. Unconventional working fluids in organic Rankine-cycles for waste heat recvoery. Applied Thermal Engineering 2001;21(3):381-390.

[11] Dai Y, Wang J, Gao J. Parametric optimization and comparative study of organic Rankine cycle (ORC) for low grade waste heat recovery. Energy Conversion and Management 2009;50(3):576-582.

[12] Borsukiewicz-Gozdur A, Nowak W. Comparative analysis of natural and synthetic refrigerants in application to low temperature Clausius-Rankine cycle. Energy 2007;32(4):344-352.

[13] Madhawa Hettiarachchi HD, Golubovic M, Worek WM, Ikegami Y. Optimum design criteria for an organic Rankine cycle using low-temperature geothermal heat sources. Engery 2007;32(9):1698-1706.

[14] Lemort V, Devlaye S, Quoilin S. Experimental characterization of a hermetic scroll expander for use in a micro-scale Rankine cycle.

Proceedings of the Institution of Mechanical Engineers, Part A: Journal of Power and Energy 2012;226(1):126-136.

[15] Yue C, Huang Y, Wu Y. Experimental study of low-temperature organic Rankine cycle with axial flow turbine. International Conference on Applied Energy 2015;75:1583-1589.

[16] Zhao P, Wang J, Gao L, Dai Y. Parametric analysis of a hybrid power system using organic Rankine cycle to recover waste heat from proton exchange membrane fuel cell. International Journal of Hydrogen Energy 2012;37:3382-3391.

[17] Centre d'études et de recherches économiques sur l'énergie (CEREN). Potentiel de récupération de chaleur à partir des effluents industriels. Paris, France. 2011.

[18] Wang D, Ling X, Peng H. Performance analysis of double organic Rankine cycle for discontinuous low temperature waste heat recovery. Applied Thermal Engineering 2012;48:63-71.

[19] Lemmon EW, Huber ML, McLinden MO. Refprop: reference fluid thermodynamic and transport properties, NIST standard reference database 23, version 9.1. National Institute of Standards and Technology, Gaithersburg, Maryland, USA. 2013.

[20] Muhammad U, Imran M, Lee DH, Park BS. Design and experimental investigation of a 1 kW organinc Rankine cycle system usign R245fa as working fluid for low-grade waste heat recovery from steam. Energy Conversion and Managament 2015;103:1089-1100.

[21] Quoilin S. Sustainable energy conversion through the use of organic Rankine cycles for waste heat recovery and solar applications. PhD thesis. University of Liège, Belgium; 2011.

[22] Baik YJ, Kim M, Chang KC, Lee YS, Ra HS. Power maximization of a heat engine between the heat source and sink with finite heat capacity rates. Korean Journal of Air-Conditioning and Refrigeration Engineering 2011;23:556-561.

[23] Declaye S, Quoilin S, Guillaume L, Lemort V. Experimental study on an open-drive scroll expander integrated into an ORC (Organinc Rankine Cycle) system with R245fa as working fluid. Energy 2013;55:173-183.

국 문 초 록

최근 수 십여 년간 전지구적 에너지 위기와 기후 변화가 큰 화제로 대두되고 있다. 이를 해결하기 위해, 기존 발전 시스템의 효율 향상, 새로운 형태의 발전 시스템 개발, 신 재생 에너지, 대체에너지와 같은 새로운 유형의 에너지원에 대해 연구되고 있으며, 그 중에서도 폐열 회수를 통한 발전 시스템 효율 향상에 대한 연구가 활발히 진행되고 있다. 250°C 이상의 중·고온 폐열 발전에 대해서 기존 스팀 사이클을 이용하여 실제 발전 산업 현장에서 폐열이 원활히 회수되고 있지만, 물의 비교적 높은 비등점으로 인해 저온 폐열은 충분히 활용되지 못하고 있다. 이러한 배경에서 유기 냉매를 작동 유체로 이용함으로써 저온 열원에 적합하게 구성된 것이 유기 랭킨 사이클이며, 지난 수 십 년간 연구가 진행되었다. 하지만 기존에 수행된 유기 랭킨 사이클에 대한 연구마저도 150~350°C 의 지열, 태양열, 바이오매스 연소 폐열 등의 열원에 집중되어 있다.

따라서 본 연구는 전체 폐열원의 상당 부분을 차지하나 온도가 낮아 이용가능성이 떨어지는 100°C 이하의 열원에 적용된 유기 랭킨 사이클에 대한 실험을 수행하였다. 그 중에서도 전체 산업 폐열의 약 30%를 차지하며 그 중 54%가 80°C 이하인 식품 및 섬유 산업의 폐열과 앞으로 차량용, 소규모 발전용 등으로 이용될 것으로 예상되는 60~80°C 의 연료전지 폐열에 주안점을 두었다. 이에 대한 실험적 연구를 진행하기 위해 기어 펌프, 스크롤 팽창기, 증발기, 응축기 등으로 구성된 기본 랭킨 사이클을 구성하고, 작동유체를 간단한 사이클 해석을 통해 R245fa 로 선정하여 실험장치를 구성하였다. 이를 통해 증발압력, 응축압력, 질량유량, 폐열량, 냉매 충전량 등의 변수를 변화시켜가며 다양한 작동 조건에서의 유기 랭킨 사이클의 성능을 분석하였다.

냉매 충전량 실험을 통해 시스템이 최대 출력을 내는 최적 냉매 충전량은 8.50 kg 인 것을 확인하여 이를 냉매 충전량으로 고정하고, 고온열원과 저온열원의 온도를 각각 70°C, 15°C 로 설정하고 3~6 kW 로 변화시켜가며 실험을 진행하였다. 그 결과, 최대 출력은 증발압력 4.40 bar, 열원 크기 6.07 kW 에서 약 234 W 로, 최대 열효율은 증발압력 4.29 bar, 열원 크기 4.80 kW 에서 4.07%로 확인되었다. 또한, 스크롤 팽창기의 고정된 built-in volumetric ratio 에 의한 성능 저하에 대한 현상도 확인할 수 있었다.

본 연구를 통해 유기 랭킨 사이클이 100°C 이하의 열원에도 적용 가능함을 확인하였고, 다양한 운전 조건에서의 성능을 면밀히 파악할 수 있었다.

주요어: 유기 랭킨 사이클, 스크롤 팽창기, 폐열 회수, 저온열원, 산업 폐열, 고분자 전해질막 연료 전지 폐열, R-245fa

학 번: 2013-23833